2013

Assessment of riparian conditions in the Nooksack River Basin with the combination of LiDAR, multi-spectral imagery and GIS

Erica M. Capuana
Western Washington University

Follow this and additional works at: https://cedar.wwu.edu/wwuet

Part of the Environmental Sciences Commons

ASSESSMENT OF RIPARIAN CONDITIONS IN THE NOOKSACK RIVER BASIN WITH THE COMBINATION OF LIDAR, MULTI-SPECTRAL IMAGERY AND GIS

By

Erica M. Capuana

Accepted in Partial Completion
Of the Requirements for the Degree
Master of Science

Kathleen L. Kitto, Dean of the Graduate School

ADVISORY COMMITTEE

Chair, Dr. David O. Wallin

Dr. James M. Helfield

Dr. Leo R. Bodensteiner

MASTER'S THESIS

In presenting this thesis in partial fulfillment of the requirements for a master's degree at Western Washington University, I grant to Western Washington University the non-exclusive royalty-free right to archive, reproduce, distribute, and display the thesis in any and all forms, including electronic format, via any digital library mechanisms maintained by WWU.

I represent and warrant this is my original work, and does not infringe or violate any rights of others. I warrant that I have obtained written permissions from the owner of any third party copyrighted material included in these files.

I acknowledge that I retain ownership rights to the copyright of this work, including but not limited to the right to use all or part of this work in future works, such as articles or books.

Library users are granted permission for individual, research and non-commercial reproduction of this work for educational purposes only. Any further digital posting of this document requires specific permission from the author.

Any copying or publication of this thesis for commercial purposes, or for financial gain, is not allowed without my written permission.

Erica M. Capuana

November 14, 2013

ASSESSMENT OF RIPARIAN CONDITIONS IN THE NOOKSACK RIVER BASIN WITH THE COMBINATION OF LIDAR, MULTI-SPECTRAL IMAGERY AND GIS

A Thesis
Presented to
The Faculty of
Western Washington University

In Partial Completion
Of the Requirements for the Degree
Master of Science

By
Erica M. Capuana
November 2013

Abstract

Riparian areas are a complex component of stream ecosystems and provide critical habitat for Pacific salmon (*Oncorhynchus* spp.). Comprehensive techniques are needed for assessing riparian areas that can be used on small and large regional scales. I examined the application of airborne LiDAR and high resolution multi-spectral imagery from the World View-2 (WV-2) satellite to analyze riparian landcover and riparian forest structure in the Nooksack River Watershed. I employed an object-oriented approach to segment the imagery into meaningful objects consisting of groups of pixels. I examined the advantages of the four additional spectral bands from the 8-Band World View-2 Image compared to the traditional four spectral bands provided from conventional high resolution multi-spectral imagery. Using the Random Forest algorithm, I developed classification and regression models to predict the features of interest across the study area.

The classification results from the 8-Band WV-2 image were improved over the traditional 4-Band WV-2 image that is comparable to other high resolution sensors such as IKONOS and Quickbird. Analyzing the combined LiDAR and 8-Band WV-2 spectral data improved the results for landcover classification but did not improve the results for riparian forest structural predictions. However, the results generated from the LiDAR only image was comparable to the 8-Band WV-2 spectral imagery at classifying forest classes and remarkably better at predicting forest structure data. The overall results indicate that classification of forested cover type and structural properties of riparian forest stands can be determined accurately for relatively large study areas with LiDAR-based approaches. From the final LiDAR image output, I applied the models to categorize the riparian forest based on forest class, size, and density to show one application of the results generated in this study. The categorized map provides a tool to prioritize restoration and preservation needs within the riparian forest landscape in the Nooksack River Basin study area.

Acknowledgments

Table of Contents

List of Figures

List of Tables

1.0 Introduction

The degradation of freshwater habitat has contributed to the decline of anadromous Pacific salmonids (*Oncorhynchus* spp.) (Nehlsen et al. 1991; Beechie and Bolton 1999; Rot et al. 2000). Because riparian areas directly influence instream freshwater habitat, restoration and preservation efforts in the Pacific Northwest have focused extensively on riparian areas and the aquatic habitat they support (Naiman and Latterell 2005).

A well-functioning riparian area provides many services to the aquatic habitat. Large woody debris (LWD) recruitment is a critical function of riparian areas. Trees, large branches, and root wads that fall into a stream create refuge pools for salmon that allow them to forage for food, save energy, and gain protection from predators (Beechie and Sibley 1997). The pools also serve as thermal refuges in streams with elevated temperatures. The combination of LWD and vegetation along the stream edge provides stream bank stabilization and protects soils from surface erosion (Gregory et al. 1991; Naiman et al. 2005). Decreased erosion helps to reduce the amount of fine sediment in the channel which can clog salmonid spawning gravel reducing aeration of buried eggs and ultimately leads to decreased survival of eggs. Riparian vegetation also provides shade that maintains low stream temperatures vital for salmonids (Beschta et al. 1987; Gregory et al. 1991). Riparian vegetation can filter pollutants such as sediments, nutrients, road salt, and agricultural chemicals from upland areas that enter into the stream habitat (Duncan et al. 1987). The recruitment of particulate organic matter (POM) is another important function riparian zones provide (Naiman et al. 2000). Detrital organic matter such as leaves, cones, and needle litter are food sources for aquatic and terrestrial consumers important to aquatic food chains (Gregory et al. 1991). An intact riparian floodplain forest provides dynamic channel and floodplain interaction, which creates critical off-channel habitat for juvenile salmonids (Sommer et al. 2001; Fullerton et al. 2006). Riparian areas also provide critical wildlife habitat for aquatic habitat modifiers such as beaver and many other terrestrial predators or scavengers associated

with salmonid populations (Gregory et al. 1991; Naiman et al. 1998). This study focuses on developing remote sensing methods for describing the conditions of riparian forests.

1.1 Research Objectives

Anthropogenic influences on riparian habitat have compromised the function of the existing riparian habitat thus limiting suitable fish habitat. LWD recruitment and shade are two important contributions to stream habitat that functioning riparian forests provide to the adjacent stream segment. In particular, large conifers are key characteristics of a mature riparian forest because they can provide both functional LWD and shade. Characterizing riparian habitat into landcover classes is important for discriminating between forested and non-forested areas and specifically isolating conifer forest from deciduous forest. A deciduous dominated forest does not provide LWD of the size that is needed to function in most Pacific Northwest streams and decays more rapidly than conifer species (Latterell and Naiman 2005, Naiman et al. 2005). The ability to identify riparian forest structural attributes is important for assessing LWD and shade potential because it will give an indication of the tree size and developmental stage. In many stream reaches, extensive restoration is needed to recover these features. Other stream reaches may have functioning riparian habitat or are on a pathway to recovering functioning conditions. Identification of high quality riparian habitat is critical for prioritizing areas for preservation or assessing restoration efforts. Analysis of riparian areas with LiDAR and advanced multi-spectral imagery has the potential to provide a rapid, objective, and cost-effective tool to assist in prioritizing locations for riparian preservation and restoration efforts.

The objectives of this study are to:

- Evaluate the potential of LiDAR and multispectral imagery for assessing riparian forest condition
    - Specifically, evaluate LiDAR and WorldView-2 multispectral imagery for:
        i. Classification of riparian landcover classes
        ii. Predicting riparian forest structural attributes

- Generate a map of riparian forest condition based on the riparian landcover classification and riparian forest structural attributes that are relevant to LWD recruitment and shade potential.

1.2 Study Area

The study area is a subset of the Nooksack River Watershed in the Water Resources Inventory Area 01 (WRIA 01) in northwestern Washington (Figure 1). The Nooksack River runs through two hydrologic provinces, the steep uplands originating on the western slopes of the Cascades which cut through bedrock, and the lowlands which pass through glacial and interglacial sediments and alluvium at a much lower gradient (USGS 2002). The lower elevation areas are part of the Puget Sound lowlands. In the upland area east of Deming, WA, the river system is composed of three forks: the North Fork, Middle Fork, and the South Fork of the Nooksack River. After passing through Deming, the reaches converge to form the mainstem Nooksack River, which then flows through the lowlands before entering Bellingham Bay in the Puget Sound (USGS 2002). The study area specifically includes the lower South Fork Nooksack River and the associated tributaries and a portion of the upper mainstem Nooksack River and the associated tributaries.
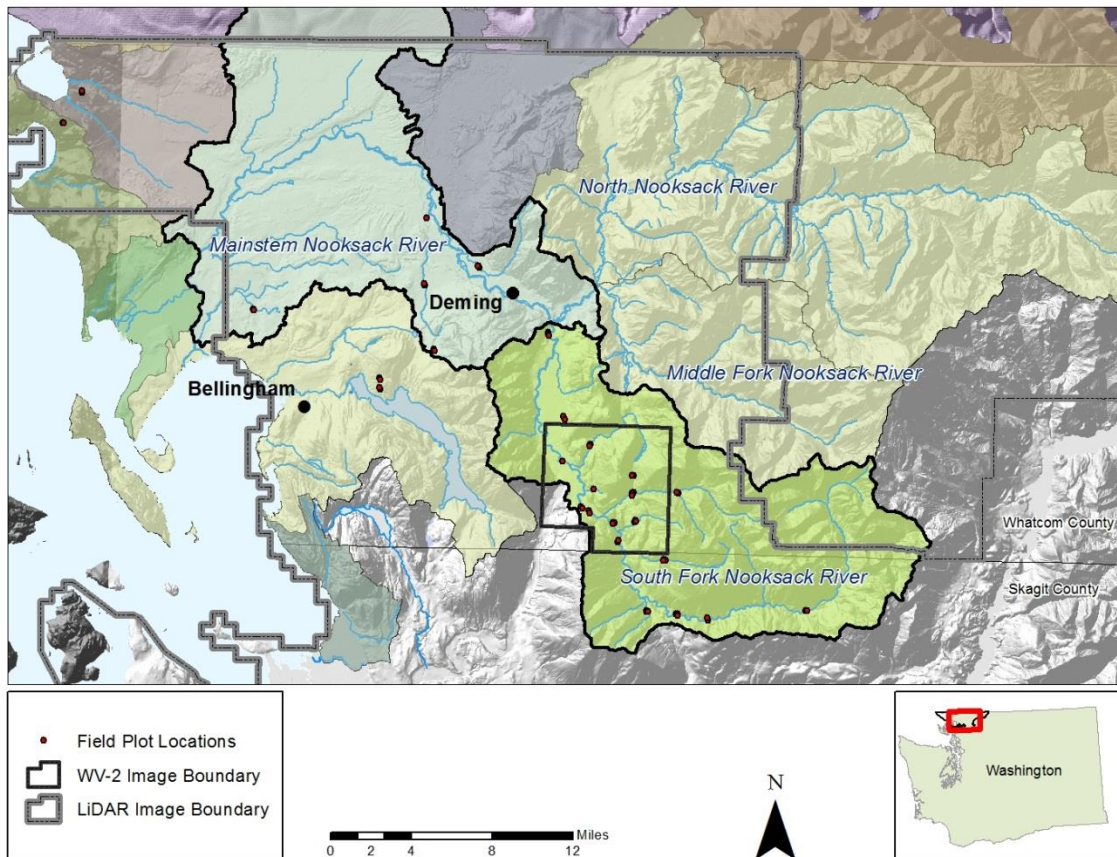
Figure 1. Nooksack River Basin study area with extent of available imagery areas.

Historically, Native Americans used the basin for subsistence fishing, hunting, and gathering. In the late 1800s, European settlers began to harvest timber in the uplands and cleared land in the lowlands to farm (Maudlin et al. 2002). Currently, the study area includes a mixture of rural-agriculture (53%), commercial forestland (28%), federal forestland (10%), urban-UGA zone (4%), and Lummi Indian Reservation (2%) (Hyatt 2000).

The study area was selected due to the presence of anadromous and resident fish populations that have been classified as "threatened" under federal law and a "candidate" species under state law (NMFS 2013; WDFW 2013), the diversity of upland and lowland habitat, and the diversity of land use practices along riparian zones. The South Fork Nooksack River supports all five North American species of Pacific salmon: chinook (*Oncorhynchus tshawytscha*); chum

(*Oncorhynchus keta);* coho (*Oncorhynchus kisutch);* pink (*Oncorhynchus gorbuscha);* sockeye (*Oncorhynchus nerka);* as well as steelhead (*Oncorhynchus mykiss)*, bull trout (*Salvelinus confluentus*), and sea-run cutthroat (*Oncorhynchus clarkii);* (WRIA 01SRB 2005). The South Fork Nooksack River is the focus of the study because of the threatened status of the Spring Chinook populations in the river. Threatened native summer-run and winter-run steelhead and bull trout also utilize this fork of the river. South Fork Nooksack Chinook are close to extirpation, with only a few dozen adults returning annually. To recover this and other species, there are intensive restoration efforts underway to restore habitat and habitat-forming processes and to protect high quality areas along the South Fork Nooksack. Elevated stream temperatures in the South Fork are considered to be a key factor that is limiting recovery of the Chinook population, and this especially affects adults holding in the river during the summer months (WRIA 01 SRB 2005). Threatened adult summer steelhead and bull trout also migrate up-river in the summer, and are also likely affected by the elevated temperatures. The Mainstem Nooksack was chosen because it has the combined influence of all forks of the Nooksack River, and it is the first segment salmon and trout populations travel through in their anadromous journey back from marine waters.

　　Riparian areas in this system were historically dominated by red alder (*Alnus rubra*), black cottonwood (*Populus trichocarpa*), Sitka spruce (*Picea sitchensis*), and western red cedar (*Thuja plicata*) (Collins and Sheikh 2004). In the lower watershed and delta, red alder was the most common riparian tree, but Sitka spruce was the only large-diameter tree and by far the dominant conifer by basal area. In the upper Nooksack and forks, alder was the most common tree and cedar the largest streamside tree. Present day riparian forest conditions are dominated primarily by deciduous species such as alder and cottonwood (Hyatt et al. 2004). Recent surveys of LWD in the South Fork Nooksack documented few key logs and stable log jams (NNR 2008). Historic records indicate the rivers contained extensive amounts of large woody debris, primarily sitka spruce in the delta, black cottonwood in the lower Nooksack, cedar in the upper Nooksack

followed by spruce, fir and cottonwood, and in the forks, cedar and fir followed by cottonwood and big leaf maple (*Acer macrophyllum*) (Collins and Sheikh 2004).

2.0 Background

2.1 Riparian Forests

Logging, agriculture, urban development and many other anthropogenic factors have dramatically altered riparian areas in the Pacific Northwest, causing a sharp decline in their ability to provide terrestrial and aquatic habitat (Duncan et al. 1987; Beechie and Sibley 1997). Until the 1980s there were limited restrictions on timber harvest activity in the riparian zone, and forests were logged to the streams edge. For this reason, the legacy of past harvest activity is still apparent. Currently riparian forests are often dominated by deciduous species such as red alder which are important components of the riparian regime but do not typically provide large enough or decay resistant LWD to the stream (Mikkelson 2001; Compton et al. 2003; Volk et al. 2003; Gergel et al. 2007; Mollot et al. 2007). This change in species composition, size and stem densities post-harvest has caused the reduction in coniferous woody debris of sufficient size to provide instream habitat (Beechie and Sibley 1997; Bilby and Bisson 1998; Hyatt et al. 2004; Mollot et al. 2007). The reduction of LWD in streams can degrade instream habitat by increasing sediment loads, increasing water temperatures, and decreasing channel complexity leading to channel incision (Bilby and Ward 1989; Kreutzweiser and Capell 2001; Steiger et al. 2001; Kiffney et al. 2003; Fullerton et al. 2006). Alterations to riparian forests have reduced the inputs of LWD to streams, but historical management practices also involved the active removal of LWD from stream channels.   Up until the 1950s splash dams were used to transport logs, which also reduced the amount of wood in streams (Wendler and Deschamps 1955; Bilby and Ward 1991). A splash dam is a temporary dam made from wood that was built in the stream adjacent to a harvest operation. The buildup of water allowed more logs to be transported downstream when the dam was released, but also flushed any existing large woody debris from the stream and

scoured the stream channel corridor. As recently as the late 1980s, instream wood –both naturally occurring and logging debris-- was also actively removed for navigation and, at the time, as a perceived improvement to upstream access for anadromous fish (Sedell and Luchessa 1982; Bilby 1984; Bisson et al. 1987; Bilby and Ward 1991). However, the negative impacts of this wood removal are now widely recognized.

The loss of an active channel migration zone through bank armoring and levees has also dramatically decreased the recruitment of LWD to streams and rivers (WRIA 1SRB 2006). These flood protection measures were instituted to protect infrastructure and agriculture in floodplains but at the time did not integrate with fish habitat needs. A floodplain that is well connected to the active channel provides multiple functions for the river-floodplain ecosystem, such as off-channel habitat for salmonids, attenuation of high flows, reduction of sediment loads, and recruitment of LWD (Naiman et al. 1998). Reconnection of rivers to their associated floodplains is a way to restore natural river process which makes the system more resilient to future changes by allowing the system to make necessary physical and biological adjustments (Beechie et al. 2010). As river management progresses into the 21st century, balancing the recovery of ESA-listed salmon species while protecting infrastructure is a controversial and challenging issue.

Washington Forest Practice Rules under Title 222-30 WAC were enacted in 2001 to establish riparian buffers to decrease active logging in the riparian zone (WADNR 2010). The width of these buffers zones and restrictions within them vary based on the sensitivity of the associated stream reach (WADNR 2010). However, having only been in place for approximately 10 years, there are still legacy effects of past harvest practices within the riparian zone.

A mature riparian forest is comparable to an old growth forest and is composed of large, living and dead trees; massive fallen logs; a multi-layered canopy with openings; and a diverse understory (Naiman et al. 2000; Bigley and Deisenhofer 2006). Compared to other successional stages, a mature riparian forest has greater amounts of horizontal and vertical variation (Alaback

1982a; 1982b; Naiman et al. 1998). A well-functioning riparian zone exhibits many features of an old growth forest (Naiman et al. 2005). The Washington State Department of Natural Resources (WADNR) habitat conservation plan (HCP) for managing state owned forested land dictates management for structurally complex riparian forest that are assumed to be at a fully functional development stage or equivalent to the ecological definition of old growth forest conditions (Bigley and Deisenhofer 2006). Functional riparian habitat is characterized by three main elements, large conifer trees, a complex stand structure, and long-lived tree species composition to provide stability to stream banks, channels, and floodplains (Bigley and Deisenhofer 2006). Large conifers over time are recruited to the stream providing stable LWD that in turn modifies the channel to provide critical salmon spawning, rearing, holding, and over-wintering habitat. Shade is also directly provided by large conifers in the riparian zone. Due to the mosaic of site conditions near streams, the riparian forest exhibits diverse stand structure with canopy gaps and patches of variably spaced trees throughout the stands (Bigley and Deisenhofer 2006).

Historically, mature riparian forests in the Pacific Northwest included not just a wide, almost continuous corridor of mature trees but also off-channel wetlands and complex floodplain areas (Naiman et al. 1998). The trees species in the riparian forest were primarily conifers but there were also patches of alder and willow in areas of recent disturbance and a mosaic of dense, diverse understory species (Gregory et al. 1991; Naiman et al. 1998).

Historically, the lower Nooksack River maintained extensive wetlands, multiple channels, sloughs, and forested islands (Collins and Sheikh 2004). The riparian forest was dominated by red alder, western red cedar, Sitka spruce, and black cottonwood (Collins and Sheikh 2004). The intact riparian forest provided large wood to the Nooksack River with geographic variability in species contribution,

"Wood jams were historically abundant and had a variety of geomorphic and habitat functions in the Nooksack. The GLO bearing tree data indicate species that would have contributed very large wood that could potentially function as key pieces in jams. Sitka spruce was the sole source on the delta; black cottonwood would have augmented spruce in the lower Nooksack; in the upper Nooksack cedar would have been the most common, and secondarily spruce, fir and cottonwood. In the forks, primarily cedar and fir and secondarily cottonwood and maple would have commonly provided very large wood." (Collins and Sheikh 2004).

Large amounts of wood in the Nooksack riverine environment would have caused a dynamic channel pattern characterized by frequent avulsion. However, due to the frequency of large stable log jams acting as hard points for vegetation to remain, there would have been a patchwork, mosaic forest across the active channel migration zone (Maudlin et al. 2002).

2.2 LWD Function

LWD enters the streams when riparian trees fall or when trees are transported from upstream or the adjacent riparian forest. Delivery of trees to the stream can be through biological processes such as tree mortality due to insect and disease or by physical processes such as wind throw and undercutting of root systems by the aquatic environment (Bisson et al. 1987). LWD recruitment can occur more frequently at smaller scales of a single tree falling in the river and also at less frequent but larger scales that deliver a large number of trees to the river at one time (Bilby and Ward 1989). The greater episodic events contribute large pulses of wood that are usually caused by tree mortality driven by epidemic scale insect infestations and disease, landslides, avalanches, large-scale patches of blow down, and bank erosion caused by high flows (Bisson et al. 1987; Naiman et al. 2000). While input processes vary based on tree species composition, soil stability, valley form, climate, lateral channel mobility, and streamside management history, the density of streamside trees is positively correlated with LWD amounts in some systems (Bisson et al. 1987; Long 1987; Bilby and Ward 1989). Studies comparing the recruitment of trees from a second growth riparian forest in which large trees have been previously harvested show the inputs are greatly reduced compared to old growth riparian stands (Bisson et al. 1987).

The persistence of LWD in the fluvial system is a function of the wood size and species recruited from the riparian forest (Naiman et al. 2000). The amount, characteristics, and function of LWD differ with stream size (Bilby and Ward 1989; Hyatt et al. 2004). Riparian derived LWD interacts with the geomorphology and hydrology of the associated fluvial system exerting a strong influence on channel morphology and as a result the composition of the adjacent riparian forest (Fetherston et al. 1995; Abbe and Montgomery 1996; Naiman et al. 2000; Bailan and Naiman 2005). Debris jams formed by LWD exert localized control on channel hydraulics and can provide stable locations for vegetation to withstand flood scour. These protected locations allow riparian succession to progress for decades and in some cases centuries in a riverine environment where rapid channel migration can cause frequent disturbance (Bisson et al. 1987; Fetherston et al. 1995). LWD in the aquatic environment acts as refuge for aquatic invertebrates and fish species from high flows and predation. The logs function to form associated scour pools and deepen existing pools. The logs also provide locations for sediment and organic matter to build up and increase the channel roughness and complexity (Bilby and Bisson 1998; Naiman, et al. 2000).

2.3 Shade Function

Stream temperature is influenced by multiple factors such as direct solar radiation, ambient air temperature, groundwater inputs, hyporheic exchange, humidity, and elevation (Brown 1969; Brown and Krygier 1970). High water temperatures can be detrimental to all life stages of salmonids and can affect multiple factors such as disease resistance, timing of life history events, egg survival, and more (Spence et al. 1996; WRIA 01 2005). The dominant source of heat to streams comes from direct solar radiation (Johnson 2004; Naiman et al. 2005). Riparian forests can dictate the amount and duration of direct solar radiation reaching an adjacent stream. Canopy density, canopy height, stream channel width, and orientation of the channel in relation to the path of the sun also influence stream temperature (Naiman et al. 2005). Riparian

vegetation can also indirectly influence stream temperature by altering the stream micro-climate variables such as air temperature, humidity, and wind speed (Rutherford et al. 1997). The micro-climate then affects evaporation, conduction, ground temperature, and water temperature.

During the summer when solar radiation levels are highest due to higher sun angles, longer periods of daylight, clear skies and the discharge of the stream is low, the interception of solar radiation by riparian canopies is critical (Beschta et al.1987). The exposed surface area of a stream segment and stream discharge determines the degree to which solar radiation increases the water temperature (Sheridan and Bloom 1975; Beschta et al. 1987). For example a stream with a large exposed surface area and a low discharge will have higher temperature increases. Several studies have observed increases in stream temperature immediately downstream of removal of riparian forests (Brown 1969; Brown and Krygier 1970; Brazier and Brown 1973).

2.4 Riparian Assessment

Riparian areas extend through land under multiple jurisdictions with diverse land use practices. For this reason, many different groups and agencies are involved in the management of riparian areas. Riparian area assessment is a critical component in predicting salmon habitat quality because riparian areas directly influence instream freshwater habitat (Naiman and Latterell 2005; Fullerton et al. 2006). Riparian structure, composition, and succession vary substantially based on spatial variability in elevation and slope, and as a result there is fine-grained spatial variability in responses to regional disturbance regimes (Mollot and Bilby 2008). Ground-based surveys combined with aerial photos or Landsat imagery with a pixel size of 30 meters have been the main methods for riparian zone inventory by forested land managers and habitat biologists. Ground-based techniques are labor intensive and expensive for regional application. Aerial photos and Landsat imagery do not capture the diversity of riparian zone features in enough detail. Conducting a field based survey campaign of the entire riparian forest is typically logistically impractical and the current methods for extrapolating the conditions to

areas not sampled may not capture the heterogeneity of the riparian forest and also require extensive time and labor to digitize aerial photographs. There is potential to improve the methodology for riparian forest inventory by developing an efficient fine-grained assessment method that can effectively survey narrow, complex riparian forest.

In riparian forest assessment, similar to traditional forestry assessments, it is common to use one forest metric as a predictor of another forest metric because forest stand structural, functional, and compositional attributes are often highly correlated (Franklin et al. 2002; Bormann et al. 2006). Forest structure can be defined by a diverse set of variables such as: number of canopy strata, canopy cover, tree diameter, tree height, spacing, abundance (basal area and volume), species, understory vegetation (richness, height, total cover), and dead wood components (Bormann et al. 2006). Spies and Franklin (1991) found that mean diameter at breast height (DBH), standard deviation of DBH, tree density, and density of trees greater than 100 cm are strongly correlated with mature forest structural stage in the Pacific Northwest. Later work found that the quantity and size of canopy gaps are also important features of old growth stands (Spies 1998; Van Pelt and Franklin 2000).

2.5 Restoration Strategies

Two main strategies for improving salmon habitat occur in the Pacific Northwest, introducing conifer trees into riparian stands and introducing large wood into the stream itself. Large wood designed to mimic naturally occurring logjams, is the most common strategy for introducing large wood to the stream. In the Nooksack River Watershed alone there have been over 100 ELJ structures installed in the North Fork and South Fork Nooksack combined (Maudlin and Coe 2012).

The strategy of planting conifers in hardwood stands is low cost compared to the addition of wood to the aquatic environment but requires a longer time frame to achieve the habitat benefits. The main objective of conifer introduction is to provide a future source of large logs and

shade for the stream (Mollot and Bilby 2008). The majority of wood introduced to the channel from the adjacent riparian forest is produced within 50 m of the channel edge (Murphy and Koski 1989; McDade et al. 1990; Mollot and Bilby 2008).

2.6 Image Assessment

Multiple efforts are underway to develop new forest assessment methods using LiDAR, satellite imagery, and also combinations of LiDAR and satellite imagery. There is potential to apply these newer remote sensing methodologies to riparian forests as well. Classification of remotely sensed data for forest assessment can be divided into two approaches: pixel based and object based. Pixel based is the traditional method of image analysis based on a per pixel classification. Object-based image analysis (OBIA) is an emerging analysis method for image classification based on segmenting the image into groups of adjoining pixels that are referred to as "objects." The objects are defined based on spectral similarities among adjoining pixels and other analyst-determined constraints such as object shape, size, and texture (Campbell and Wynne 2011). Objects then become the carriers of image information derived from the underlying pixels (Chubey et al. 2006). An advantage to OBIA is that the segmentation process aggregates individual pixels of the forest stand into one image object that combines the spectral response of all of the included pixels. The image objects are then used in subsequent analyses (Chubey et al. 2006). OBIA is an attempt to reconcile digital imagery, with a pixel size of perhaps 1 to 4 m, with forest inventory data for stands or individual trees (Hall 2003). This is particularly useful when evaluating heterogeneous riparian areas.

2.6.1 LiDAR

Airborne LiDAR or Light Detection and Ranging is a relatively new technology that is becoming more widely available to natural resource practitioners. LiDAR is primarily used for terrain mapping (Reutebuch et al. 2003) but is also becoming more commonly used in forest management as an important tool for vegetation assessment (Sullivan et al. 2009). LiDAR data

13

can provide high-resolution topographic maps and also accurate estimates of vegetation height, cover, and canopy structure. The benefit of using LiDAR sensors is the ability to sample a three-dimensional distribution of plant canopy components as well as sub-canopy topography (Bormann et al. 2006).

The relationship between LiDAR-derived height and cover measurements and traditional field measurements of canopy structure is well understood. This approach is referred to as area level metrics (ALM) (Bormann et al. 2006). LiDAR data has been used to measure crown height (Means et al. 1999; Næsset and Bjerknes 2001; Næsset 2004; Andersen et al. 2006), measure crown height and length (Næsset and Økland 2002), mean DBH (Lefsky et al. 1999; Kane et al. 2010a), variation in tree diameter (Lefsky et al. 1999; Kane et al. 2010a), basal area (Lefsky et al. 1999; Means et al. 1999; Næsset 2004; Goerndt et al. 2010), above ground biomass (Lefsky et al. 1999; Means et al. 1999; Lefsky et al. 2002; Lefsky et al. 2005a), cover (Means et al. 1999, Kane et al. 2010a), stem count (Næsset and Bjerknes 2001; Næsset 2004), density (Goerndt et al. 2010; Kane et al. 2010a) and fuel loads (Andersen et al. 2005). The metrics are most often related via regression, non-parametric and discriminate analysis (Hyyppä et al. 2008). Three categories of LiDAR metrics, mean height of LiDAR returns, variation in height such as standard deviation of LiDAR returns, and canopy closure were found to correlate with field measurements of forest structure when used in combination with each other (Lefsky et al. 2005a; Kane et al. 2010a)

The use of individual-tree level LiDAR metrics (ITM) has been documented as well, but is not as common (Brandtberg et al. 2003; Holmgren et al. 2003; Holmgren and Persson 2004; Popescu 2007; Yu et al. 2011). Individual tree height, location and crown size can be derived for individual-tree level metrics from the canopy height point clouds and pixels of canopy height models. Identification of species from LiDAR data is also being developed using both LiDAR elevation and intensity points (Holmgren and Persson 2004).

LiDAR metrics have been incorporated into object-based analysis of forest stands (Pascual et al. 2008; Sullivan 2009). Pascual et al. (2008) used OBIA to characterize *Pinus*

14

sylvestris stands using LiDAR data. They first defined forest stands in eCognition, software that specializes in OBIA, with a digital canopy layer derived from the LiDAR data and then used cluster analysis (k-means) to separate the different forest types. The best predictors of forest structure were median and standard deviation of height.

2.6.2 Multi-spectral Imagery

There are many satellites that provide multi-spectral data for image analysis. Several satellites, QuickBird, IKONOS, Spot 4 and 5, Orbview-3, and WorldView-2 can acquire multi-spectral imagery at spatial resolutions below 4 m and panchromatic data at less than 1 m pixel resolutions. The sensors carried by IKONOS and Quickbird have three spectral bands in the visible spectrum, 0.45 to 0.70 µm and one in the near infrared, 0.76 to 0.85 µm. The IKONOS sensor provides a spatial resolution of 4 m for the four multispectral bands listed in Table 1 and 1 m for the panchromatic band. Spot 5 also has a band in the mid-infrared, 1.58 to 1.75µm. WorldView-2 is a relatively new satellite launched in 2009 and the only satellite that currently has eight spectral bands. The satellite provides a spatial resolution of 0.5 m on the panchromatic band and 2 m on the eight multispectral bands (Table 1). In addition to the four standard spectral bands (blue, green, red, and near infrared) carried by other satellites, Worldview-2 carries four additional spectral bands, (coastal blue, yellow, red edge, and near IR2) (Table1). The new Yellow, Red-Edge and the second near-IR bands provided by the WorldView-2 sensor should increase the capacity to differentiate between conifer and deciduous trees (Digital Globe 2010).

Table 1. Band comparison for World View-2 and IKONOS.

WorldView-2 -			IKONOS	
Band Name	Band #	Wavelength Interval (μm)	Band #	Wavelength Interval (μm)
Coastal	1	0.40-0.45	-	-
Blue	2	0.45-0.51	1	0.45-0.52
Green	3	0.51-0.58	2	0.51-0.60
Yellow	4	0.59-0.63	-	-
Red	5	0.63-0.69	3	0.63-0.70
Red Edge	6	0.71-0.75	-	-
NIR-1	7	0.77-0.79	4	0.76-0.85
NIR-2	8	0.86-1.04	-	-

High resolution satellite imagery has been used in forest assessments with assorted mapping objectives, such as the mapping of invasive species (Everitt et al. 2008), merchantable timber, fire fuels (Mutlu et al. 2008), riparian species (Johansen and Phinn 2006; Johansen et al. 2007; Gergel et al. 2007), and old growth tropical rainforests (Clark et al. 2004). QuickBird imagery has been used recently to measure riparian vegetation with high levels of accuracy (Johansen and Phinn 2006; Gergel et al. 2007; Johansen et al. 2007). Johansen and Phinn (2006) used QuickBird satellite imagery to analyze the structural attributes of savanna riparian zones in northern Australia, such as canopy gaps, foliage clumping, tree crowns, stand density, and vegetation communities. Johansen et al. (2007) used QuickBird imagery to classify riparian vegetation on Vancouver Island, British Columbia They used a combination of spectral, vegetation and texture bands in an object-oriented image classification to classify vegetation structural stages with accuracies of 78.95%. Gergel et al. (2007) used QuickBird imagery to classify riparian forest structure classes using OBIA as well with accuracies ranging from 70 to 90%. Hyperspectral imagery has also been used to classify riparian forests using a supervised classification method with an overall accuracy of approximately 80% (Mollot et al. 2007).

In Costa Rica Clark et al. (2004) used IKONOS imagery to map old growth forests, tree crown location and growth for large trees. Stand basal area, estimated above ground biomass, and percentage of the canopy 15 m tall were significantly correlated with indices derived from IKONOS data. Chubey et al. (2006) used multi-resolution segmentation in eCognition to segment an IKONOS image to extract the forest inventory parameters: species, height, and crown closure, and stand age. Radoux and Defourny (2007) compared IKONOS imagery and Spot-5 imagery to delineate forest stands using multi-resolution segmentation in eCognition.

Recent studies have used WorldView-2 imagery for forestry applications (Borel 2010; Omar 2010; Sridharan 2010; Wolf 2010). Sridharan (2010) used the WorldView-2 imagery to map urban forests in Texas with classification accuracies of 62-64% at the species level for up to 40 tree species and accuracies of greater than 91% at the landcover level. Omar (2010) mapped tree species in Malaysia using WorldView-2 imagery with an overall accuracy of 90% using the random forest classification technique. Another study used textural and spectral indices extracted from WorldView-2 data to estimate plot-level basal area, volume, mean height and mean DBH in New South Wales, Australia (Shamsoddini et al. 2010). They found better results for mean height and DBH compared with volume and basal area. The red edge, yellow and NIR2 bands performed well in combination for estimation of biophysical parameters. Chávez and Clevers (2010) used object-based analysis to segment a WorldView-2 image into individual trees and then apply three vegetation indices to quantify tree health. Chen (2010) compared WorldView-2 imagery and IKONOS-2 imagery for tree identification in Hawaii. He tested three types of classifications at the pixel and object level: discriminant analysis, support vector machine, and random forest. Comparing the four comparable bands that both satellites share (blue, green, red, and NIR) he found the WorldView-2 image achieved higher accuracies than the IKONOS image at the pixel and object level, 6 % and 13% higher, respectively. Chen found the four new WorldView-2 bands (coastal, yellow, red-edge, and NIR2) were among the top bands for classifying tree species at the pixel level. Ozdemir and Karnieli (2010) used correlation analysis

to predict forest structural parameters from texture indices derived from WorldView-2 imagery in dryland forest in Israel. They looked at number of trees, basal area, stem volume, Clark-Evans index, diameter differentiation index, contagion index, Gini coefficient, and standard deviation of breast heights. Basal area, standard deviation of diameter at breast heights, and Gini coefficient were the best fitting models. Multi-spectral imagery has been useful at characterizing tree species and structure. This study examines the potential of multi-spectral imagery for characterizing riparian landcover and structural attributes. It is also examines the capacity of the additional four bands provided by the 8-Band WV-2 image for this purpose. At this time there are no studies that have examined the role of the additional spectral bands from the 8-Band WV-2 image for riparian forest assessment in the Pacific Northwest.

2.6.3 Data Fusion

Many studies use a combination of imagery to increase accuracy of forest classification. There are several studies that have fused LiDAR with aerial photography, multispectral or hyperspectral imagery (Popescu et al. 2004; Lefsky et al. 2005b; Geerling et al. 2007; Packalen and Maltamo 2007; Secrest 2007; Voss and Sugumaran 2008; Anderson et al. 2009; Arroyo et al. 2010; Jones et al. 2010). Lefsky et al. (2005b) combined SLICER-derived LiDAR estimates of stand height and above ground biomass and Landsat estimates of stand age to estimate above ground net primary production of wood (NPP_{Aw}). Packalen and Maltamo (2007) used a combination of LiDAR and aerial images to predict species specific plot-level tree volumes. Anderson et al. 2009 conducted an image analysis of ombrotrophic peatlands in the United Kingdom using both LiDAR and IKONOS imagery. They calculated the following textural data products from a LiDAR dataset at the same 4-m resolution as accompanying IKONOS imagery: minimum and maximum land surface height, and variance and semi-variance calculated from semi-variogram analysis of land surface height. They achieved an accuracy of 72% for peatland landcover classes using IKONOS data only and increased accuracy levels to 88% when the

LiDAR semi-variance product was used. The LiDAR minimum and maximum local heights and variance product also increased accuracies compared to just using IKONOS imagery, 86% and 83 %, respectively.

A study by Hudak et al. (2006) integrated canopy height, LiDAR return intensity, and canopy metrics derived from LiDAR and Advanced Land Imager (ALI) spectral data to predict basal area and tree density using stepwise regression in conifer-dominated forests in northern Idaho. The LiDAR variables proved much more valuable than the ALI variables for predicting the structural variables. They found LiDAR height variables predicted basal area best followed by LiDAR intensity. Tree density was predicted based by LiDAR canopy cover variables and then also LiDAR intensity. Overall they explained ~90% of variance in basal area and tree density. Voss and Sugumaran (2008) used hyperspectral data from Airborne Imaging Spectrometer for Applications (AISA) and LiDAR to classify seven tree species in Cedar Falls, Iowa, USA using an object-oriented approach. Adding LiDAR height information to the classification increased the accuracies by 19% for both seasons. In a study classifying floodplain vegetation in the Netherlands, Geerling et al. (2007) used Compact Airborne Spectrographic Imagery (CASI) data combined with LiDAR. They implemented an object-based multi-resolution segmentation followed by a supervised classification. Using the LiDAR data alone their classification accuracy was only 41%. The CASI data performed better with an accuracy of 74%. After fusing the two datasets, the accuracy was increased to 81%. Arroyo et al. (2010) fused LiDAR data with QuickBird imagery to map riparian biophysical parameters and land cover types: plant projective cover (PPC) or groundcover, riparian vegetation, woodlands, rangelands, bare ground, streambed, streambed width, riparian zone width, and overhanging vegetation. They used OBIA to analyze the data and achieved an overall accuracy of 86%. The fusion of LiDAR and multi-spectral imagery provides improved results based on previous work from the unique advantages that each dataset brings to the analysis. I would expect the

fusion of LiDAR and multi-spectral imagery to be the most useful for characterizing riparian landcover and forest structural attributes.

3.0 Materials and Methods

3.1 Materials: Data sources

There are four main types of data used in this analysis: LiDAR, multi-spectral satellite imagery, field or ground truth vegetation data, and GIS data.

3.1.1 LiDAR

The 2006 USGS LiDAR dataset was part of a regional LiDAR survey campaign covering 1735 square miles of western Whatcom and Skagit counties contracted by U.S. Geological Survey (USGS; Sanborn 2008; Figure 1). The data were acquired in May, 2006 (Table 2). Two platforms, the Leica ALS-50 (Airborne Laser Terrain Mapping) and the Optech 2050 LiDAR systems, were used to collect the data. The two platforms have comparable specifications. The LiDAR data was processed by the vendor to obtain first and last return point data. The last return was further filtered to yield a LiDAR surface representing the bare earth. The vendor also provided a first return point data DEM in ArcInfo Grid File Format, a bare earth point data DEM in both an ArcInfo Grid File Format and ASCII xyz file format, and all return data in ASCII text file format and las format.

The data acquisition was an experiment by the USGS in collecting LiDAR data over a large area for a low cost. The final product did not meet the task order specifications for completeness or accuracy and did not meet the specifications for vertical accuracy (Haugerud 2008). The incomplete areas and sparse return areas are beyond the boundaries of the study area for this project. The errors associated with the decreased vertical accuracy within the dataset made mapping the ground surface challenging; however, because this study evaluates the LiDAR point cloud in relation to the last return on the surface, absolute vertical accuracy was not a critical issue.

Table 2. LiDAR specifications for USGS 2006 LiDAR dataset.

Data source	Specifications
date	May 11, 2006
vendor	Sanborn
Leaf on or off	on
Area (km^2)	5096
Pixel size (m)	1.83
Accuracy (cm)	18.5- 37 RMSE (vertical) 100 (horizontal)
Scan angle (^{o}) - hm +- or total	36-40 (half angle)
Flying height above ground level (AGL)	1200-1500 (m)
Scan pulse rate (kHz)	50-60
Scan width (m)	NA
Sampling density all returns (points/m^2)	1.3-1.4
Sampling density all returns (points/m^2)[1]	2.58
Sampling density first returns (points/m^2)[1]	1.36

[1]within the sample plots in this study

The 2006 LiDAR dataset has an overall all returns point density of 1.3-1.4 points/m^2 (Table 2). Within the sample plots, the average all returns point density was higher, 2.58 points/m^2. The first return point density was closer to the overall average at 1.36 points/m^2. A top down view of a small portion of the maximum tree height layer can be seen in Figure 2b. An example of the distribution of the first returns points for one of the sample plots as viewed in the Forest Service Software FUSION Version 3.30 can be seen in Figure 3 (McGaughey 2013).

Figure 2. Imagery sources: (a) Visible bands (5, 3, 2; RGB) from 8-band World View-2 September 29, 2010; (b) LiDAR 2006 tree height layer, May 11, 2006.
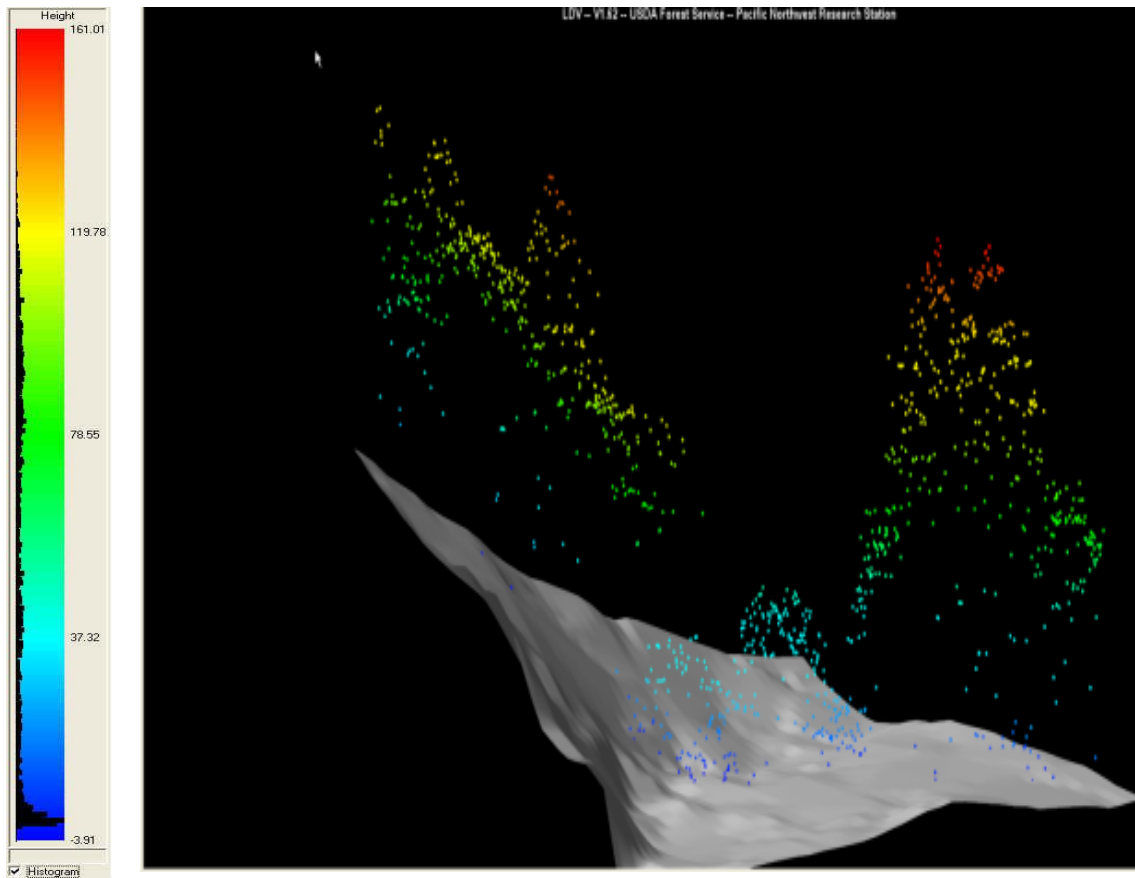
Figure 3. Example of First Returns height above the ground data points in ft. for Plot POBLB (76) displayed over the bare earth ground layer. Point density 1.28 points/m^2, Total points 1174.

3.1.2 WorldView-2

One high resolution World View-2 eight band image was obtained on September 29, 2010. This is considered a leaf-on time period although some of the deciduous trees were beginning to senesce by this date. The World View -2 image covers an area centered on the lower South Fork Nooksack River, approximately river mile 7.7 to 16.5 (Figure 1). The image was delivered with the multispectral bands separate from the panchromatic band and was divided into eight tiles. A close up of the visible bands from the World View-2 imagery can be seen in Figure 2a.

3.1.3 GIS data

A summary of the GIS data used in the analysis is listed in Table 3. The hydrology data and watershed boundaries data were provided by the Northwest Indian Fisheries Commission (NWIFC 2008). Anadromous fish usage includes both current and historical/potential distribution (NNR 2004). I digitized the active channel boundaries directly from the 2010 WorldView-2 Image. The riparian condition zone and channel migration zone were delineated from aerial photo interpretation from aerial photos from both 1991 and 1995 (Coe 2001).

Table 3. GIS data, date and source of data.

Data description	Source
Stream Gradient (SSHIAPP[1])	NWIFC 2008[2]
Anadromous fish usage	NNR 2004
Active Channel South Fork Nooksack	digitized from WV-2 Image
Riparian vegetation (RCU)[3]	Coe 2001
Channel Migration Zone	NNR 2001
Watershed boundaries (SSHIAPP)	NWIFC 2008

[1]SSHIAPP – Salmon and Steelhead Stock Inventory Assessment Program
[2]NWIFC – Northwest Indian Fisheries Commission
[3]RCU - Riparian Condition Units based on aerial photo interpretation

3.1.4 Field data

Field sites were identified through a stratified random sampling scheme developed from existing landcover datasets, fish distribution data, stream gradient information, and riparian

vegetation from a previous assessment (Table 3). The sites were distributed throughout the study area and were selected to sample a full range of riparian forest composition and structural attributes adjacent to anadromous fish habitat within the study area. The plots were limited to anadromous fish-bearing streams and adjacent stream segments with gradients less than 20%. To restrict the study area to the riparian zone, I used a buffer width of 300 ft. from the stream edge or active channel. While buffer regulations vary among streams, I chose a buffer of 300 ft. that represents the target buffer distance for riparian reserves as recommended by the Forest Ecosystem Management Assessment Team (FEMAT 1993). The 300-ft. buffer distance is greater than most regulated buffers; however, to fully assess the riparian forest I wanted to include a riparian buffer that was somewhat larger than the regulated buffer. Also, the larger buffer compensates for some of the inaccuracies in the GIS stream layer.

The World View-2 data were acquired later in the project as grant funding became available and, due to funding constraints, do not cover the full spatial extent of the 2006 LiDAR dataset. As a result, there are fewer field plots within the area covered by the World View-2 imagery. There are 63 field plots in the LiDAR data area and 22 in the World View-2 study area (Figure 1). Field data were collected during summer and fall 2008 and 2009 and three additional plots were collected in 2010 to augment the World View-2 imagery dataset which was acquired in 2010.

From each randomly generated point I ran a transect perpendicular to the stream segment that was 10 m wide and extended 60 m into the riparian zone (0.06 ha). In a few instances the perpendicular distance was extended beyond 60 m if there was a distinct break in the forest from a road or harvest operation beyond 60 m but less than 100 m. The locations of the four plot corners were determined with a Trimble Pro XT differential GPS receiver. At all plots, I was able to obtain coordinates for a minimum of one plot corner. When dense forest cover precluded obtaining coordinates for all four plot corners, I calculated the coordinates for the other corners using distance and bearing from the one location. The data were post-processed using Trimble

Pathfinder software to establish horizontal accuracies of ≤ 2 m. Within each transect tree species composition, diameter at breast height (DBH), and distance to stream was measured for all standing trees greater than 10 cm DBH. For dead trees, the mortality agent and decay class adapted from Maser et al. (1988) were recorded. However, mortality agent proved difficult to determine and most often was recorded as unknown.

All live trees ≥ 10 cm DBH were included in the analysis. For each field plot I calculated summary statistics and derived basal area and stem density metrics from the DBH measurements and stem counts. Washington Department of Natural Resources (DNR) Timber Fish and Wildlife (TFW) riparian forest methodology includes measuring live and dead trees because standing dead trees have high potential for contributing wood to the stream (WADNR 1996). However, quantifying dead trees from LiDAR and multispectral imagery is beyond the scope of this project, although dead tree data were collected at field sites.

Ideally, the image and field data would have been acquired simultaneously, but logistics did not allow this. An analysis of potential factors affecting riparian vegetation in the time interval between image and field data acquisition showed that the derivation of relationships between the data sets is still possible. However, one field plot that was sampled in 2008 was dropped from the analysis due to harvest in the plot in 2010.

3.2 Methods

The general workflow for data analysis was: (1) preprocessing of raw LiDAR data to create plot level metrics; (2) pre-processing of raw LiDAR data to create seven raster grids describing LiDAR height and density metrics which can be used for input into image segmentation; (3) pre-processing of 8-Band WV-2 image to prepare image for input into image segmentation; (4) segmentation of different image datasets; (5) evaluation of the use of different combinations of segmented images to predict both categorical (land cover classes) and

continuous (forest structure attributes) response variables; (7) mapping of riparian forest using best classification methods.

3.2.1 Image pre-processing

3.2.1.1 LiDAR

I conducted a preliminary exploratory analysis of relationships between metrics derived from the LiDAR first returns data and the field metrics to validate using a subset of the LiDAR metrics for the image segmentation and classification component of this project. Key stand structural attributes derived from field data were: maximum DBH, mean DBH, standard deviation (SD) of DBH, maximum basal area, mean basal area, SD basal area, plot basal area , stem density, and stem density of trees with DBH > 50cm (Table 4). Instead of using the metric of trees > 100 cm DBH as in Kane et al. (2010a), the metric of trees > 50 cm DBH was used because it applies to riparian forest size classes (WFPB 1997). Trees > 50 cm DBH are categorized in the large size class for riparian forest classification (WFPB 1997). The choice of field metrics was based on metrics that are commonly used to describe forest complexity and specifically riparian forest complexity (Spies and Franklin 1991; Naiman et al. 2005). The choice of LiDAR metrics used in this analysis was based on a literature review of LiDAR applications in forestry and then applied to the context of riparian forest. Lefsky et al. (2005a) found that a combination of three LiDAR metrics (mean height of LiDAR returns, SD of height of LiDAR returns, and canopy closure) closely correlate with field measurements of structural attributes. Each of the three LiDAR metrics relate to a different element of stand structure: 1) biomass (height measurement), 2) canopy structural complexity (variability in height), and 3) canopy gaps and leaf area index (LAI) (Lefsky et al. 2005a; Kane et al. 2010a; Kane et al. 2010b). In order to fully cover the three broad categories of LiDAR metrics described by Lefsky et al. (2005a), I used seven LiDAR metrics: maximum height, mean height, 95th percentile of height, SD height, CV of height, rumple (described below), and cover (Table 4). I included three LiDAR metrics representing

26

height (maximum height, mean height, and 95th percentile height) and three metrics of canopy structural complexity or variability in height (SD height, CV of height and rumple) to explore differences in performance of the metrics. All LiDAR metrics were extracted from the raw first-return point data using the LiDAR software FUSION (McGaughey 2012). The LiDAR data are projected in State Plane coordinate system with units in feet; however, all units are reported in metric units.

Table 4. Field and LiDAR metrics.

Field Metric	Description
DBH SD (cm)	Variation in size
DBH mean (cm)	Average size
DBH max (cm)	Maximum size
Plot Basal area (m^2/ha)	Size of trees adjusted for plot area
Stem density (trees/ha)	Density or cover
Density of trees DBH ≥ 50 cm (trees/ha)	Density of large trees with high riparian function
LiDAR Metric	**Description**
Height maximum (ft.)	Maximum height of first returns above the ground surface; The highest point in canopy, sensitive to outliers.
Height mean (ft.)	Mean height of first returns; An average height but is sensitive to outliers.
Height 95th Percentile	95th percentile height of first returns; Refers to the height where 95% of the LiDAR returns fall below. Metric is a representation of maximum heights and is less sensitive to outliers.
Height SD (ft.)	Standard deviation of first return heights; Sensitive to vertical variation in canopy structure.
Height CV	Coefficient of Variation first return heights; Sensitive to vertical variation in canopy structure relative to mean heights.
Cover	Canopy cover; Proportion of first returns greater than a lower height limit of 3.05m (10 ft.) above ground. Height limit is used to eliminate returns from herbaceous and shrub cover.
Rumple	The ratio of 3-D canopy surface model area to ground area. Sensitive to vertical and horizontal variation in canopy structure (Kane et al. 2010a).

I calculated the LiDAR metrics using first returns elevation data at the plot level for the 10 m x 60 m field plots and not at the individual tree level. I calculated all LiDAR metrics using the US Forest Service FUSION software package (McGaughey 2013).

I used the vendor-provided bare earth digital elevation model (DEM) tiles to produce a mosaicked digital terrain model (DTM) in FUSION. The DTM is then used as the ground surface for generating other LiDAR metrics from the first returns point data in FUSION. The output of this tool is a raster in GeoTiff format with pixel size of 1.83 m (6 ft.). Because I was interested in the height difference between the bare earth and the vegetation points, it was acceptable to use the vendor provided bare earth tiles to create a DTM rather than generating a bare earth model from the all returns point data. Previous studies have had success using the vendor provided DTM (Næsset 2004; Pascual et al. 2008).

I extracted the first returns LiDAR data points located within the associated field data plot from the raw LiDAR all returns las file provided from the vendor using FUSION.   I then calculated a full suite of LiDAR metrics from the clipped data using the CLOUDMETRICS tool (McGaughey 2013). I used CLOUDMETRICS to generate a csv table with all LiDAR metrics for each plot which I then used in the correlation analysis with the field data plots. A more detailed description of data processing in FUSION can be found in Appendix A.

In FUSION, canopy cover is defined as the percentage of returns (first returns or all returns) over a specified height threshold (McGaughey 2013). Overstory canopy cover is typically defined as any vegetation greater than the height break of 3 meters above ground. For example, if 21 LiDAR pulses enter the canopy and 16 first returns are recorded above the 3-m height threshold, then the LiDAR-based cover estimate would be computed as 76% (Figure 4). The Cover function in FUSION estimates canopy cover using a grid with output values form 0.0 to 100.0 percent. I calculated cover as the percentage of first returns above 3.05 m (10 ft.) out of the total number of first returns for each plot. A height threshold of 3.05 m was chosen because it eliminates understory vegetation typically encountered in the study area (McGaughey 2013).
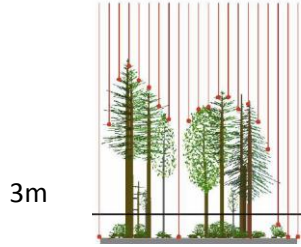
Figure 4. Example cover measurements in FUSION (McGaughey 2013).

The Rumple index is the ratio of 3-D canopy surface model area to ground area. It is a sum of 3-D area of triangles formed by canopy surface model grid points divided by the 2-D area of grid cell surface (Kane et al. 2010a). The Rumple index is another way to quantify canopy structural complexity and can qualify variation that might not be apparent when looking only at standard deviation (Figure 5). In both artificial canopy surface models in Figure 5, half of the points are at a height of 50 m and half are at 100 m (from Kane et al. 2010a). The higher the rumple index is the more heterogeneous the three-dimensional vertical and horizontal heterogeneity is. To calculate Rumple, I first generated canopy surface models (CSM) for each plot by subtracting the ground return elevations from the first return elevations. Rumple is then calculated by dividing the surface area of the CSM by the ground area.
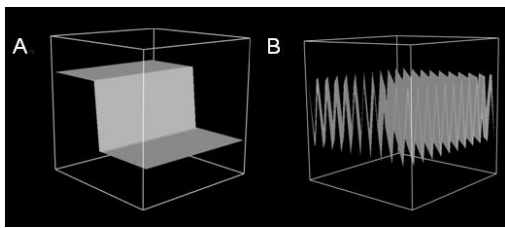
	Surface A	Surface B
Rumple	1.4	14.2
95% height	100	100
Mean height	75	75
SD height	25	25

Figure 5. Rumple example. Comparison of two artificial canopy surfaces with comparable descriptive height metrics but different rumple indexes (Kane et al. 2010a).
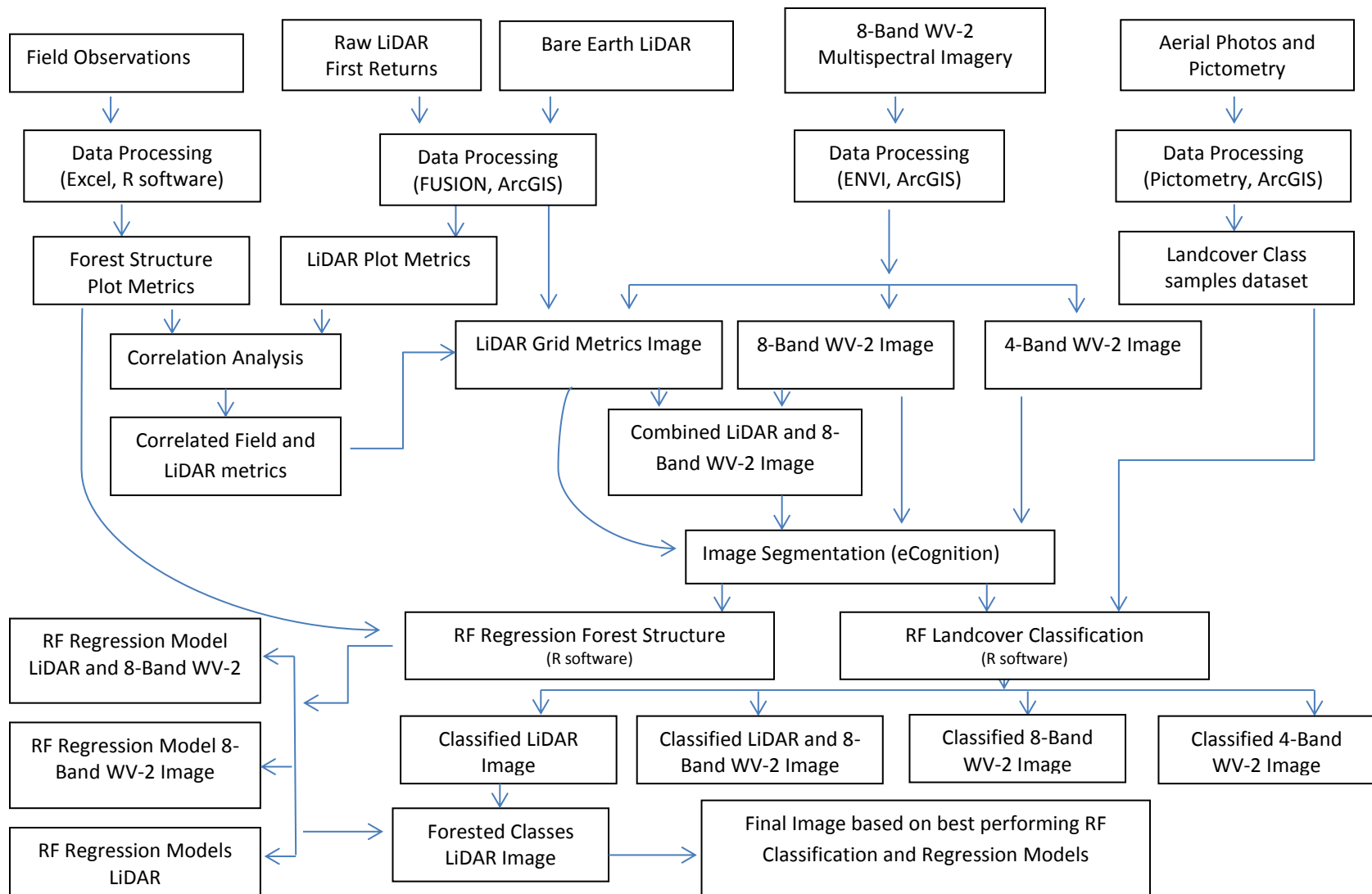
Figure 6. Data flow diagram describing the combination of field observations, LiDAR, Multispectral Imagery, and Aerial Photos used in data analysis.

All LiDAR metrics were calculated in FUSION (Figure 6). LiDAR and field metrics were compared using the Kendall's tau correlation coefficients. Kendall's tau correlation coefficient was chosen due to non-normality and heteroscedasticity within multiple variables. Kendall's correlation operates with ranks of the measurements for each variable.

For the following image segmentation and classification, I generated seven raster grids from the LiDAR first return elevation points in FUSION: Maximum Height, Mean Height, the 95th Percentile of Height, Standard Deviation Height, Coefficient of Variation of Height, Cover, and Rumple. A grid cell size of 3.66 m (12 ft.) was used to capture enough data points per grid (~10 points/grid cell) but still retain adequate detail to relate to field plots which were 10 m x 60-100 m. The raster grids were imported into ArcGIS for additional processing before importing into eCognition (Definiens 2010). ECognition is the software used for image segmentation described below. The grids were projected to the same coordinate system as the WorldView-2 Imagery (WGS 1984 UTM Zone 10). At the 3.66 m resolution there were still locations, primarily water, with no returns for the LiDAR data. I used a conditional equation in ArcGIS to interpolate data in the no-data locations for all seven grids because the summary statistics calculated in eCognition would not ignore the no-data values. Finally, I clipped the raster grids to correspond to the WorldView-2 image tiles, resulting in eight tiles for each of the raster grids. A detailed data flow diagram is included in Appendix A.

3.2.1.2 WorldView-2 pre-processing

The LiDAR went through multiple pre-processing steps as described in the previous section. The WorldView-2 image was provided by the Digital Globe as eight separate tiles. The WorldView-2 image underwent radiometric correction on the raw data by the vendor to reduce visible banding and streaking. The image also underwent orthorectification by the vendor. I pan-sharpened the 2-m resolution WorldView -2 multispectral bands with the 0.5 m resolution panchromatic band using the Gram-Schmidt method in ENVI (Figure 7). In order to evaluate the influence of additional four bands that the WV-2 image provided, I also examined the WV-2 image isolating the four conventional bands, Blue (2), Green (3), Red (5), and NIR-1 (7) (Table 2). This did not require any pre-processing or creating a separate image because the different image bands of the entire 8-Band WV-2 image can be included or excluded on a band by band basis in the image segmentation software. I refer to the 4-Band dataset as an image (4-Band WV-2 image) to make the comparisons between datasets simpler even though it is not technically a separate image.

Figure 7. WV-2 image pan-sharpening. From left to right: visible WV-2 bands 2-m resolution; Panchromatic WV-2 band, 0.5-m resolution; and Pan-sharpened visible WV-2 bands, 0.5-m resolution.

3.2.2 Image Segmentation

The imagery was classified using an object-based classification technique with the eCognition V 8.0 software (Definiens 2010). The objectives of the segmentation phase were to generate meaningful objects that would support: 1) delineation of landcover classes within the riparian zone, and 2) prediction of riparian forest structure metrics within field plots. Four sets of data were individually segmented: 1) the 4-Band WV-2 image including only the Blue, Green, Red, and

NIR-1 bands that correspond to the four conventional spectral bands of other high spatial resolution satellites such as IKONOS, 2) the 8-Band WV-2 image including the four conventional bands (Blue, Green, Red and NIR-1) plus the four additional bands (Coastal, Yellow, Red-Edge, and NIR-2), 3) LiDAR metrics alone, and 4) WV-2 image with all 8 bands and the LiDAR metrics. For predicting landcover classes I compared the use of four segmentation inputs: (1) 4-Band WV-2 Image, (2) 8-Band WV-2 Image, (3) LiDAR data metrics, and (4) 8-Band WV-2 Image combined with the LiDAR metrics data.   For predicting riparian forest structure metrics within field plots, I compared the use of three out of the four segmentation results: 1) WV-2 image all 8 bands, 2) the seven LiDAR grids alone, and 3) WV-2 image all eight bands with the seven LiDAR grids.

Within eCognition, there are multiple image segmentation algorithms. I used the multi-resolution segmentation process to generate meaningful objects from the four datasets. The image layers were first imported into eCognition, creating a layer stack of spectral bands and LiDAR metrics that can be used in the analysis. The LiDAR datasets were resampled, using nearest neighbor, to the 0.5-m pixel size of the pan-sharpened WV-2 imagery upon input into eCognition. I also added three shapefiles: 1) the WorldView-2 image boundary, 2) a 300 ft. riparian buffer, and 3) field plot boundaries. I used an image pre-processing step known as a chessboard segmentation that incorporated the WV-2 image boundary and the riparian buffer to constrain the subsequent multi-resolution segmentation for the landcover classification to the riparian zone and also eliminate issues associated with the image border. Once the analysis zone was isolated I ran the multi-resolution segmentation algorithm.

 I used all three shapefiles to constrain unit of observation for the subsequent regression analysis of the riparian forest structure variables to just the field plots. I did not run the multi-resolution segmentation on the field plots but instead exported the spectral and LiDAR metric statistics for each plot from eCognition to incorporate into the regression analysis of riparian forest structure statistics with the field plots. I then applied the model results of RF regression analysis to the objects from the above mentioned segmentation process that were developed for the entire study

area. . The segmentation divides an image into multi-pixel objects based on similarities in user-defined parameters affecting size, spectral homogeneity, spatial homogeneity, and shape of output objects (Chubey et al. 2006). The input parameters for the segmentation algorithm consist of the scale parameter, the shape parameter and the compactness parameter. The scale parameter creates a threshold of how much heterogeneity is retained in an object based on the spectral and/or LiDAR metric inputs but is not prescriptive of size of an object. However, a larger scale parameter value allows greater variance within objects, which usually creates larger objects. To find the appropriate object size, I examined different scale parameters, ranging from 15 to 300, as inputs to the multi-resolution segmentation algorithm. Both the shape and compactness parameters range from 0 to 1. For all segmentations algorithms I used a shape parameter of 0.3 and a compactness parameter of 0.5 after trying a suite of values. If the shape parameter is too high, the spectral information and/or LiDAR metric information will be ignored. Specific weights can be assigned to different bands as part of the segmentation settings. I assigned all bands a weight of 1, except the NIR-1 band, which was weighted as 2. The NIR portion of the EM spectrum is closely associated with the ability to discriminate changes in vegetation (Campbell and Wynne 2011). I only weighted the NIR-1 band in order to compare the results between the full 8-Band WV-2 image and the segmentation limited to the 4-Band WV-2 image. I weighted the NIR-1 band as 2 is in the 4-Band WV-2, 8-Band WV-2, and the combined LiDAR and 8-Band WV-2 image segmentation processes. I segmented the image in the eight tiles that corresponded to the image tiles provided by the vendor due to computer processing limitations when attempting to segment the entire image (20,216 x 20,216 pixels = 102 km^2). The results were mosaicked together into one image after all segmentation processing was complete.

I calculated summary statistics for each image object and each input band or metric in eCognition (Table 5). The number of metrics ranged from 12 for the 4-Band WV-2 Image to 29 for the combined LiDAR and WorldView-2 Image Analysis. For each input band or layer, the mean and standard deviation of the pixel values (spectral data and/or LiDAR metrics) within each object was exported. Mean of the band or layer refers to the mean value of all pixels within an object (e.g.,

Mean RED is the mean value of the red band of all pixels within an object.). The standard deviation features were also derived from the analysis of all pixels included in each object. The standard deviation serves as an estimation of the level of variability within each object. The mean brightness index for each object was also exported. The brightness index calculates the mean intensity value of all spectral bands within the object. To examine object size and shape, I exported the object area, object length/width ratio, and compactness. Compactness for each object is calculated as the product of the length and the width, divided by the number of pixels in the object. The export output for each tile is a raster tif and an associated csv file that contain the specified object statistics. These two files are the inputs for the image classification (described below). I also exported a shapefile of object boundaries to examine in ArcMap.

To export the metrics isolated to the field plots, I exported the spectral band metrics and/or LiDAR metrics but restricted them to the boundaries of the field plots. The output was a csv file with the unique plot id identifying the data that I combined with the field metrics associated for each plot. This product is the input for the following Random Forest Regression analysis.

Table 5. Object statistics calculated for each object based on the segmentation inputs. See text for description of each metric.

Metric Number	Metrics	Metrics from WV-2 - 8 Bands	Metrics from WV-2 - 4 Bands	Metrics from WV-2 and LiDAR	Metrics from LiDAR
1	Mean Band 1	x		x	
2	Mean Band 2	x	x	x	
3	Mean Band 3	x	x	x	
4	Mean Band 4	x		x	
5	Mean Band 5	x	x	x	
6	Mean Band 6	x		x	
7	Mean Band 7	x	x	x	
8	Mean Band 8	x		x	
9	SD Band 1	x		x	
10	SD Band 2	x	x	x	
11	SD Band 3	x	x	x	
12	SD Band 4	x		x	
13	SD Band 5	x	x	x	
14	SD Band 6	x		x	
15	SD Band 7	x	x	x	
16	SD Band 8	x		x	
17	Area	x	x	x	x
18	Length/Width	x	x	x	x
19	Compactness	x	x	x	x
20	Brightness Index	x	x	x	
21	Mean Max Height			x	x
22	Mean Mean Height			x	x
23	Mean 95th % Height			x	x
24	Mean Cover			x	x
25	Mean Rumple			x	x
26	SD Max Height			x	x
27	SD Mean Height			x	x
28	SD 95th Height			x	x
29	SD Cover			x	x

3.2.3 Image Classification

After image segmentation, I classified image objects, using multi-spectral and/or LiDAR derived information (Table 5), into the following landcover types: Water, Gravel bar, Pasture,

Developed, Deciduous, Conifer, and Roads. In order to classify the image I mosaicked the eight

eCognition output rasters into one image. I also merged the eight original csv outputs into one csv

that corresponded with the mosaicked raster. The final merged csv and mosaicked raster are the

inputs for the classification process.

Prior to image segmentation, I generated a dataset of training and testing data that represented

the seven different landcover types used in the image classification. The primary goal of the

landcover classification was to distinguish between conifer and deciduous riparian trees. The five

additional classes represent broad non-forested landcover types found in the riparian buffer. I used a

combination of Pictometry imagery from 2008 and 2010, 2006 NAIP imagery, and the WV-2 image

to digitize the training and testing data within the riparian buffer. I identified a minimum of 100

samples for each class with the exception of the "developed" class which consisted mostly of man-

made structures in the riparian zone (Table 6). It was difficult to identify additional "developed"

training points because the proportion of developed structures in the study area is minimal compared

to the other landcover classes. The training and testing points were stored in a shapefile with the

associated Class ID in the attribute table.

Table 6. Distribution of training and testing data among landcover classes.

Number of Classes	Class	Number of samples in each class
1	Water	152
2	Gravel Bar	102
3	Pasture	199
4	Developed	42
5	Deciduous	227
6	Conifer	230
7	Road	109

I used the Random Forests (RF) algorithm (Breiman 2001) to both classify the landcover

types and predict forest structure metrics in the field plots. RF operates similarly to classification and

regression trees (CART) (Hudak et al. 2008). RF can operate as a classification algorithm and a

regression algorithm depending on the response variable being categorical or continuous (Breiman 2001). It is referred to as RF classification when the response variable is categorical. When the response variable is continuous the algorithm is referred to as RF regression. The RF algorithm randomly subsets the training data to estimate a large number of classification trees. The trees are split based on a random subset of the predictor variables (Breiman 2001; Martinuzzi et al. 2009). After running the iterations, (100s to >1000s), the predictions are combined using a rule of majority votes (Martinuzzi et al. 2009). By generating multiple trees compared to a single classification tree, the RF algorithm typically achieves higher accuracies (Breiman 2001). Another advantage to the RF algorithm is that it is nonparametric making it unaffected by distributional assumptions (Breiman 2001; Cutler et al. 2007). Two main metrics of error are output from the model that differs slightly depending on the RF algorithm operating via classification or regression. For RF classification, the Out of Bag error estimate (OOB) is an overall error measure describing the proportion of times the result is not accurate over all samples (Breiman 2001; Horning 2011). For classification, a confusion matrix is also generated describing the class error. For regression, the "percent variance explained" is given which is also referred to as a pseudo R-squared value (Horning 2011). For both RF classification and RF regression an estimate of variable importance is given indicating the amount of influence that one variable has over another. In RF classification it is referred to as the Mean Decrease in Gini (MSG) or the Gini index and in RF regression it is referred to as Percent Increase in Mean Squared Error (MSE; Breiman 2001; Cutler et al. 2007; Hudak et al. 2008). The Gini index is described by Hudak et al. (2008) as,

> "a measure of node impurity, or the degree to which a variable produces terminal nodes in the forest of classification trees. Splitting a node on a variable causes the Gini index for the two descendant nodes to be less than the parent node. Summing these decreases in the Gini index for a variable across the forest of classification trees provides a measure of variable importance (Breiman et al. 2001)."

For RF regression the Percent Increase in MSE is measured by the degree to which the inclusion of a variable decreases the mean squared error (Liaw & Wiener 2002). I used the RF package (Breiman et al. 2012) in R (www.r-project.org; R Development Core Team 2013) to run the

RF regression algorithm to predict riparian forest structure. The RF regression analysis builds a predictive model using the spectral and/or LiDAR metrics as the predictor variables and the field measured riparian forest structure metrics as the response variables. The predictive model is then applied to the image objects classified by the RF classification algorithm as conifer and deciduous to create a predicted map of riparian forest structure. I ran the analysis separately for each of the six field-measured riparian forest structure metrics but with all of the predictor variables included in each run. I then generated a final map of riparian forest condition based on the classification and regression predictions to be used for restoration and conservation prioritization.

4.0 Results

4.1 Field Summary

The majority of trees in the field plots were in the smallest size class, between 10 cm and 30 cm (Table 7). The most common tree species were red alder, followed by western hemlock (*Tsuga heterophylla*), western red cedar, and Douglas fir (*Pseudotsuga menziesii*) (Figure 8). Additional species located in the field plots were: big leaf maple, cascara (*Rhamnus purshiana*), paper birch (*Betula papyrifera*), vine maple (*Acer circinatum*), and willow species (*Salix spp.*). Western red cedar had the greatest basal area overall, followed closely by red alder and Douglas fir (Figure 9). The average DBH of trees was 29.86 cm for all sites and 30.59 cm for the WV-2 sites. The field plots exhibited a range of riparian vegetation (Figure 10). A summary of all field plots and associated LiDAR metrics is included in Appendix B.

Table 7. Summary statistics for live trees in all field plots. Deciduous dominated: >70 percent deciduous species; Conifer dominated: >70 percent conifer dominated species; Mixed: neither deciduous or conifer dominated**.**

Variable	Conifer dominated LiDAR (n=17)	Deciduous dominated LiDAR (n=21)	Mixed LiDAR (n=25)	All LiDAR sites (n=63)	All WV-2 sites (n =22)
Minimum DBH (cm)	10.00	10.00	10.00	10.00	10.00
Maximum DBH (cm)	116.40	141.00	213.50	213.50	153.20
SD DBH (cm)	17.38	17.17	20.88	19.11	19.67
Average DBH (cm)	32.00	25.46	30.99	29.86	30.59
Average basal area (m^2/ha)	62.73	33.92	54.06	49.69	49.53
Stem density (trees/ha)	540.09	406.51	502.24	482.93	491.95
Stem density $10 \leq DBH < 30$ cm (trees/ha)	283.77	299.96	306.12	298.12	289.38
Stem density $30 \leq DBH < 50$ cm (trees/ha)	181.05	71.63	134.51	127.73	140.00
Stem density DBH $\geq$ 50 cm (trees/ha)	75.27	34.92	61.62	57.08	61.63
Total stem count (# trees)	531	454	758	1743	733
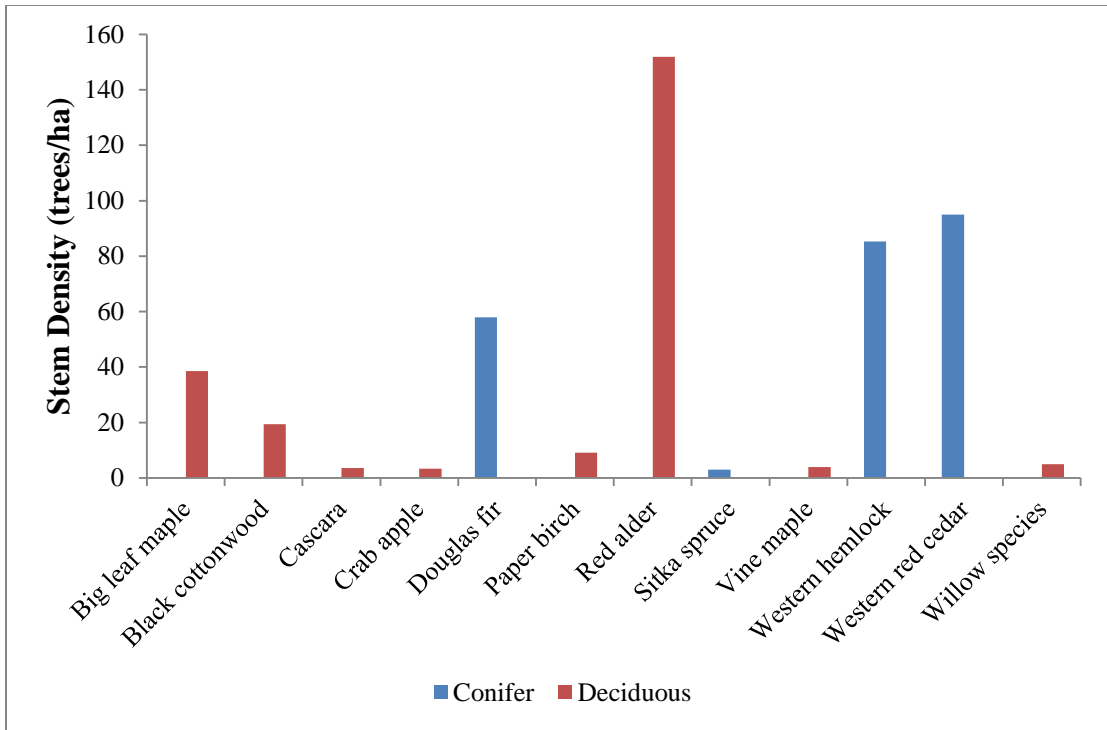
Figure 8. Stem density of live trees for all 63 LiDAR field plots by tree species for major species. Major species had greater than 10 individuals counted in all plots.
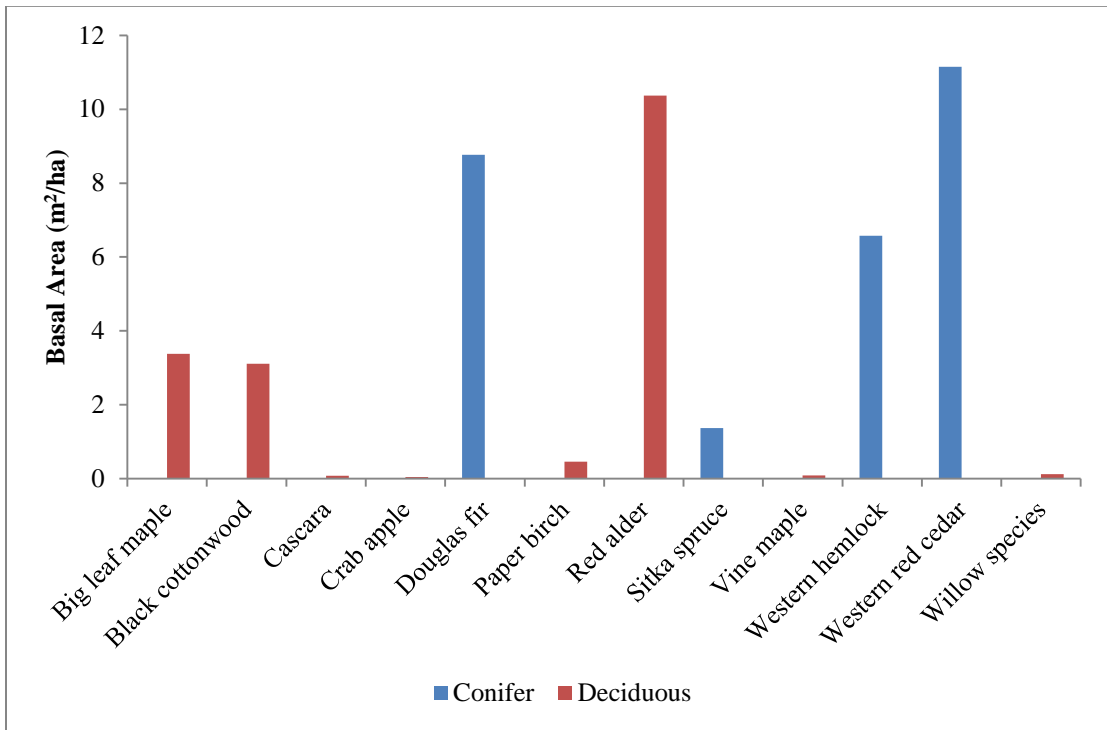
Figure 9. Total basal area (m^2/ha) of live trees for all 63 LiDAR field plots by tree species for major species. Major species had greater than 10 individuals counted in all plots.
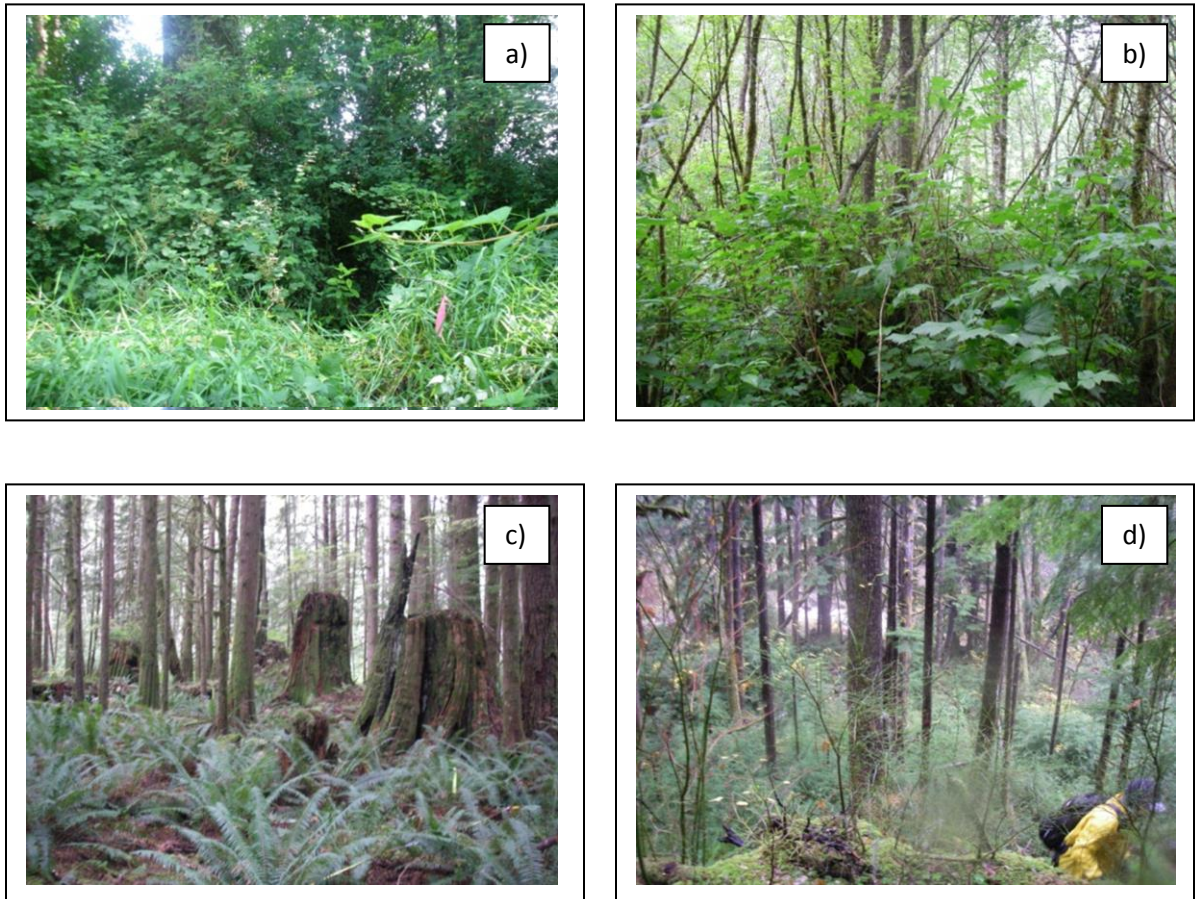
Figure 10. Examples of field plots: a) narrow buffer dominated by reed canary grass, alder and cottonwood (Plot #58); b) young alder dominated (Plot #42); c) second growth cedar and hemlock dominated (Plot #29); d) second growth hemlock dominated with regenerating hemlock understory (Plot #22).

4.2 Correlations between LiDAR and field based forest metrics

There was a significant correlation between most field and LiDAR metrics (Table 8). The LiDAR height metrics, with the exception of CV of height, were correlated with field metrics for size, DBH and Basal area. The LiDAR height metrics were not correlated with Stem density of all trees but were correlated with Stem density of trees ≥ 50 cm DBH. Mean height had lower correlation coefficients for most field metrics but had the highest overall correlation coefficient with Basal area, tau = 0.48. SD height and Rumple correlated with all six field metrics. SD height had the strongest correlation with SD DBH and SD Basal area. Rumple also had the highest correlation mean DBH

followed by Stem density trees $\geq$ 50 cm, tau = 0.34 and tau = 0.31 respectively. Rumple was negatively correlated with Stem density, tau = -0.21. Cover and CV of height did not correlate with the three DBH metrics but did correlate with Basal area. CV of height negatively correlated with Basal area plot and Stem density. Conversely cover was positively correlated with Basal area plot and Stem density.

Field metric SD DBH was strongly correlated with Maximum height, tau = 0.39, 95th percentile height, tau = 0.42, and SD height, tau = 0.35 (Table 8). Mean DBH was correlated with Maximum height, tau = 0.42, and 95th percentile height, tau = 0.43. Maximum DBH had the strongest correlation with Maximum height, tau = 0.45, followed by 95th Percentile Height, tau = 0.40. Basal area had the strongest correlation with Mean height, closely followed by 95th Percentile height, and then maximum height. Stem density was negatively correlated with SD height, CV height, and Rumple but positively correlated with Cover. Stem density of trees $\geq$ 50 cm had the strongest correlation with Maximum height closely followed by the 95th percentile height, tau = 0.41 and tau = 0.39 respectively. Stem density of trees $\geq$ 50 cm DBH was also correlated with Maximum height, Mean height, SD height and Rumple but not with cover.

Table 8. Kendall's tau values for correlations of LiDAR metrics with field metrics. Significant correlations only, $p \leq 0.05$. (n=63). *p<0.05, **p≤0.001.

Field Metrics	LiDAR Metrics						
	Maximum Height (ft.)	Mean Height (ft.)	SD[1] Height (ft.)	CV[2] Height	95th Percentile Height	Cover (%)	Rumple
SD DBH (cm)	0.39**	0.19*	0.35**		0.36**		0.28**
Mean DBH (cm)	0.42**	0.32**	0.33**		0.43**		0.34**
Maximum DBH (cm)	0.45**	0.28**	0.28**		0.40**		0.23**
Basal Area Plot (m²/ha)	0.44**	0.48**	0.18*	-0.24*	0.47**	0.28**	0.20*
Stem Density (trees/ha)			-0.30**	-0.38**		0.38**	-0.21*
Stem Density DBH ≥ 50cm (trees/ha)	0.41**	0.27*	0.27*		0.39**		0.31**

[1]SD: Standard deviation
[2]CV: Coefficient of Variation

4.3 Image Segmentation

In order to compare the four datasets I used the same segmentation settings. However, the

LiDAR objects were typically larger than the spectral image objects (Table 9). For the subsequent

Random Forest classification and regressions, I used a scale setting of 50 for all image combinations

because the setting segmented the image into objects that in general were not too large to misclassify

the classes of interest and were too small to generate too much heterogeneity within the objects. For

example the higher scale settings created objects that spanned the channel and the forest for the

LiDAR only image in more frequent places than the 50 scale setting (Figure 11). The Scale settings of

100 and 150 segmented the 8-Band WV-2 image and the combined LiDAR and 8-Band WV-2 Image

well but created objects in the LiDAR only image that were too coarse to capture the landcover

classes. Note the 4-Band WV-2 image is not included in Figure 11 but a scale of 50 was also used to

segment this image.

Table 9. Summary statistics for image objects derived using a 50 scale setting.

Object Information	LiDAR only Image	LiDAR and 8-Band WV-2 Image	8-Band WV-2 Image	4-Band WV-2 Image
# Objects	41,596	124,109	170,461	179,610
Minimum Area (m^2)	1.75	1.50	0.25	1.00
Maximum Area (m^2)	12,643.25	4,344.75	5,476.75	4,856.25
Mean Area (m^2)	413.95	138.71	100.99	95.84
Median Area (m^2)	287.50	115.75	80.75	75.50
SD Area (m^2)	497.34	116.89	93.06	89.95
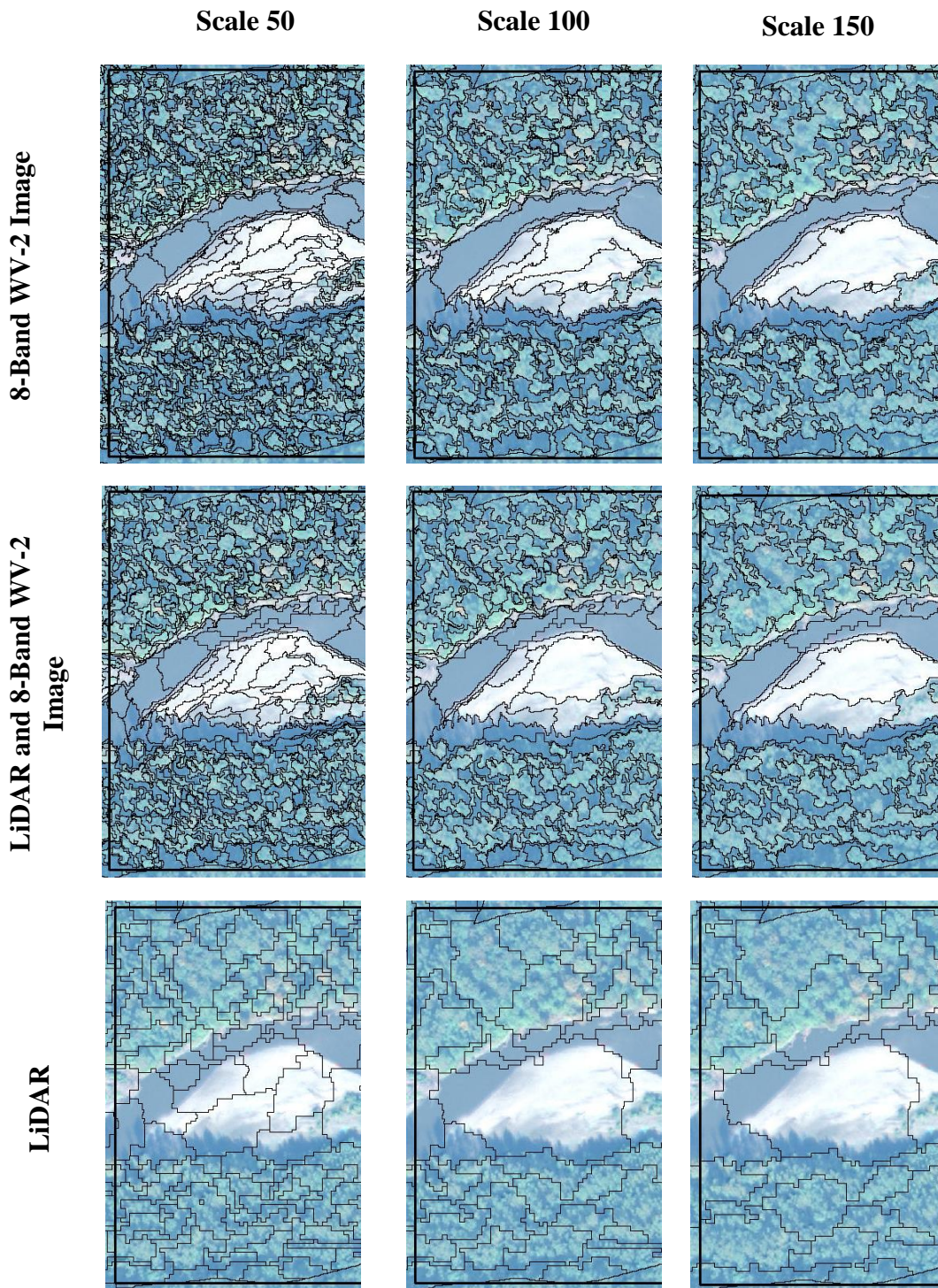
Figure 11. Example of the output of the multi-resolution segmentation with varying scale parameters for the three combinations of data. Shape parameter, 0.3 and compactness parameter, 0.5 for all combinations.

4.4 Random Forest Classification

The RF classification for the 8-band WV-2 image resulted in an overall classification accuracy of 82% compared with overall classification accuracy of 79% for the 4-band WV-2 image (Table 10, Table 11). Classifying using just the LiDAR image resulted in an overall classification accuracy of 74% (Table 12). The combined LiDAR and 8-band WV-2 image increased the overall classification accuracy to 88% (Table 13). The 8-band WV-2 RF classification had the highest Producer's accuracy for Water, followed by Pasture, and then Gravel bar (Table 10). The Developed class had the lowest Producer's and User's accuracy for all four classification processes and was confused primarily with roads. Roads were most often confused with classes Gravel bar and Conifer. Conifer and Deciduous exhibited the most confusion between the two classes. The conifer class had a slightly higher User's accuracy, 75%, compared with 70% for the Deciduous class as classified from the 8-Band WV-2 image. The 4-Band WV-2 image accuracies were lower for most classes compared to the 8-band WV-2 image with the exception of the User's accuracies for the Pasture and Developed classes and the Producer's accuracies for the Gravel bar, Pasture, and Developed classes. The LiDAR only image class error decreased for Deciduous and Conifer when combined with the 8-band WV-2 image from 20% and 2% to 16% and 18% respectively (Table 10, Table 13). Overall, the combined LiDAR and 8-Band WV-2 image was the most useful for classifying all classes. However, the spectral imagery had the most influence on classifying the Water, Gravel bar, and Pasture classes based on the high class accuracies for the 4-Band WV-2 image and the 8-Band WV-2 image compared with the low class accuracies for the LiDAR only image. However, the LiDAR only image was the most useful for classifying the Developed and almost as accurate as the combined LiDAR and 8-Band WV-2 image at classifying the forested classes, Deciduous and Conifer.

Table 10. Random forest classification results confusion matrix for 8-band WV-2 image.

		Reference Data									
		Water	Gravel Bar	Pasture	Developed	Deciduous	Conifer	Roads	Total	Class Error	Users Accuracy
Classified Data	Water	150	0	0	0	1	1	0	152	1.32%	98.68%
	Gravel Bar	1	95	0	0	0	0	6	102	6.86%	93.14%
	Pasture	0	0	187	1	5	2	3	198	5.56%	94.44%
	Developed	0	1	0	17	0	1	22	41	58.54%	41.46%
	Deciduous	0	0	4	0	159	62	2	227	29.96%	70.04%
	Conifer	1	0	1	0	55	171	1	229	25.33%	74.67%
	Roads	1	7	1	3	2	5	90	109	17.43%	82.57%
	Total	153	103	193	21	222	242	124	1058	**Overall Accuracy:**	
	Producer's Accuracy	98.04%	92.23%	96.89%	80.95%	71.62%	70.66%	72.58%		**82.14%**	

Table 11. Random forest classification results confusion matrix for 4-band WV-2 image.

		Water	Gravel Bar	Pasture	Developed	Deciduous	Conifer	Roads	Total	Class Error	Users Accuracy
					Reference Data						
Classified Data	Water	148	0	0	1	1	2	0	152	3.00%	97.37%
	Gravel Bar	0	94	0	0	0	0	8	102	8.00%	92.16%
	Pasture	0	0	189	1	4	1	3	198	5.00%	95.45%
	Developed	2	3	1	20	2	0	13	41	51.00%	48.78%
	Deciduous	0	0	1	0	144	82	0	227	37.00%	63.44%
	Conifer	1	0	0	1	71	153	3	229	33.00%	66.81%
	Roads	3	4	2	5	2	6	87	109	20.00%	79.82%
	Total	154	101	193	28	224	244	114	1058	**Overall Accuracy:**	
	Producer's Accuracy	96.10%	93.07%	97.93%	71.43%	64.29%	62.70%	76.32%		**78.92%**	

Table 12. Random forest classification results confusion matrix for LiDAR only image.

		Water	Gravel Bar	Pasture	Developed	Deciduous	Conifer	Roads	Total	Class Error	Users Accuracy
						Reference Data					
Classified Data	Water	89	16	20	0	7	2	10	144	38.19%	61.81%
	Gravel Bar	19	63	19	0	2	0	7	110	42.73%	57.27%
	Pasture	18	12	159	1	2	0	8	200	20.50%	79.50%
	Developed	0	0	1	33	5	1	1	41	19.51%	80.49%
	Deciduous	0	1	0	2	182	41	1	227	19.82%	80.18%
	Conifer	1	1	0	1	42	183	1	229	20.09%	79.91%
	Roads	3	4	16	5	3	3	73	107	31.78%	68.22%
	Total	130	97	215	42	243	230	101	1058	**Overall Accuracy:**	
	Producer's Accuracy	68.46%	64.95%	73.95%	78.57%	74.90%	79.57%	72.28%		**73.91%**	

Table 13. Random forest classification results confusion matrix for the combined LiDAR and 8-Band WV-2 Image.

Reference Data

	Water	Gravel Bar	Pasture	Developed	Deciduous	Conifer	Roads	Total	Class Error	Users Accuracy
Water	149	0	0	0	0	0	3	152	1.97%	98.03%
Gravel Bar	0	92	0	0	0	0	10	102	9.80%	90.20%
Pasture	0	1	191	1	1	0	4	198	3.54%	96.46%
Developed	2	0	1	31	1	2	4	41	24.39%	75.61%
Deciduous	0	0	0	0	191	36	0	227	15.86%	84.14%
Conifer	1	0	0	0	40	188	0	229	17.90%	82.10%
Roads	4	5	0	3	3	0	94	109	13.76%	86.24%
Total	156	98	192	35	236	226	115	1058	**Overall Accuracy:**	
Producer's Accuracy	95.51%	93.88%	99.48%	88.57%	80.93%	83.19%	81.74%		**88.47%**	

Classified Data

For each of the three image classifications that incorporated spectral information, the NIR-1 band was one of the three most important variables. For the 8-band WV-2 image, the three variables of most importance were: 1) Mean NIR-1, 2) Mean NIR-2, and 3) Mean Red Edge (Figure 12). For the 4-band WV-2 image, the three variables of most importance were: 1) Mean NIR-1, 2) Mean Blue, and 3) Mean Brightness Index (Figure 13). For the LiDAR only image, the three variables of most importance were: 1) Mean Max Height, 2) Mean Mean Height, and 3) Mean 95th percentile height (Figure 14). For the combined LiDAR and 8-band WV-2 image the three variables of most importance were: 1) Mean NIR-1, 2) Mean Max Height, and 3) Mean NIR-2 (Figure 15). The combined LiDAR and 8-Band WV-2 image maintained two of the top predictors for each image as the top predictor variables in the RF classification. Object area, compactness, and length to width ratio had minimal influence on landcover classification in all four classifications.
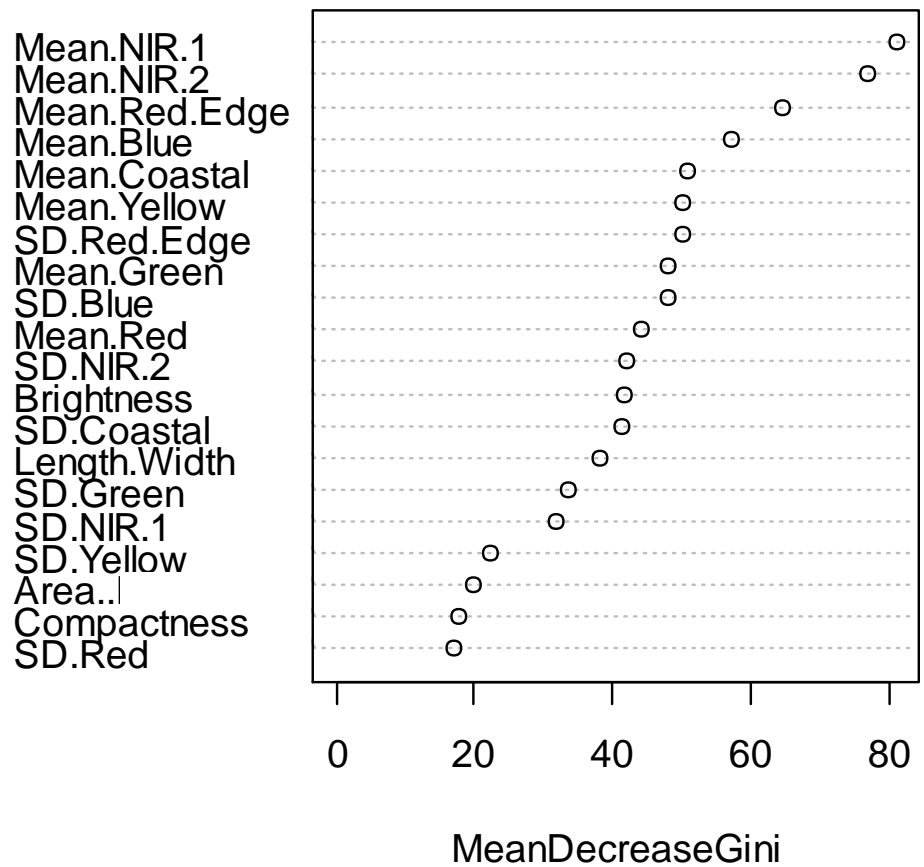
Figure 12. Variable importance plot represented by the Mean Decrease Gini values for the 8-band WV-2 image RF classification.
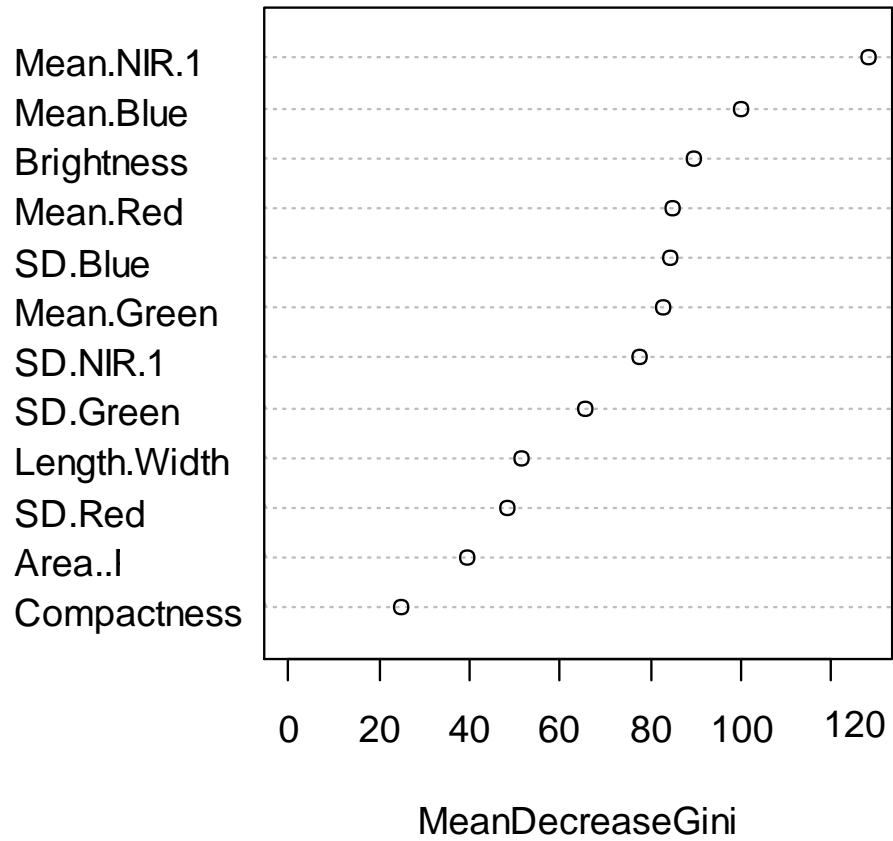
Figure 13. Variable importance plot represented by the Mean Decrease Gini values for 4-band WV-2 image RF classification.
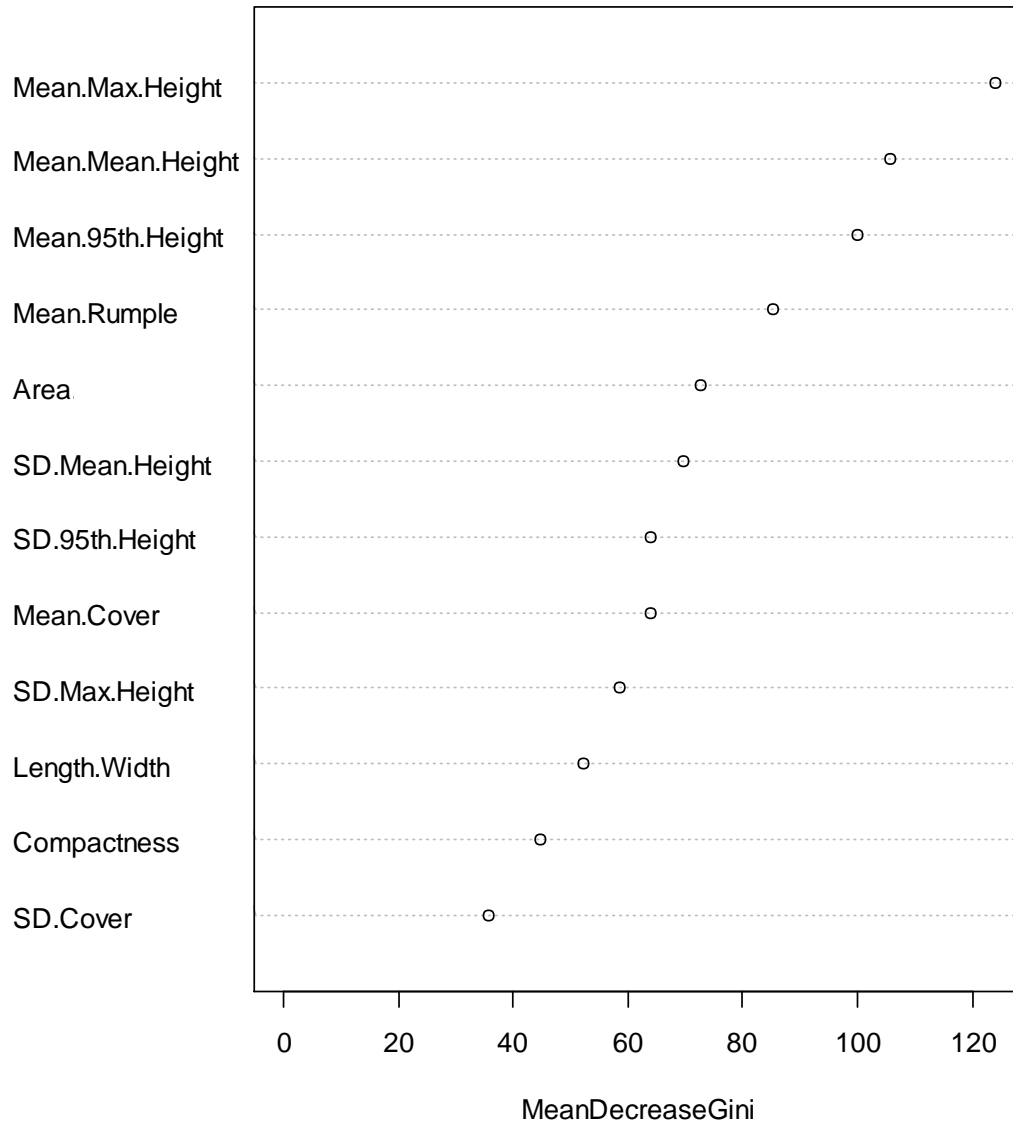
Figure 14. Variable importance plot represented by the Mean Decrease Gini values for LiDAR only image RF classification.
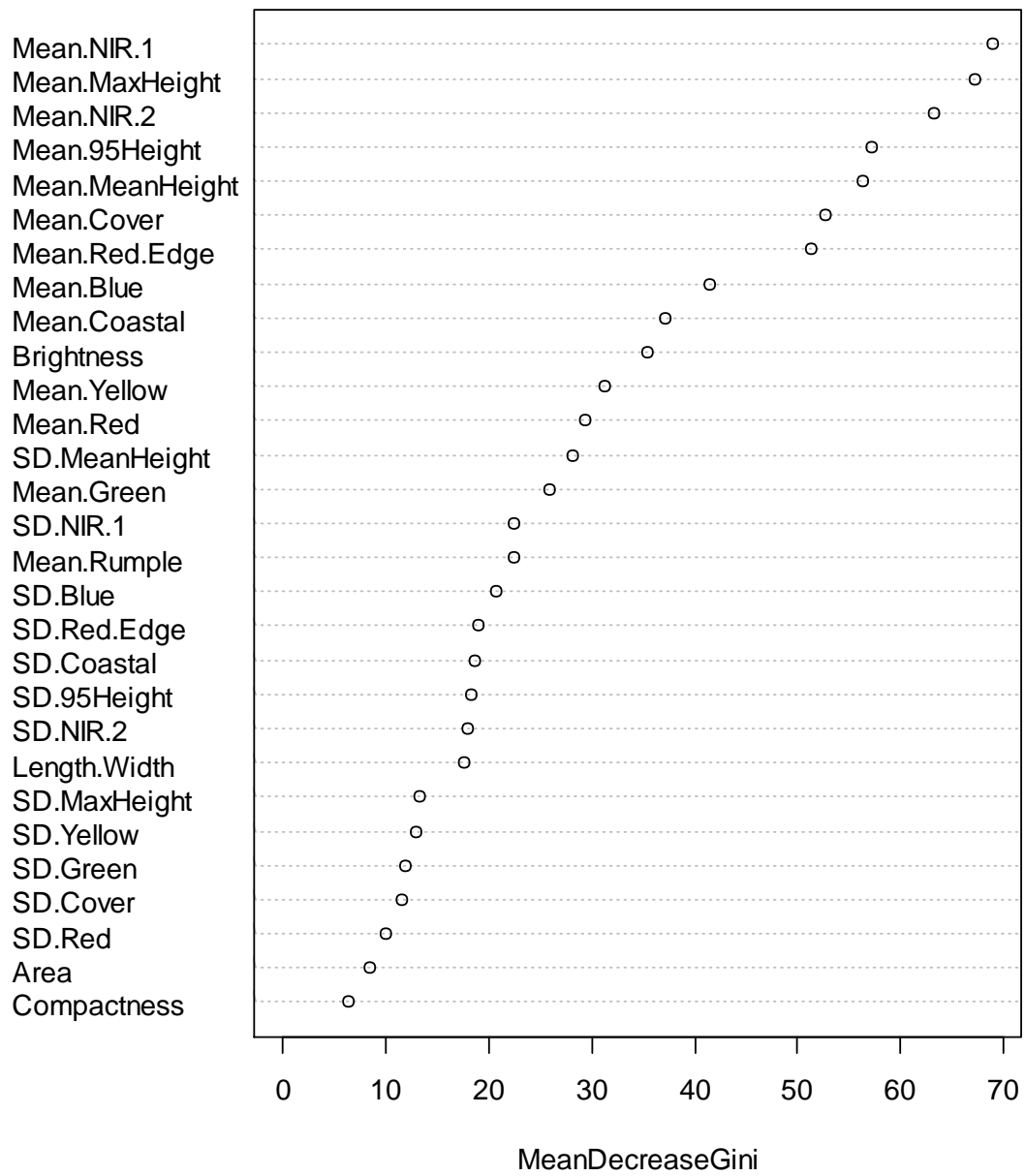
Figure 15. Variable importance plot represented by the Mean Decrease Gini values for combined LiDAR and 8-band WV-2 image RF classification.

A mapped classification from the entire 8-Band WV-2 image is shown in Figure 16 with subsets for two zones illustrating all four classifications. In Zone 1, the road was misclassified as water in all three datasets that contained spectral data, the 4-Band WV-2 image, 8-band WV-2 image and combined LiDAR and 8-Band WV-2 image (Figure 16). In Zone 2 the gravel bar was misclassified as road for the same three datasets. The classified 4-band WV-2 image shown in Zone 2 contains larger patches of the conifer class compared to the other three datasets. The classification of the LiDAR only dataset contains fewer small classifications of both the conifer and deciduous classes compared to the other three datasets. In Zone 1 the 8-band WV-2 image and the combined LiDAR and 8-band WV-2 image incorrectly identified pasture on the gravel bar which was not apparent in either the 4-Band WV-2 image or the LiDAR only image.
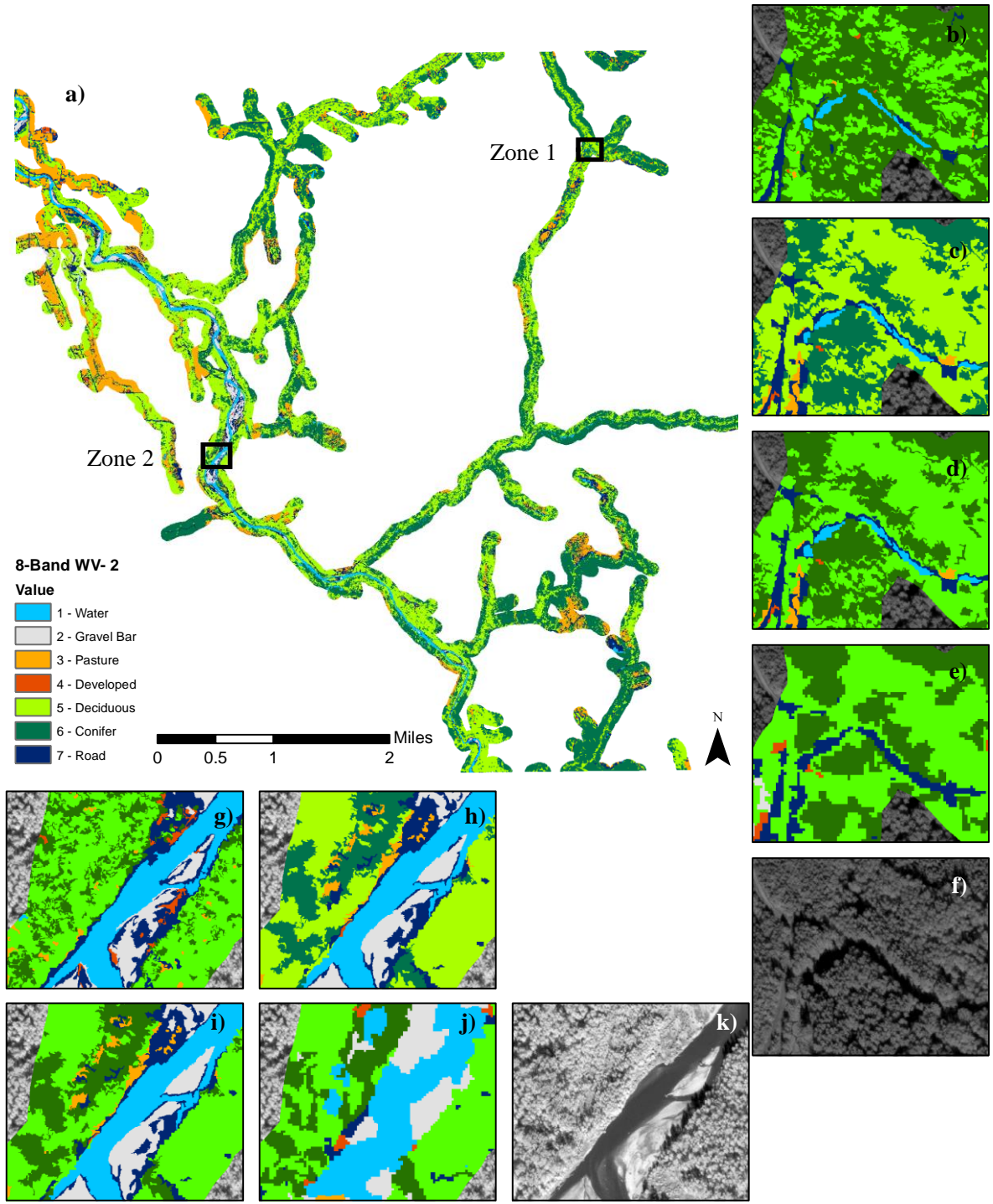
Figure 16. a) Random forest classification map for 8-Band WV-2 image showing full classification area. For Zones 1 and 2: b. and g.) 4-Band WV-2 Classification, c. and h.) 8-Band WV-2 Classification, d. and i.) LiDAR and 8-Band WV-2 Classification, e. and j.) LiDAR Only Classification, f. and k.) Panchromatic Image.

4.5 Random Forest Regression

The LiDAR metrics alone described the largest amount of variance out of the three datasets (Table 13). For SD DBH, Max DBH, and Basal Area, the LiDAR only dataset explained greater than 50% of the variance. For the response variables Mean DBH and Stem Density DBH >50cm, the LiDAR dataset explained less than 50% of the variance, 46 % and 40 % respectively. The RF regression analysis for the LiDAR metrics explained the most variance for the response variable SD DBH, 64% (Table 14). SD 95th percentile height, SD of Mean height, and SD of Max height were the best predictors of SD DBH (Table 15, Figure 17). SD Max Height and SD 95th % Height were the best predictors of Max DBH (Table 15, Figure 18). The top three predictor variables for Basal Area for the LiDAR only image were all mean statistics, specifically, Mean 95th percentile height, Mean Max Height, and Mean Mean Height (Table 15, Figure 19). For the LiDAR only image, SD 95th percentile height, SD Mean Height, and SD Max Height were the top overall predictors for all response variables (Table 15). The top three predictor variables for the combined LiDAR and 8-Band WV-2 image dataset were SD Mean Height, SD Max Height, and Mean 95th % Height (Table 16). The top three predictor variables for Basal Area and SD DBH were the same for both the LiDAR only and the 8-Band WV-2 image dataset and were all LiDAR metrics. This was similar to Max DBH but the order was different with SD Max Height as the top predictor for the LiDAR only dataset and SD 95th % Height as the top predictor for the combined LiDAR and 8-Band WV-2 image dataset. Plots of predicted values by the LiDAR only image compared with the observed response variables are shown in Figure 20.

The 8-Band WV-2 image alone was a poor fit for all riparian forest structure response variables (Table 14). All values for percent variance explained were negative indicating no significant relationship (Horning 2011). Only the percent variance explained is reported for this dataset because the variables of importance do not explain any of the variance to provide meaningful results. The percent variance in the riparian forest structure variables explained by the 8-Band WV-2 and LiDAR image was considerably higher compared with the 8-Band WV-2 alone (Table 14).

However, the top three predictors were still all LiDAR metrics, with the exception of the variable Stem density which contained SD Coastal band as a top predictor (Table 16). The model for Stem density was poor for all three datasets as indicated by the negative values % variance explained for the 8-Band WV-2 and the combined LiDAR and 8-Band WV-2 datasets and the low value, 6%, for the LiDAR only datasets. While the LiDAR only dataset performed the best, the combined LiDAR and 8-Band WV-2 dataset explained over 50 % of the variance for SD DBH, 57%, and close to 50 % for Max DBH, 47%.

Table 14. Percent variance explained by the RF regression models for the 8-Band WV-2 image, the LiDAR only image, and the combined LiDAR and 8-Band WV-2 image (n=22).

	Percent Variance Explained		
	8 Band WV-2	LiDAR	8 Band WV-2 and LiDAR
Mean DBH	-15.8	45.87	33.23
SD DBH	-14.94	64.41	56.61
Max DBH	-5.91	55.44	47.37
Basal Area	-17.42	57.05	33.65
Stem Density	-28.31	6.11	-3.57
Stem Density DBH >50 cm	-53.26	40.31	12.42

Table 15. Top three predictor variables of the field based riparian forest structure metrics from the RF regression models developed for the LiDAR only image as described by %Increase Mean Square Error (MSE).

Forest Structure Variable	RF Predictor 1	RF Predictor 2	RF Predictor 3
Mean DBH	Mean 95th % Height	Mean Max Height	SD 95th % Height
SD DBH	SD 95th % Height	SD Max Height	SD Mean Height
Max DBH	SD Max Height	SD 95th % Height	SD Mean Height
Basal area	Mean 95th % Height	Mean Max Height	Mean Mean Height
Stem density	SD Mean Height	SD Max Height	SD 95th % Height
Stem density trees > 50 cm DBH	Mean Rumple	Mean Max Height	SD Mean Height

Table 16. Top three predictor variables of the field based riparian forest structure metrics from the RF regression models developed for the combined LiDAR and 8-Band WV-2 image as described by %Increase Mean Square Error (MSE).

Forest Structure Variable	RF Predictor 1	RF Predictor 2	RF Predictor 3
Mean DBH	Mean Max Height	Mean Rumple	Mean 95th % Height
SD DBH	SD 95th % Height	SD Max Height	SD Mean Height
Max DBH	SD 95th % Height	SD Max Height	SD Mean Height
Basal area	Mean 95th % Height	Mean Max Height	Mean Mean Height
Stem density	SD Mean Height	SD Max Height	SD Coastal
Stem density trees > 50 cm DBH	Mean Rumple	SD Mean Height	Mean 95th % Height
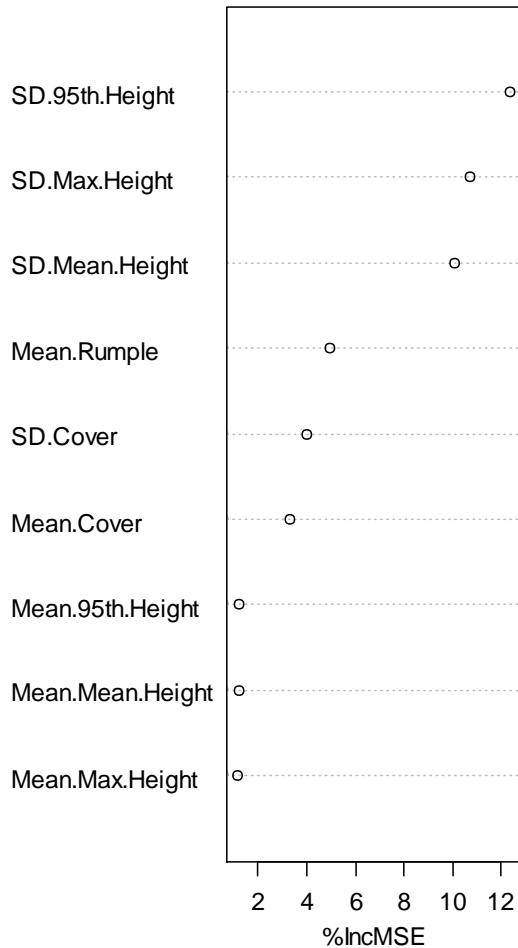
Figure 17. Percent Increase in Mean Square Error (%IncMSE) for the LiDAR only RF regression model developed for SD DBH.
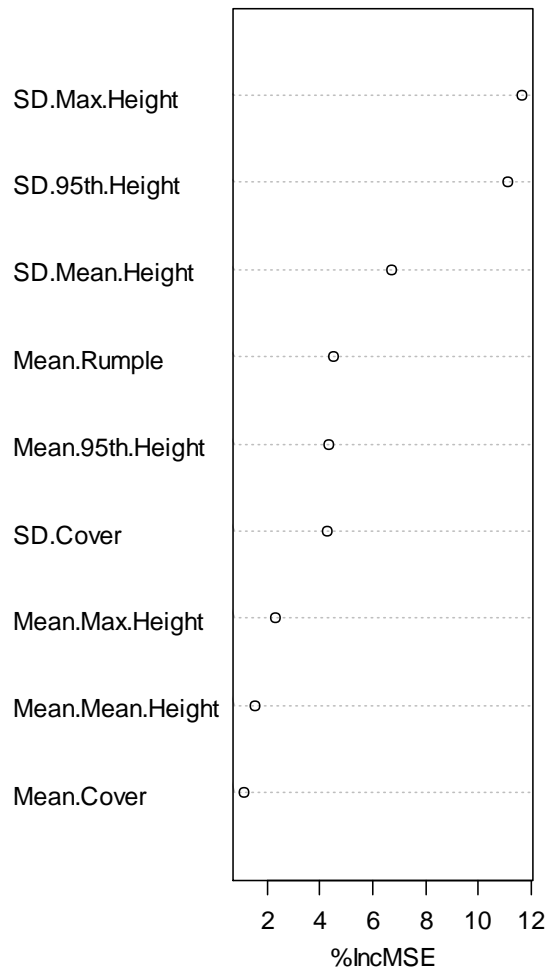
Figure 18. Percent Increase in Mean Square Error (% Inc MSE) for the LiDAR only RF regression model developed for Max DBH.
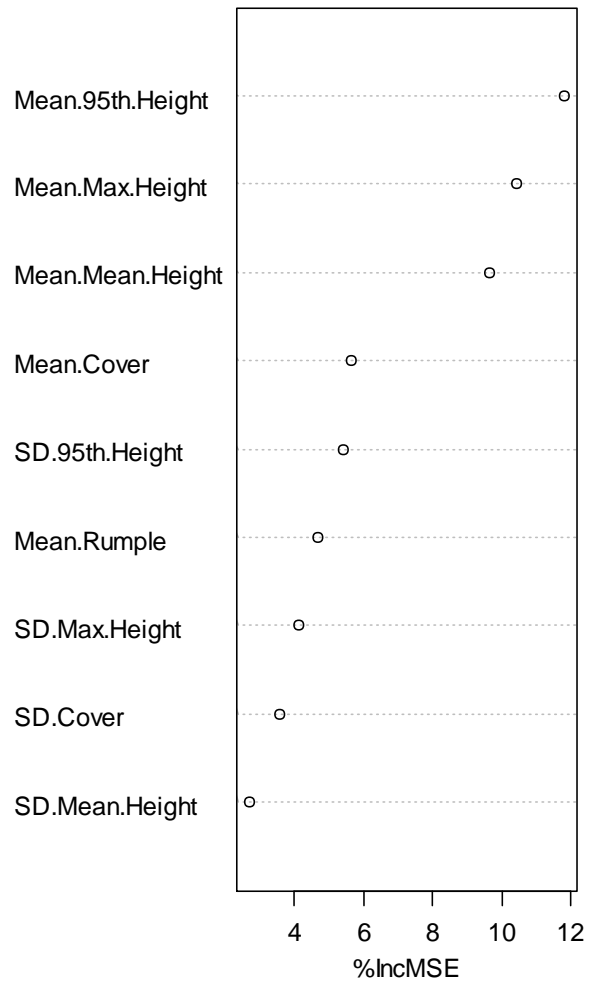
Figure 19. Percent Increase in Mean Square Error (% Inc MSE) for the LiDAR only RF regression model developed for Basal Area.
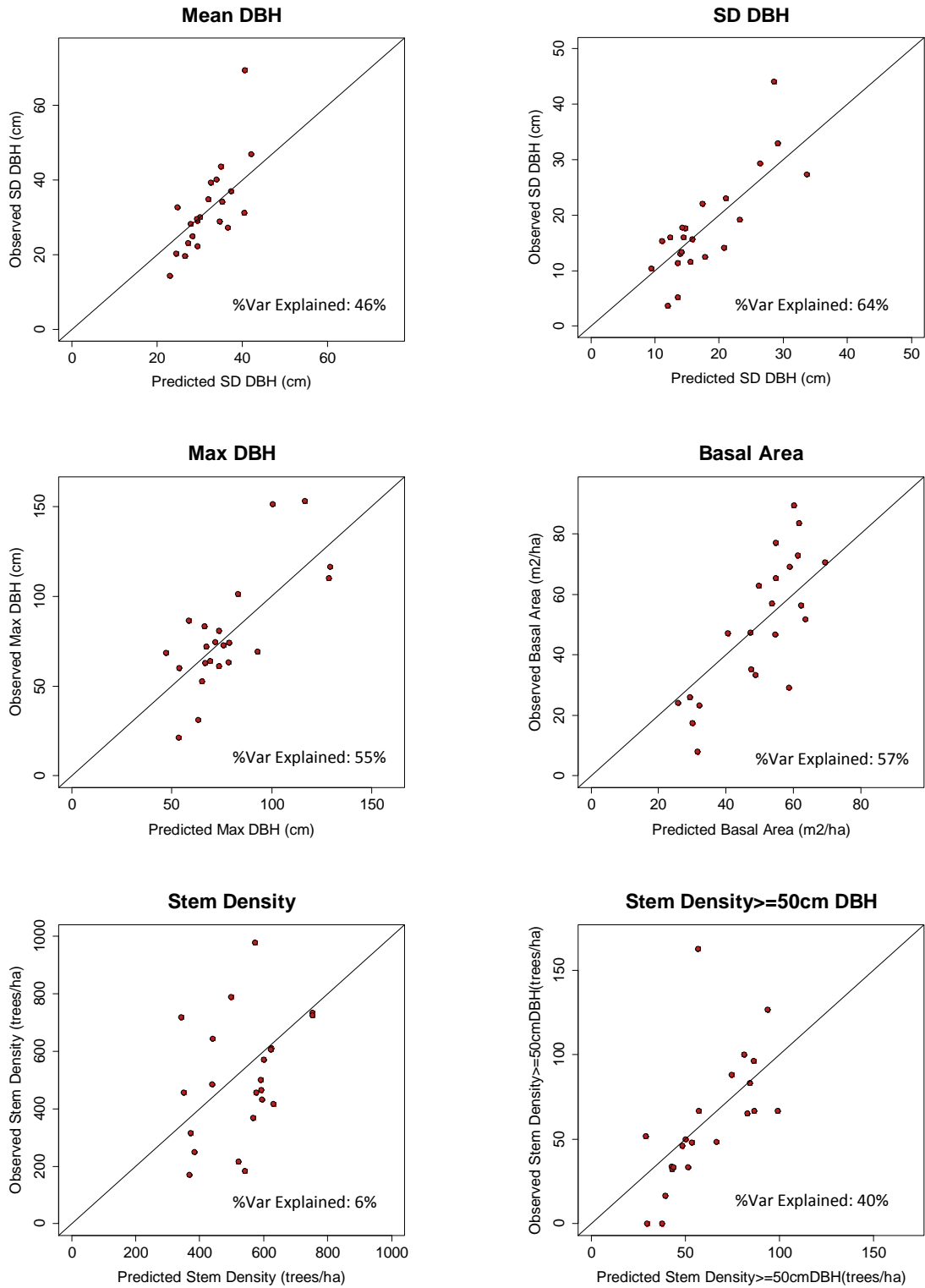
Figure 20. Observed vs. predicted variables from the LiDAR only image RF regression analysis, n = 22. Line represents 1:1 ratio. % Var (Variance) Explained describes model fit.

4.5.1 Mapped Random Forest Regression Predictions

I applied the RF regression models from the LiDAR only dataset to the forested classes (conifer and deciduous) identified from the LiDAR only RF classification. The Stem density model was not applied to the classified image due to poor predictive power (Table 13). The differences between the models are shown for a subset of the study area in Figure 21. The left bank of this location is dominated by conifer forest of greater height and maturity than the younger, deciduous dominated right bank forest. The predicted RF regression models reflect these differences. The left bank forest has a higher Mean DBH values, greater variability with higher SD DBH values, higher Max DBH values, larger Basal area values, and a higher stem density of trees > 50 cm DBH compared to the right bank.
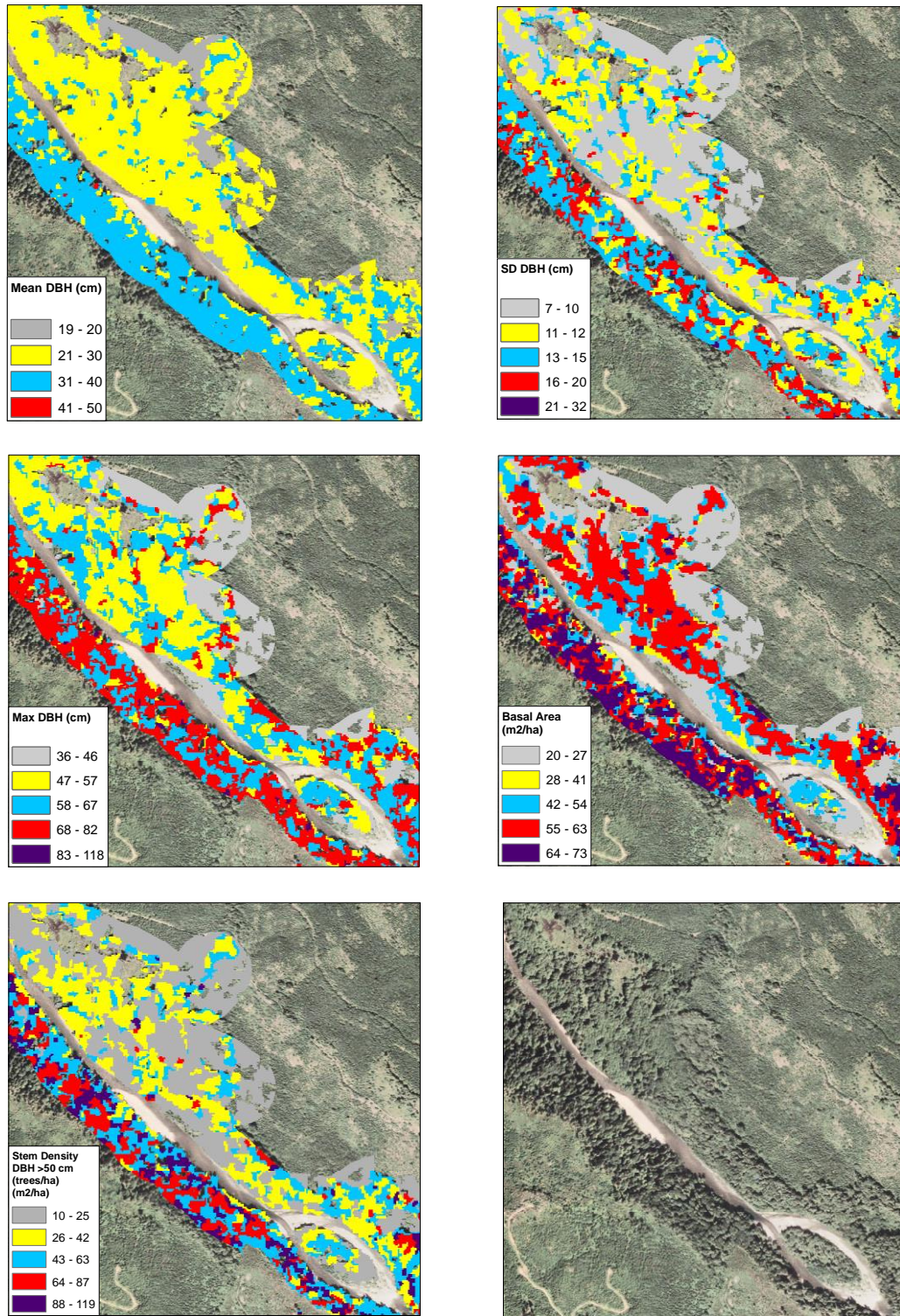
Figure 21. Image subsets of LiDAR only image RF regression models for riparian forest structure metrics predicted from the LiDAR RF regression analysis across the LiDAR RF classification of conifer and deciduous forests.

66

4.6 Application of Random Forest Analysis

After applying the best-performing RF regression models to the forested classes in the

LiDAR only RF classified image, I categorized the riparian forest metrics to illustrate one potential

application of these products for restoration prioritization based on the large woody debris

recruitment potential of the riparian forest. Due to the poor performance of the Stem density model, it

was not included. I included the classified LiDAR metric for cover as a substitute for stem density.

Canopy cover can provide an indication of stem density because increased stem density provides

higher canopy cover and a less dense stand will have less canopy cover. Visual inspection of the

raster grid for cover derived from LiDAR suggested the results provided a suitable surrogate to aid in

prioritization of riparian forest and the correlation analysis of showed a significant relationship

between LiDAR derived cover and Stem density. I categorized the dataset by riparian forest class,

size, and density based on similar methods previously used for watershed analysis (WFPB 1997).

This approach generated 14 unique categories that can be further grouped for restoration prioritization

(Table 17). The code is a combination of the first letter in each category. For example, CSD is a

Conifer, Small, Dense classification. The LWD recruitment potential is based on a low, medium, and

high scale as identified in the watershed analysis methods (WFPB 1997). The final classified dataset

provides individual raster grids that can be used in GIS to categorize the riparian forest as provided in

this application. A final map of the riparian forest categories can be seen in Figure 22. The largest

category based on percentage of total area classified was Deciduous Small Dense (DSD) followed by

Conifer Small Dense (CSD) (Table 18).

Table 17. Riparian forest vegetation categories. Categories and LWD (Large Woody Debris) Recruitment Potential based on WFPB (1997). Code indicates the first letter of each category, for Riparian Forest Class, Size (Mean DBH), and Density.

Riparian Forest Class	Size	Density	Code	LWD Recruitment Potential
Conifer	Small[1]	Dense[4]	CSD	Low
		Sparse[5]	CSS	Low
	Medium[2]	Dense	CMD	High
		Sparse	CMS	Med
	Large[3]	Dense	CLD	High
		Sparse	CLS	Med
Deciduous	Small	Dense	DSD	Low
		Sparse	DSS	Low
	Medium	Dense	DMD	Med
		Sparse	DMS	Low
	Large	Dense	DLD	Med
		Sparse	DLS	Low
No Forest	na	na	NF	Low
Active Channel [6]	na	na	AC	na

[1] Small: mean dbh <=30 cm

[2] Medium: mean dbh>30 dbh and <=50 cm dbh

[3] Large: mean dbh > 50 cm

[4] Dense: cover >=60%

[5] Sparse: cover <60 %

[6] Active Channel Digitized from 2006 NAIP Aerial Photo
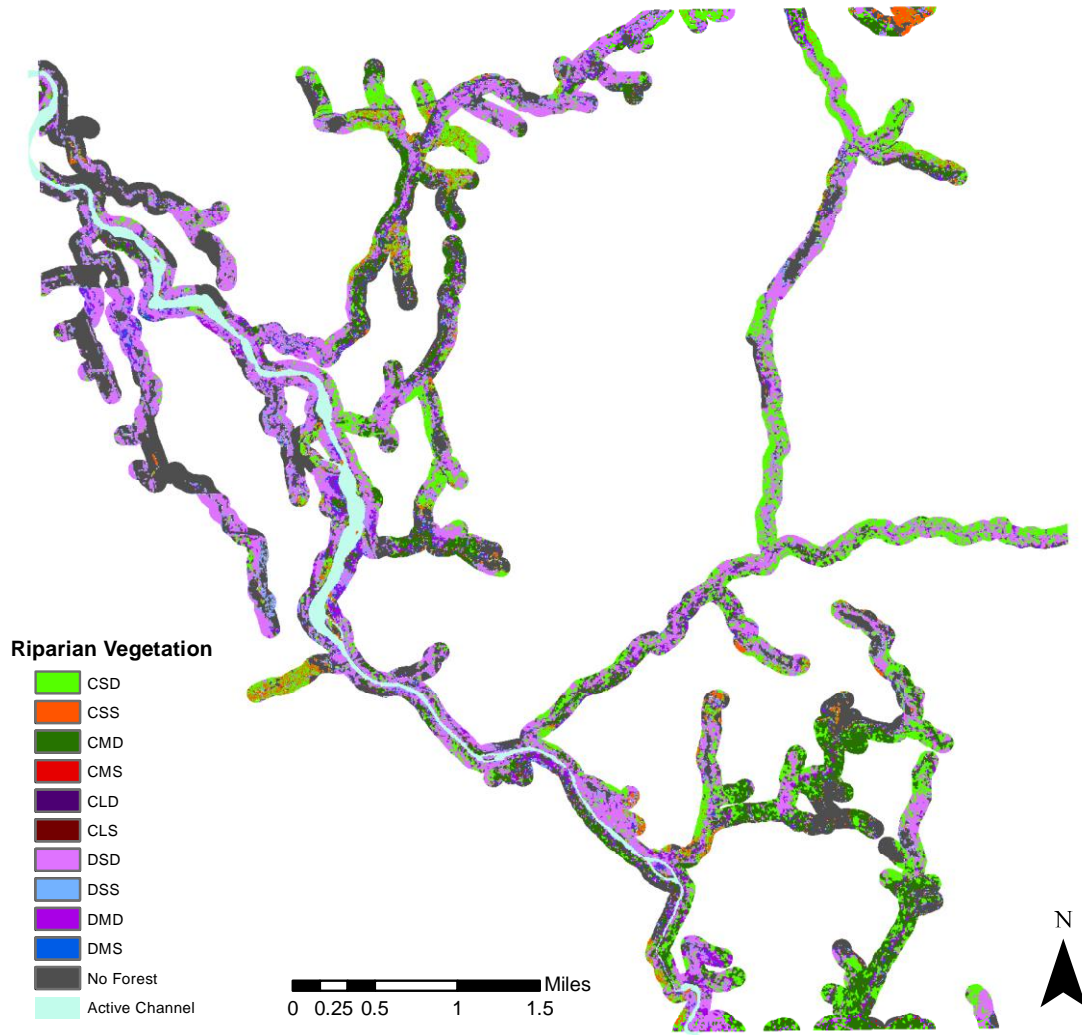
Figure 22. Riparian vegetation by forest class, size, and density. See Table 16 for riparian vegetation codes. No large deciduous trees (DLS or DLD) were found in the study area.

Table 18. Area of riparian forest categories in acres, percentage of total area, and percentage of forested area. The categories conifer large dense (CLD) and conifer large small (CLS) were less than 0.00002% of total area and forested area.

Category	Area (Acres)	Percentage of Total Area	Percentage of Forested Area
CSD	715.34	1.10%	23.09%
CSS	113.40	0.17%	3.66%
CMD	561.99	0.86%	18.14%
CMS	30.30	0.05%	0.98%
CLD	0.01	0.00%	0.00%
CLS	0.01	0.00%	0.00%
DSD	1,153.34	1.77%	37.23%
DSS	168.18	0.26%	5.43%
DMD	262.21	0.40%	8.46%
DMS	93.26	0.14%	3.01%
DLD	0.00	0.00%	0.00%
DLS	0.00	0.00%	0.00%
No Forest	61,722.58	94.86%	na
Active Channel	243.43	0.37%	na

5.0 Discussion

5.1 Correlations between LiDAR and field based forest metrics

The preliminary analysis of LiDAR metrics provided support for using the seven selected LiDAR metrics in the image classification and regression phases of this study. All field metrics were significantly correlated with at least one LiDAR metric and often with more than one metric. The strength of the correlations were modest but illustrate significant relationships between field metrics and LiDAR metrics (Table 8).

Certain relationships were stronger than others. In particular, Basal Area was correlated with all LiDAR metrics but showed the strongest correlations with Mean Height, followed by 95th Percentile Height, and Maximum Height. This is similar to the results of Lefsky et al. (1999) where basal area was predicted by number of waveforms > 55 m, indicating the relationship between basal area and the height of the upper percentiles. However, in the same study the basal area of just Douglas fir was predicted by mean canopy surface height and open gap volume. Means et al. (1999) found basal area predicted by maximum canopy height from LiDAR. SD DBH had the strongest relationships with Maximum Height, SD Height, and the 95th Percentile Height. This is expected because a stand with taller trees would typically represent a more mature forest which would exhibit greater variability in tree size and greater maximum tree size. Lefsky et al. (1999) also found maximum canopy height to be a strong predictor of SD DBH.

Mean DBH had the strongest correlations with Maximum Height and 95th Percentile Height which is surprising because both height metrics are representative of the maximum measurements and not averages of height distribution. Similarly, Maximum DBH had the strongest correlation with Maximum Height followed by the 95th Percentile Height. Stem Density was negatively correlated with all three LiDAR metrics that measure height variability: SD Height, CV Height, and Rumple but positively correlated with cover. These is expected as mature forests exhibit greater variability and are less dense than younger less developed stands. Younger stands, especially stands following

71

commercial timber harvest, have a higher proportion of even aged, dense trees.   Lefsky et al. (2005a) also found relationships between LiDAR derived canopy cover and stem density. Hudak et al. (2006) found that LiDAR cover was the strongest predictor variable of basal area and tree density for dominant tree species in Idaho. However, they also found LiDAR canopy height variables predicted basal area better than tree density and the LiDAR canopy cover variable predicted tree density better than basal area. Stem Density DBH ≥50 cm was not correlated with cover and instead the strongest relationships were with Maximum Height and 95th Percentile Height. This reflects the concept that older forests have higher variability in canopy structure and a greater proportion of larger trees (Alaback 1982a, 1982b; Naiman et al. 1998).   While Rumple correlated with all field metrics, the correlation coefficients were lower compared to other LiDAR metrics that correlated with field metrics.

Previous studies have found the 95th percentile height to align closer to the field measure of canopy maxima (Kane et al. 2010a; Nord-Larsen and Riis-Nielsen 2010). However, in this study there was not a large difference in the strength of correlations between maximum height and 95th percentile height and the response variables.

Previous studies have found that LiDAR metrics that came from three categories of stand structure were highly correlated with stand structure (Lefsky et al. 2005a; Kane et al. 2010a). The three LiDAR metrics are height, variation in height, and canopy density. Kane et al. (2010a) found the strongest correlations with 95th percentile height, rumple, and canopy cover.   While the LiDAR metrics and field metrics in this study were not highly correlated, the results demonstrate similar relationships that provide support for using the seven LiDAR metrics derived from the first returns LiDAR dataset as part of an image classification scheme to describe riparian stand structure complexity.

5.2 Random Forest Classification

In this study, I described the individual and integrated capabilities of multispectral data and LiDAR data to estimate riparian landcover classes and riparian forest structural attributes. I also

explored the additional spectral bands provided by the WV-2 image for landcover classification by comparing the full 8-Band WV-2 image with the subset of the 8-Band image that only contained the 4 spectral bands used by the conventional satellites (e.g., IKONOS and similar). Classification accuracy for the main classes of interest (conifer and deciduous) was higher when using the full 8-Band image rather than the 4-Band image. Overall, the use of the combined LIDAR and 8-band WV-2 image improved the outcome of the landcover classification for all classes compared to the use of either dataset alone. However, classification accuracy for the forest classes with the LiDAR-only image was similar to the combined LIDAR and WV-2 8-band image. Both the 4-band WV-2 image and 8-band WV-2 image were more useful at classifying the active channel classes, water and gravel bar classes, compared to the LiDAR only image.

The 8-Band WV-2 image was more useful for classifying landcover classes compared to the 4-Band WV-2 image, the main differences occurred between the two forest classes, deciduous and conifer. The inclusion of the additional four bands in the 8-Band WV-2 Image increased the User's accuracy of both the deciduous, 7%, and conifer, 8%, classes. This is not surprising because the four additional bands were designed to improve differentiation among vegetation classes (Digital Globe 2010). However, the 4-Band image had slightly higher User's accuracies for the two classes pasture and developed. The NIR-1 band was the variable of most importance for both the 4-Band WV-2 image and the 8-Band WV-2 image. However, the 2nd and 3rd variables of most importance differed between the two images. The Blue band and the Brightness index were the next most important variables for classifying landcover classes for the 4-Band WV-2 image, and the two of the new bands, NIR-2 and Red Edge, were the next most important for the 8-Band WV-2 image (Figure 13, Figure 12). These results are similar to another study in Malaysia that found the NIR-2 band, NIR-1 and the Red Edge to be the top three bands of importance in classification of tree species also using a RF classification algorithm for a WV-2 image (Omar et al. 2010). Chen (2010) also found the additional four bands of a WV-2 image increased classification accuracy for Hawaiian tree species using both a pixel-based and object-based classification. Immitzer et al. (2012),found the 8-bands of the

WorldView-2 classified tree species in Austria better than the four standard bands using the RF algorithm when classifying 10 different tree species. However, the results were similar between the 4-band and 8-bands when only looking at the four major species. Specifically, they found, Green, NIR-1, Blue followed by Red and NIR-2 as the bands of most importance in predicting forest species. Overall, the inclusion of the four new spectral bands in the WV-2 image, in particular the NIR-2 band and the Red-Edge band, increased the capacity to distinguish conifer and deciduous classes. Including the NIR-2 band may have improved the results because it is less likely to be affected by atmospheric influence (Immitzer et al. 2012; Digital Globe 2010).

The LiDAR only image produced lower overall classification accuracies compared to the other three images. However, the Producer's accuracy and User's accuracy for the forested classes were comparable to, but slightly lower, than the combined LIDAR and 8-Band WV-2 image. Use of the LiDAR only image results in classification accuracies that are high for the developed and pasture classes (Table 11). The variables of most importance according to the Mean Decrease in the Gini coefficient were Mean Max Height, Mean Mean Height, and Mean 95th Percentile Height followed by Mean SD Height and Mean Rumple (Figure 14). This suggests that for the LiDAR only image, the LiDAR metrics which represent the upper surface of the canopy, Max Height and 95th Percentile Height, are most useful for discriminating between landcover classes. The most confusion was between the water, gravel bar, and road classes. The results for water and gravel bar classes is not surprising because the channel alignment and flow would have been different at the time of LIDAR data acquisition (2006) compared to the Pictometry datasets (2008, 2010) that the training data was derived from, meaning different portions of the gravel bar would be exposed and different areas covered by water. The Pictometry dataset was from the same year as the WV-2 dataset. I did not generate a separate reference dataset to test these two classes for the LiDAR only image which had the greatest difference between the two different images from different dates. The challenges associated with classifying gravel bar likely caused error in the road class as well because the road class and gravel bar class share similar spectral properties. However, water differs spectrally from

both the road and gravel class and it is likely that spectral imagery such as the WV-2 imagery will be more useful for separating those classes despite the differences in dataset acquisition times. Ideally the LiDAR and multispectral imagery would be collected during the same time frame, if not the same day for more accurate comparison and/or integration.

In addition to the problems associated with the differences in the timing of acquisition for the LIDAR and WV-2 data, delineation of the active channel area, including the gravel bar and water classes, is problematic for the LiDAR because of the difficulty in obtaining LiDAR data over water surfaces in general. LiDAR instruments emit pulses of energy in the near IR portion of the spectrum and record this energy as it reflects from earth surface features. Vegetation, bare soil and gravel are highly reflective in the near IR portion of the spectrum, but clear water absorbs strongly in this portion of the spectrum. A LIDAR pulse that hits a clear, deep water body results in no return and a "no data" value for this area. Very shallow, clear water and water with a high silt load will result in returns that are comparable to those for exposed gravel. For this reason, it is likely that spectral data will continue to outperform LiDAR data for classifying the water.

An issue associated with LiDAR pre-processing likely had a larger effect on the utility of this LiDAR dataset for classifying water, especially on the margins of the channel. In order to run the segmentation algorithm and export the mean and standard deviation for the seven LiDAR metrics, I interpolated values to the no-data locations based on neighboring pixel values. The 3.7-m pixel size for the LiDAR grids resulted in some of the interpolated pixels containing erroneous data, such as elevations more similar to neighboring trees on the stream bank than to the water elevation (Figure 11). This was one of the drawbacks to the object-based analysis compared to a pixel-based approach. A potential solution to remedy this issue is to generate a stream layer from the LiDAR dataset that incorporates a more sophisticated algorithm to assign values to the no-data pixels. Arroyo et al. (2010) developed an algorithm to classify areas of steep slope adjacent to potential stream as stream bank based on a LiDAR derived digital terrain model and slope map. The defined streambed layer was then incorporated into the following image segmentation. Defining the stream is also helpful in

75

quantifying overhanging vegetation from the bank and the amount of shade on the channel. A

LiDAR derived stream layer would also improve the accuracy of stream locations in heavily forested

areas. Often the GIS stream dataset does not line up with actual stream location due to rapid channel

migration and seasonal and diurnal variation in water levels. This is problematic for developing the

riparian buffer area, which is based on distance from the stream location. Critical areas of riparian

forest could be excluded from the analysis if a buffer is based on geographically incorrect

hydrological dataset. Developing a stream layer from the LiDAR dataset was beyond the scope of this

project.

The combination of LiDAR metrics and the 8-Band WV-2 image produced the highest

overall accuracy of the landcover classification compared to the other three datasets. The mean error

decreased considerably for the developed, deciduous, conifer, and road classes compared with the 8-

band WV-2 image and the 4-Band WV-2 image. The deciduous and road classifications for the

LiDAR only image were improved by the integration of the LiDAR and spectral data. However, the

producer's and user's accuracy for the water and gravel bar classes decreased slightly compared with

the 8-Band WV-2 image. This is likely due to the errors associated with the LiDAR dataset for the

active channel described above. Combining the LiDAR and 8-Band WV-2 image resulted in

changes to the variables of most importance as well. The top four variables of most importance

included both the spectral and LiDAR metrics, specifically in order of importance, Mean NIR-1 band,

Mean Max Height, Mean NIR-2 band, and Mean 95th % Height, (Figure 15). These respective

spectral and LiDAR metrics were in the top three variables of importance for each respective dataset

on their own. It is not surprising that the two LiDAR metrics representing the upper portion or top of

the canopy surface model are important for deciphering landcover classes that have different vertical

structure. LiDAR Max Height and 95th Percentile Height also exhibited strong relationships in the

correlation analysis with the riparian forest field metrics and in predicting riparian forest structure.

Other studies have found increased accuracies in classification of WV-2 imagery with the addition of

LiDAR height information (Aguilar et al. 2012).

For all RF classifications the mean values for the various bands and LiDAR metrics explained more variance than the SD of the spectral bands and metrics. The shape and size metrics ranked low for importance in predicting the response variables. Out of the three shape and size metrics, the length/width ratio was higher in importance based on the mean decrease in Gini except for the LiDAR only dataset. This is not surprising because there were features in the study area that were long and thin, such as roads and edges of gravel bars compared with features that were wider such as pasture. These two classes included objects with different length/width ratios. This indicates that the spectral bands and LiDAR metrics are more accurate predictors of different riparian landcover classes than object shape and size metrics.

Overall, all four images were valuable for separating the seven landcover classes. The 8-Band WV-2 Image was better overall compared to the 4-Band WV-2 image for classifying the forested classes but not necessarily the other landcover classes. The LiDAR only image had a lower overall accuracy compared to the three other datasets but was similar at classifying the forested classes. The combined LiDAR and 8-Band WV-2 image had the highest overall accuracy compared to the other three datasets but was not dramatically better than the LiDAR only dataset at classifying the forest classes. The LiDAR only image was least successful for classifying the landcover classes, water, gravel bar, and pasture, which were the categories that both the 4-Band WV-2 and 8-Band WV-2 images were most effective at classifying. These results suggest that depending on the classes of interest, combining spectral and LiDAR imagery might not be necessary to achieve high classification accuracies. To separate conifer and deciduous classes, the LiDAR only image was sufficient. Another way to examine the landcover classification would be to reduce the seven landcover classes to three classes by grouping all non-forest classes into one class and preserving the deciduous and conifer classes. The overall accuracies when the seven classes are reduced to the three that are the most applicable to riparian restoration (non-forest, conifer, and deciduous) for the 4-Band WV-2, 8-Band WV-2, LiDAR only, Combined LiDAR and 8-Band WV-2 images were: 83%, 86%, 91%, and 92% respectively.

For the RF classification analysis, increasing the sample size for the landcover classes would be beneficial. Due to the high variability in riparian stands, more samples are needed to represent the differences compared to an upland forest. For example, often a deciduous patch would have small segments of conifer classifications that were smaller than an actual tree crown. In this study I digitized landcover classes for a point location from high resolution aerial photos, but entire stands of a homogeneous forest type in the form of a polygon could be used as training samples for the landcover classification as in Gergel et al. (2007).

The segmentation phase was a pre-classification phase where I performed basic operations in order to keep the methods and results comparable. To optimize the segmentation phase, additional information could be generated from the objects and also other levels of segmentation could be performed on the output to further refine the results. For example, long, thin objects classified as roads but surrounded by gravel bar are likely gravel bar and be reclassified based on their shape and proximity to other classes. In addition to incorporating context, spectral and spatial enhancements could be applied to the multispectral imagery such as the Normalized difference vegetation index (NDVI) or image texture features such as entropy or contrast (Johansen and Phinn 2006; Sridharan 2010). Other biological, geographic and edaphic variables could also be incorporated to improve the model such as soil moisture, slope, aspect, precipitation, and tree distance to stream.

5.3 Random Forest Regression

The results from the RF regression analysis indicate forest structure metrics can be derived from LiDAR only images and combined LiDAR and 8-Band WV-2 images. The LiDAR only image was the most useful for predicting riparian forest structure variables out of the three images (Table 14). The 8-Band WV-2 image had no predictive power as indicated by the negative values for percent variance for all six response variables. The percent variance explained (% Var Explained), is defined as 1- mean squared error (MSE)/[variance (response)] and is used in place of the Out of Bag (OOB) error rate reported in RF classification (Pang et al. 2006). Negative values can occur when the ratios of MSE and the variance of the response are greater than one. Integrating the LIDAR and the

8-Band WV-2 images resulted in less predictive power than the LiDAR only image. This is likely due to the lack of a relationship between the spectral data from the 8-Band WV-2 image and the response variables. The poor RF regression results for the 8-Band WV-2 image suggest that spectral data alone does not predict forest structure well despite success in other studies (Clark et al. 2004). Clark et al (2004) found significant correlations between basal area in old growth tropical forest and the mean NIR-1 Band in IKONOS multispectral imagery. They also found the panchromatic band correlated more often with forest structure than the multispectral bands. Other studies have found metrics such as band mean, band ratios, and various texture metrics, derived from the Red and NIR bands correlated to stand height (Gemmell 1995; Gerylo et al. 2002; Chubey et al. 2006). Taller trees typically have more foliage which causes red reflectance to decrease as it is absorbed by the foliage and the NIR reflectance to increase because foliage is highly reflective in the NIR (Chubey et al. 2006). However, Erdody and Moskal (2010) only found a slight increase in prediction accuracy of fuel load when NIR imagery added was to LiDAR. Hudak et al. (2006) also found that the addition of multispectral imagery to LiDAR did not improve the predictions of basal area and stem density in coniferous forests in Idaho.

The LiDAR only image outperformed the other two datasets in predicting all six riparian forest metrics. The LIDAR metrics explained the most variance for SD DBH, followed by Max DBH, Mean DBH, Stem Density of trees > 50 cm DBH, and Stem density. Specifically, LiDAR metrics 95th Percentile Height, Maximum Height, and Mean height were the best predictor variables of the response variables. Stem density was not predicted well by any of the three images despite other studies producing models with greater predictive power (Næsset and Bjerknes 2001; Hudak et al. 2008). Hudak et al. (2008) found that LiDAR cover was the strongest predictor variable of species basal area and tree density in Idaho using an RF algorithm. The cover metric generated in LiDAR tends to have a bias towards overestimating cover when the grid cell size is smaller than individual tree crowns (McGaughey et al. 2013). Increasing the grid cell size to15 m or more might produce more meaningful cover metrics that could potentially predict stem density better. This would require

79

increasing the plot width as well, which could be beneficial for predicting cover as well as other variables because the plot could capture more variability within a full tree canopy width for dominant trees. Næsset and Bjerknes (2001) found LiDAR-derived canopy cover to be the only LiDAR variable that predicted stem density in young conifer stands in Norway. Analyzing the data on an individual tree level compared to the plot level used in this analysis could be helpful in predicting stem density better because it would isolate individual trees in the imagery (Chubey et al.2006; Yu et al. 2011). Stem Density DBH $\geq$ 50 cm was predicted much better than Stem density overall by the RF regression models for the LiDAR only image. Interestingly, Stem Density DBH $\geq$ 50 cm was the only response variable with Mean Rumple as a top predictor for the LiDAR only image and the combined LiDAR and 8-Band WV-2 image. This suggests stands that have trees $\geq$ 50 cm DBH exhibit more variability in tree DBH sizes, which is a characteristic of mature stands. The combined LiDAR and 8-Band WV-2 image was less useful for predicting Stem Density DBH $\geq$ 50 cm.

Increasing the sample size of field plots could improve the RF regression model. RF relies heavily on the quality and representation of the training data (Chubey et al. 2006). It is likely that the small sample size of 22 plots does not represent the variability within the riparian forest in this study area. Applying the methods for RF regression to the 63 plots located within the LiDAR only image boundaries (Figure 1) could potentially improve the model performance. Research is needed into the minimum amount of training data needed for optimal model performance. Also, doing a preliminary analysis of the study area to aid in stratifying the study area would be helpful. For example trying to identify homogeneous stands of conifer or deciduous prior to field sampling and then generating points based on those areas could target the field sampling. Obtaining field samples from stands with a greater diversity of tree height and DBH would also be useful. Wondzell et al. (2011) segmented a LiDAR height raster and classified it into height classes before generating a random set of sample locations within the different height classes. The plots in my study area likely exhibit greater within plot variability than between plot variability. A stratified sampling approach that can target multiple stand variation categories would cover more variation across the riparian forested landscape. This

could improve the capacity to capture a broader spectrum of forest stands in the field data. Although, the availability of old growth riparian stands in this study area and many Puget Sound watersheds is limited by past land use practices, and it would likely be difficult to generate numerous plots in this category. Heumann (2011) suggests a thorough assessment linking field sampling schemes with (OBIA) of natural landscapes is needed because remote sensing field sampling protocols have been based on pixel based analysis at a lower resolution (e.g., 25 m Landsat pixels) than newer imagery. He suggests large-scale quadrat sampling or mapping boundaries of homogenous patches as areas to explore for OBIA field sampling methods. In addition to increasing the quantity of plots, increasing the width of the plots would also be helpful because 10 m is typically insufficient to capture a tree canopy width.

5.4 Application of Random Forest Models

The application of my RF classification and regression models to categorize the riparian forest condition shows promise for increasing the efficiency and effectiveness of modeling large areas of riparian forest in order to prioritize sites for preservation and restoration. I applied only results from the LiDAR only image for the riparian forest classes, deciduous and conifer (Figure 16), the mean DBH model (Figure 21) and the LIDAR Cover metric to examine the riparian function of large woody debris recruitment potential. LWD recruitment potential is a function of tree size, species composition, either conifer or deciduous species, and the density or amount of recruitable trees (Bigly and Diesenhofer 2006). However, the other RF regression models could be used to address additional research and management questions. For example the current WA Department of Natural Resources Forest and Fish regulations for timber harvest are intended to manage the riparian forest zone to create desired future conditions (DFC) which are based on stream type, site class index and basal area (WADNR 2010). These three items could easily be incorporated to develop a model that addresses the DFC requirements. To examine shade potential, I would integrate the models for Max height and Stem density of trees > 50 cm DBH with elevation and aspect information. Explaining the Maximum height and also the density of large trees would show the potential of the trees to cast shadows over

81

the stream channel which would help to maintain cooler water temperatures. Aspect provides an important description of the trees and can be related to the solar azimuth at specific times to show where the shadows would be cast. Elevation is an important element to a shade model because there are different shade requirements based on elevation that would be important for categorizing the shade potential and current status (WADNR 2010).

The results exhibited in the final map show that the lower portion of the South Fork Nooksack watershed is dominated by deciduous trees of small to medium sizes and non-forested areas (Figure 22). While the upper portion of the watershed contains a larger area of conifers, very little forest contains large conifers, either sparse or dense classes. It is surprising that there were no large deciduous trees identified throughout the entire study area. However, this model is categorizing based on mean DBH. While there are likely trees in the large size class, ≥ 50 cm DBH, this model suggests there are not enough to increase the mean DBH over that size threshold. The results suggest a need for restoring large conifers throughout much of the study area and provide a tool to point to specific areas where these large trees are lacking. The upper watershed is on a trajectory for recovery in many areas but still needs time to reach optimal size of > 50 cm DBH for recruitment of functional pieces of large wood to the system. This prioritization map can be used to target areas for future restoration which could involve conifer riparian planting, conifer release, or the addition of in stream large wood, but should be incorporated with local expert knowledge of the sites. Potential sites should be examined in person prior to planning on the ground restoration. In addition, the RF riparian forest structure models developed in this study can be used to further examine forest understory. The portions of the study area that are currently dominated by deciduous trees could be targeted for planting of conifers in the understory, if ground surveys confirm that conifers are absent in the understory. This is an interesting area for future development for remote sensing riparian forest modeling.

5.5 Future Research

It would be worthwhile to explore the use of LiDAR intensity metrics, in conjunction with the LiDAR metrics used in this study to differentiate riparian conifer and deciduous classes, tree species, and describe riparian forest structure. LiDAR intensity data has been used to identify and classify individual species successfully in other studies (Holmgren and Perrson 2004; Brandtberg et al. 2003). The fusion of hyperspectral data and LiDAR has also been successfully in mapping species of the coastal Pacific Northwest (Jones et al. 2010).

Future research could also explore analysis of riparian stands at the individual tree level compared to the stand level. Research into the capacity of the LiDAR data to evaluate riparian forest at the individual tree level would be helpful in determining stem density and tree crown characteristics (Suratno et al. 2010). Also, analyzing the forest at an individual tree level could aid in distinguishing different tree species. Current LiDAR datasets are typically higher density (≥ 8 points/m^2) than the dataset used in this analysis (1.3-1.4 points/m^2). The increased point density will increase the capacity to conduct individual tree analysis and evaluate additional stand development characteristics. For example identifying forest stands with deciduous overstory with conifer regeneration below, which is an important functional class because it identifies the recovery stage of the riparian forests. However, it is difficult to classify due to obscuring canopy cover. In addition to higher point densities, previous studies have suggested incorporating multi-temporal data to get leaf on and leaf off data with one growing season could help identify those differences (Gergel et al. 2008).

One of the challenges for modeling riparian forest using LIDAR and high resolution satellite imagery is the large volume of data that must be stored and processed. For example, I had to process WV-2 study area as eight separate tiles rather than as a single dataset. This added a significant amount of time to the image processing and added several pre-processing and post-processing steps to combine the results. Tiling the image, which was required because the image segmentation software could not analyze the full WV-2 image area, also created edge and seam issues when putting the tiles

back together. This would be compounded if I tried to map larger areas. In addition to size of the imagery, the upfront cost of imagery is typically high and requires specialized training and software to analyze the data. The cost of the data, software and analyst might still be offset by the amount of information that can be generated from the imagery. Even though field sampling is still required to validate any image analysis, it is still likely less than the amount of field surveys that would be required to map the entire study area. These results provide an efficient way to expand the mapping to areas beyond the sample plots.

I calculated the LiDAR metrics from only first returns data after initial examination of the first returns data set revealed they were comparable to the all returns dataset. However, the field data included all trees ≥10 cm DBH and not just dominant and subdominant canopy trees. It would be difficult to partition out the dominant canopy trees post data collection in a way that would effectively capture this. In the future, this would be an important category to add in field data collection. I did not include LiDAR intensity data in this study, although previous studies have shown the potential for using LiDAR intensity to classify forest structure and species types (Holmgren & Persson 2004; Voss and Sugumaran 2008). In the future, intensity information could be added as data layers in the image analysis.

Another challenge in this study was getting precise GPS data for the field plots. Due to canopy cover interference with satellite reception, I was unable to GPS each corner of the field plots. This introduced error into the analysis because I calculated the coordinates of the other plot corners in the lab based on distance and azimuth recordings from the field. In the future budgeting additional time or perhaps having an additional field crew member to focus on getting plot GPS coordinates would be more efficient and accurate. However, in some heavily forested areas getting an accurate GPS location might still be challenging. Another solution could be to use circular plots which only require one GPS location at the center point. If the distance to stream is not a variable of interest, setting up circular plots within the riparian buffer might be sufficient to capture riparian forest characteristics.

6.0 Conclusion

In this study, I analyzed riparian landcover classes and riparian forest structural properties based on airborne LiDAR data and high resolution multispectral data from the WorldView-2 satellite. Rather than employing a pixel-based classification approach, I used an object-oriented approach to segment the imagery into meaningful objects consisting of groups of pixels. I developed classification and regression models to predict the features of interest across the entire study area using the Random Forest algorithm. Analyzing the combined LiDAR and WV-2 spectral data improved the results for landcover classification but did not improve the results for riparian forest structural predictions. Previous research suggests that each sensor can bring complementary and potentially synergistic capabilities to landcover classification and estimation of stand structure (Ackerman 1999; Lim et al. 2003; Anderson et al. 2008). The 8-Band WV-2 image did not prove useful in mapping forest structure but was useful in mapping landcover types which vary more in the spectral domain compared to forest structure. The results generated from the 8-Band WV-2 image were improved over the traditional 4-Band WV-2 image that is comparable to images from other high resolution sensors such as IKONOS and Quickbird. However, the results generated from the LiDAR only image were comparable to the spectral imagery at classifying forest classes and remarkably better at predicting forest structure data. The overall results indicate that classification of forested cover type and structural properties of riparian forest stands can be determined accurately for relatively large study areas with LiDAR-based approaches. LIDAR metrics alone explained a large percentage of the variance in many aspects of riparian forest structure (Table 14) and the predictive power of these models could likely be improved with additional ground data. The results show potential for increasing the efficiency of forest applications such as measuring forest structure, estimating forest inventory, and developing restoration scenarios. Improving the training dataset to capture more of the variability across the riparian forested landscape and increasing the GPS locational accuracy could greatly improve these results. Overall, my study shows that LiDAR metrics

generated from LiDAR first returns data can effectively capture riparian forest stand metrics of interest across a varied riparian landscape.

The availability of LiDAR data provides new opportunities to evaluate forest structure at the stand and landscape levels by providing managers with the equivalent area of hundreds or thousands of plots (Kane et al. 2010a). The cost of LiDAR is relatively low compared to the cost of traditional field measurements on a per acre basis. The cost of LiDAR is continuing to decrease while the point density has increased. A recent watershed-wide acquisition focused on the mainstem Nooksack River and Forks contained densities ≥ 8 pulses/m^2 and cost \$1.87/acre (WSS 2013). The 8-Band WV-2 imagery is cheaper than LiDAR at approximately \$0.18/acre to \$0.21/acre (\$44/km^2 – \$52/km^2) for orthorectified imagery. However, LiDAR data provides more information on forest structure which the 8-Band WV-2 imagery alone is unable to provide. LiDAR is also routinely purchased to generated bare earth models from the Last Return data points which increase the applications available from the LiDAR dataset alone. Purchasing spectral data alone would not meet the multi-faceted needs of resource managers as ground elevation cannot be derived from spectral imagery. My results suggest that the added investment of acquiring satellite imagery in addition to LiDAR at a regional or watershed-wide level may not be necessary as riparian forest classes and forest structure can be generated as well and better in some cases from the LiDAR data.

As LiDAR is becoming more widely available, having an accurate and efficient way to describe riparian forest structure is an important management tool. This tool can be applied to examine the current habitat potential of the adjacent riparian forest as in the example in this study, or also to monitor change over time if repeat datasets are available, which is an important step for monitoring the effectiveness of riparian restoration. The LiDAR metrics Maximum height, 95th % Height, and Mean height are the most effective at classifying riparian landcover and riparian forest structural attributes that are applicable to LWD recruitment and shade potential. These results suggest these three metrics can characterize both landcover classification and riparian forest structure. Combining the landcover classes conifer and deciduous with the forest structure metrics derived from

86

the RF regression models provides an important tool to analyze riparian function specific to LWD recruitment potential and shade potential.   Restoring functional riparian habitat is one of the long term goals for recovery of salmonid species in the Nooksack River Basin. Integrating the information from this analysis with current restoration strategies in the Nooksack River Basin provides valuable information about riparian forest condition and the potential to provide functional habitat.

7.0 Literature Cited

Abbe, T. B., and D. R. Montgomery. 1996. Large woody debris jams, channel hydraulics and habitat formation in large rivers. Rivers Research and Management 12(23): 201-221.

Ackermann, F. 1999. Airborne laser scanning – present status and future expectations. ISPRS Journal of Photogrammetry & Remote Sensing 54 (2): 64-67.

Aguilar, M.A., M. M. Saldaña, and F. J. Aguilar. 2012. GeoEye-1 and WorldView-2 pan-sharpened imagery for object-based classification of urban environments. International Journal of Remote Sensing 34 (7): 2583-2606.

Alaback, P. B. 1982a. Dynamics of understory biomass in Sitka spruce-western hemlock forests of southeast Alaska. Ecology 63: 1932-1948.

Alaback, P. B. 1982b. Forest community structural changes during secondary succession in southeast Alaska. Pages 70-79. *In* J.E. Means, ed. Forest Succession and Stand Development Research in Northwest: Proceedings of the Symposium. Oregon State University, Forest Research Laboratory, Corvallis, Oregon, USA.

Andersen, H. E., R. J. McGaughey, and S. E. Reutebuch. 2005. Estimating forest canopy fuel parameters using LiDAR data. Remote Sensing of the Environment 94 (4): 441-449.

Andersen, H. E, S. E. Reutebuch, and R. J. McGaughey. 2006. A rigorous assessment of tree height measurements obtained using airborne LiDAR and conventional field methods. Canadian Journal of Remote Sensing 32 (5): 355-366.

Anderson, J. E., L. C. Plourde, M. E. Martin, B. H. Braswell, M. L. Smith, R. O. Dubayah, M. A. Hofton, and J. B. Blair. 2008. Integrating waveform LiDAR with hyperspectral imagery for inventory of a northern temperate forest. Remote Sensing of the Environment 112 (4): 1856-1870.

Anderson, K., J. J. Bennie, E. J. Milton, P.D.M. Hughes, R. Lindsay, and R. Meade. 2009. Combining
LiDAR and IKONOS data for eco-hydrological classification of an ombrotrophic peatland. Journal of Environmental Quality 39 (1): 260-273.

Arroyo, L. A., K. Johansen, J. Armston, and S. Phinn. 2010. Integration of LiDAR and QuickBird imagery for mapping riparian biophysical parameters and land cover types in Australian tropical savannas. Forest Ecology and Management 259 (3): 598-606.

Bailan, E. V., and R. J. Naiman. 2005. Abundance and production of riparian trees in the lowland floodplain of the Queets River, Washington. Ecosystems 8(7): 841-861.

Beechie, T. J., G. Pess, P. Kennard, R. E. Bilby, and S. Bolton. 2000. Modeling recovery rates and pathways for woody debris recruitment in northwestern Washington streams. North American Journal of Fisheries Management 10 (2): 436-452.

Beechie, T. J., D. A. Sear, J. D. Olden, G. R. Pess, J. M. Buffington, H. Moir, and M. M. Pollock. 2010. Process-based principles for restoring river ecosystems. BioScience 60(3): 209-222.

Beechie, T. J. and S. Bolton. 1999. An approach to restoring salmonid habitat-forming processes in Pacific Northwest watersheds. Fisheries 24 (4): 6-15.

Beechie, T. J. and T.H. Sibley. 1997. Relationships between channel characteristics, woody debris, and fish habitat in northwestern Washington streams. Transactions of the American Fisheries Society 126 (2): 217-229.

Beschta, R. L., R. E. Bilby, G. W. Brown, L. B. Holtby, and T. D. Hofstra. 1987. Stream temperature and aquatic habitat: fisheries and forestry interactions. Pages 191-232. *In* Salo, E. O. Cundy, T. W. Cundy editors. Streamside Management: Forestry and Fishery Interaction. Seattle, Washington, University of Washington, College of Forest Research.

Bigley, R. E., and F. U. Deisenhofer. 2006. Implementation procedures for the habitat conservation plan riparian forest restoration strategy. DNR Scientific Support Section, Olympia, WA.

Bilby, R. E. 1984. Removal of woody debris may affect stream channel stability. Journal of Forestry 82(10): 609-613.

Bilby, R. E., and J. W. Ward. 1989. Changes in characteristics and function of woody debris with increasing size of streams in western Washington. Transactions of the American Fisheries Society 118 (4): 368-378.

Bilby, R. E., and J. W. Ward. 1991. Characteristics and function of large woody debris in streams draining old-growth, clear-cut, and second-growth forests in southwestern Washington. Canadian Journal of Fisheries and Aquatic Sciences 48(12): 2499-2508.

Bilby, B. E., and P. A. Bisson. 1998. Function and Distribution of Large Woody Debris in Streams. Pages 324-346. *In* B. E. Bilby and B. J. Naiman, editors. River ecology and management: lessons from the Pacific Coastal Ecoregion Springer Verlag Press, New York.

Bisson, P.A., R. E. Bilby, M. D. Bryant, C. A. Dolloff, G. B. Grette, R. A. House, M. L. Murphy, K. V. Koski, and J. R. Sedell. 1987. Large woody debris in forested streams in the Pacific Northwest: past, present, and future. Pages 143-190. *In* Salo, E. O. Cundy, T. W. Cundy editors. Streamside management: Forestry and Fisheries Interactions. Seattle, WA College of Forest Resources.

Borel, C. C. 2010 Vegetative canopy parameter retrieval using 8-band data. Digital Globe 8-Band Challenge. http://dgl.us.neolane.net/res/dgl/survey/_8bandchallenge_winners.jsp?deliveryId=&id *accessed March 26, 2012.*

Bormann, B. T., B. K. Kerns, J. Evans, M. Nay, A. Hudak, R. Darbyshire, and R. Kiester. 2006. Final report to the national commission on science for sustainable forestry: NCSSF project C4, using remote sensing to evaluate biodiversity indicators: implications for Biscuit post-fire restoration. USDA Forest Service, Pacific Northwest Research Station. Portland, OR.

Brandtberg, T., T. A. Warner, R. E. Landenberger, and J. B. McGraw. 2003. Detection and analysis of individual leaf-off tree crowns in small footprint, high sampling density LiDAR data from the eastern deciduous forest in North America. Remote Sensing of the Environment 85 (3): 290-303.

Brazier, J. R., and G. W. Brown. 1973. Buffer strips for temperature control. Research Paper 15. Forest Research Laboratory, School of Forestry, Oregon State University, Corvallis, Oregon.

Breiman, L. 2001. Random Forests. Machine Learning 45 (1): 5-32.

Breiman, L., A. Cutler, A. Liaw, and M. Wiener. 2012. Breiman and Cutlers's random forests for classification and regression. http://CRAN.R-project.org/ *accessed April 12, 2013.*

Brown, G.W. 1969. Predicting temperatures of small streams. Water Resources Research 5 (1): 68-75.

Brown, G.W., and J. T. Krygier. 1970. Effects of clear-cutting on stream temperature. Water Resources Research 6 (4): 1133-1139.

Campbell, J. B., and R. H. Wynne. 2011. Introduction to Remote Sensing. Guilford Press, New York. Pp 360.

Chávez, R., and J. G. P. W. Clevers. 2010. Object-based analysis of 8-band WorldView-2 imagery for assessing health conditions of desert trees. DigitalGlobe 8-Band Research Challenge. http://dgl.us.neolane.net/res/dgl/survey/_8bandchallenge_winners.jsp?deliveryId=&id *accessed March 26, 2012.*

Chen, Q. 2010. Comparison of WorldView-2 and IKONOS-2 imagery for identifying tree species in the habitat of an endangered bird species in Hawaii. DigitalGlobe 8-Band Research Challenge. http://dgl.us.neolane.net/res/dgl/survey/_8bandchallenge_winners.jsp?deliveryId=&id *accessed March 26, 2012.*

Chubey, M. S., S. E. Franklin, and M. A. Wulder. 2006. Object-based analysis of Ikonos-2 imagery for extraction of forest inventory parameters. Photogrammetric Engineering and Remote Sensing 72 (4): 383-394.

Clark, D. B., J. M. Read, M. L. Clark, A. M. Cruz, M. F. Dotti, and D. A. Clark. 2004. Application of 1-m and 4-m resolution satellite data to ecological studies of tropical rain forests. Ecological Applications 14 (1): 61-74.

Coe, T. 2001. Nooksack River Watershed Riparian Function Assessment. Nooksack Indian Tribe Natural Resources Department. Deming, WA.

Collins, B. D. and A. J. Sheikh. 2004. Historic channel locations of the Nooksack River. Report to Whatcom County, Public Works Department. Department of Earth and Space Sciences, University of Washington. Seattle, WA.

Compton, J. A., M. R. Church, S. T. Larned, and W. E. Hogsett. 2003. Nitrogen export from forested watersheds in the Oregon Coast Range: the role of N2-fixing red alder. Ecosystems 6 (8): 773-785.

Cutler, D. R., T. C. Edwards, K. H. Beard, A. Cutler, K. T. Hess, J. Gibson, and J. J. Lawler. 2007. Random forests for classification in ecology. Ecology 88 (11): 2783-2792.

Definiens. 2010. eCognition 8.0 User Guide. Definiens: München, Germany.

Digital Globe. 2010. The benefits of the 8 spectral bands of WorldView-2. DigitalGlobe White Paper. Longmont, CO, USA http://www.digitalglobe.com/sites/default/files/DG-8SPECTRAL-WP-WEB.pdf *accessed May 5, 2013.*

Duncan, S. H., R. E. Bilby, J. W. Ward, and J. T. Heffner. 1987. Transport of road surface sediment through ephemeral stream channels. Journal of American Water Resources Association 23 (1): 113-119.

Erdody, T. L., and L. M. Moskal. 2010. Fusion of LiDAR and imagery for estimating forest canopy fuels. Remote Sensing of the Environment 114 (4): 725-737.

Everitt, J. H, R. S. Fletcher, H. S. Elder, and C. Yang. 2008. Mapping giant Salvinia with satellite imagery and image analysis. Environmental Monitoring and Assessment 139 (1-3): 35-40.

FEMAT (Forest Ecosystem Management Assessment Team). 1993. Forest ecosystem management: an ecological, economic, and social assessment: report of the Forest Ecosystem Management Team. USDA Forest Service, U.S. Department of Commerce, National Oceanic and Atmospheric Administration National Marine Fisheries Service., USDI Bureau of Land Management, Fish and Wildlife Service, National Park Service, Environmental Protection Agency. Washington, D.D. 1v.

Fetherston, K. L., R. J. Naiman, R. E. Bilby. 1995. Large woody debris, physical process, and riparian forest development in montane river networks of the Pacific Northwest. Geomorphology: 13 (1): 133-144.

Franklin, J. F., T. A. Spies, R. VanPelt, A. B. Carey, D. A. Thornburgh, D. R. Berg, D. B. Lindenmayer, M. E. Harmon, W. S. Keeton, D. C. Shaw, K. Bible, and J. Chen. 2002. Disturbances and structural development of natural forest ecosystems with silvicultural implications, using Douglas-Fir forest as an example. Forest Ecology and Management 155 (1): 399-423.

Fullerton, A. H., T. J. Beechie, S. E. Baker, J. E. Hall, and K. A. Barnas. 2006. Regional patterns of riparian characteristics in the interior Columbia River basin, Northwestern USA: applications for restoration planning. Landscape Ecology 21 (8): 1347-1360.

Geerling, G. W., M. Labrador-Garcia, J. G. P. W. Clevers, A. M. J. Ragass, and A. J. M. Smits. 2007. Classification of floodplain vegetation by data fusion of spectral (CASI) and LiDAR data. International Journal of Remote Sensing 23(19): 4263-4284.

Gemmell, F. M. 1995. Effects of forest cover, terrain, and scale on timber estimation with thematic mapper data in a rocky mountain site. Remote Sensing of the Environment 51(2):291-305.

Gergel, S. E., Y. Stange, N. C. Coops, K. Johansen, and K. R. Kirby. 2007. What is the value of a good map? An example using high spatial resolution imagery to aid riparian restoration. Ecosystems 10 (5): 688-702.

Gerylo, H. T., R. J. Hall, S. E. Franklin, and L. Smith. 2002. Empirical relations between Landsat TM spectral response and forest stands near Fort Simpson, Northwest Territories, Canada. Canadian Journal of Remote Sensing. 28 (1): 69-79.

Goerndt, M. E., V. J. Monleon, and H. Temesgen. 2010. Relating forest attributes with area- and tree-based light detection and ranging metrics for western Oregon. Western Journal of Applied Forestry 25(3): 105-111.

Gregory, S.V., F. J. Swanson, A. McKee, and K. W. Cummins. 1991. An ecosystem perspective of riparian zones. Bioscience 41 (8): 540-551.

Hall, R. J. 2003. The roles of aerial photographs in forestry remote sensing image analysis. Pages 47-75. *In* M. A. Wulder and S. E. Franklin, editors Remote Sensing of Forest Environment: Concepts and Case studies. Kluwer Academic Publishers, Boston/Dordecht/London.

Haugerud, R. 2008. 2006 USGS north Puget Sound LIDAR survey: data quality. U. S. Geological Survey c/o University of Washington, Seattle, WA. March 31, 2008.

Heumann, B. W. 2011. An object-based classification of mangroves using a hybrid decision tree – support vector machine approach. Remote Sensing. 3 (11): 2440-2460.

Horning, N. 2011. Error analysis and variable significance with random forests. American Museum of Natural History, Center for Biodiversity and Conservation. Available from http://biodiveristyinformatics.amnh.org/. *accessed on July 2, 2013.*

Horning, N. 2013. Training Guide to Classify Satellite Images Using Segmentation and Random Forests v1. American Museum of Natural History, Center for Biodiversity and Conservation. Available from http://biodiveristyinformatics.amnh.org/. *accessed on July 2, 2013.*

Holmgren, J. and A. Persson. 2004. Identifying species of individual trees using airborne laser scanner. Remote Sensing of the Environment. 90 (4): 415-423.

Holmgren, J., M. Nilsson, and H. Olsson. 2003. Estimation of tree height and stem volume on plots using airborne laser scanning. Forest Science 49 (3): 419 - 428.

Hudak, A. T., N. L. Crookston, J. S. Evans, M. J. Falkowski, A. M. Smith, P. E. Gessler, and P. Morgan. 2006. Regression modeling and mapping of coniferous forest basal area and tree density from discrete-return LiDAR and multispectral satellite data. Canadian Journal of Remote Sensing 32 (2): 126-138.

Hudak, A.T., N. L. Crookston, J. S. Evans, D. E. Hall, and M. J. Falkowski. 2008. Nearest neighbor imputation of species-level, plot-scale forest structure attributes from LiDAR data. Remote Sensing of the Environment 112 (5): 2232-2245.

Hyatt, T. L. 2000. A GIS dataset of WRIA 01 land-use/zoning. Nooksack Tribal Natural Resources, Deming, WA.

Hyatt, T. L., T. Z. Waldo, T. J. Beechie. 2004. A watershed scale assessment of riparian forests with implications for restoration. Restoration Ecology 12 (2): 175-183.

Hyyppä, J., H. Hyyppä, D. Leckie, F. Gougeon, X. Yu, and M. Maltamo. 2008. Review of methods of small-footprint airborne laser scanning for extracting forest inventory data in boreal forests. International Journal of Remote Sensing. 29 (5): 1339-1366.

Immitzer, M., C. Atzberger, and T. Koukal. 2012. Tree species classification with random forest using very high spatial resolution 8-band WorldView-2 satellite data. Remote Sensing 4(9): 2661-2693.

Johansen, K., and S. Phinn. 2006. Linking riparian vegetation spatial structure in Australian tropical savannas to ecosystem health indicators: semi-variogram analysis of high spatial resolution satellite imagery. Canadian Journal of Remote Sensing 32 (3): 228-243.

Johansen, K., N. C. Coops, S. E. Gergel, and Y. Stange. 2007. Application of high spatial resolution satellite imagery for riparian and forest ecosystem classification. Remote Sensing of Environment 110 (1): 29-44.

Johnson, S. L. 2004. Factors influencing stream temperatures in small streams: substrate effects and a shading experiment. Canadian Journal of Fisheries Aquatic Sciences 61 (6): 913-923.

Jones, T. G., N. C. Coops, and T. Sharma. 2010. Assessing the utility of airborne hyperspectral and LiDAR data for species distribution mapping in the coastal Pacific Northwest, Canada. Remote Sensing of the Environment 114 (12): 2841-2852.

Kane, V.R., J. D. Baker, R. J. McGaughey, J. A. Lutz, R. F. Gersonde, and J. F. Franklin. 2010b. Examining conifer canopy structural complexity across forest ages and elevations with LiDAR data. Canadian Journal of Forest Research 40 (4): 774-787.

Kane, V.R., R.J. McGaughey, J. D. Baker, R. F. Gersonde, J. A. Lutz, and J. F. Franklin. 2010a. Comparisons between field and LiDAR based measures of stand structural complexity. Canadian Journal of Forest Research 40 (4): 761-773.

Kiffney, P. M., J. S. Richardson, and J. P. Bull. 2003. Responses of periphyton and insects to experimental manipulation of riparian buffer width along forest streams. Journal of Applied Ecology 40 (6): 1060-1076.

Kreutzweiser, D. P, and S. S. Capell. 2001. Fine sediment deposition in streams after selective forest harvesting without riparian buffers. Canadian Journal of Forest Research 31(12): 2134-2142.

Lefsky, M. A., W. B. Cohen, S. A. Acker, G. G. Parker, T. A. Spies, and D. Harding. 1999. LiDAR remote sensing of the canopy structure and biophysical properties of Douglas-Fir western hemlock forests. Remote Sensing of the Environment 70 (3): 339-361.

Lefsky, M. A., W. B. Cohen, G. G. Parker, and D. J. Harding. 2002. LiDAR remote sensing for ecosystem studies. BioScience 52 (1):19-30.

Lefsky, M.A., D. P. Turner, M. Guzy, and W. B. Cohen. 2005b. Combining LiDAR estimates of aboveground biomass and Landsat estimates of stand age for spatially extensive validation of modeled forest productivity. Remote Sensing of the Environment 95 (4): 549-558.

Lefsky, M.A., A.T. Hudak, W.B. Cohen, and S. A. Acker. 2005a. Patterns of covariance between forest stand and canopy structure in the Pacific Northwest. Remote Sensing of the Environment 95(4): 517-531.

Liaw, A., and M. Wiener. 2002. Classification and regression by randomForest. R News 2: 18-22.

Lim, K., P. Treitz, K. Baldwin, I. Morrison, and J. Green. 2003. LiDAR remote sensing of biophysical properties of tolerant northern hardwood forests. Canadian Journal of Remote Sensing 19(5): 658-678.

Long, B. A. 1987. Recruitment and abundance of large woody debris in an Oregon coastal stream. Master's Thesis, Oregon State University, Corvallis, Oregon, USA.

McDade, M. H., R.J. Swanson, W.A. McKee, J. F. Franklin, and J. Van Sickle. 1990. Source distances for coarse woody debris entering small streams in western Oregon and Washington. Canadian Journal of Forest Research. 20 (3): 326-330.

McGaughey, R. 2013. FUSION/LDV: Software for LiDAR data analysis and visualization, FUSION Version 3.10. Available online at forsys.cfr.washington.edu.fusion.html/ *accessed March 10, 2013*.

Martinuzzi S., L. A. Vierling, and W. A. Gould. 2009. Mapping snags and understory shrubs for a LiDAR-based assessment of wildlife habitat suitability. Remote Sensing of the Environment 113 (12): 2533-2546.

Maser, C., R. F. Tarrant, J. M. Trappe, and J. F. Franklin. 1988. From the forest to the sea: a story of fallen trees. PNW Research Station, USDA Forest Service; General Technical Report PNW-GTR-229, Portland, Oregon, 153 pp.

Maudlin, M., T. Coe, N. Currence, and J. Hansen. 2002. South fork Nooksack river Acme-Saxon restoration planning: analysis of existing information and preliminary recommendations. November 26, 2002. Lummi Nation, Natural Resources Department. Bellingham, WA 127 pp.

Maudlin, M. and T. Coe. 2012. South fork Nooksack River instream habitat projects. July 11, 2012. Nooksack Natural Resources, Deming, WA. 70 pp.

Means, J. E., S. A. Acker, D. J. Harding, J. B. Blair, M. A. Lefsky, W. B. Cohen, M. E. Harmon, and W. A. McKee. 1999. Use of large-footprint scanning airborne LiDAR to estimate forest stand characteristics in the Western Cascades of Oregon. Remote Sensing of the Environment 67(3): 298-308.

Mikkelson, K. N. 2001. Factors influencing the distribution of conifers and red alder in riparian zones in western Washington. Master's thesis, University of Washington, Seattle, WA.

Mollot, L. A. and R. E. Bilby. 2008. The use of geographic information system, remote sensing, and suitability modeling to identify conifer restoration sites with high biological potential for anadromous fish at the Cedar River municipal watershed in western Washington, USA. Restoration Ecology 16 (3): 336-347.

Mollot, L. A., D. Munro, and R. E. Bilby. 2007. Classifying fine-scale spatial structure of riparian forests using hyperspectral high-resolution remotely sensed imagery at the Cedar River municipal watershed in western Washington, USA. Canadian Journal of Remote Sensing 33(2): 99-108.

Murphy, M. L., and K. Koski. 1989. Input and depletion of woody debris in Alaska streams and implications for streamside management. North American Journal of Fisheries Management 9 (4): 427-436.

Mutlu, M., S. C. Popescu, C. Striplin, and T. Spencer. 2008. Mapping surface fuel models using LiDAR and multispectral data fusion for fire behavior. Remote Sensing of the Environment 112 (1): 274-285.

NMFS (National Marine Fisheries Service). 2013. Endangered Species Act Status Reviews And Listing Information. National Marine Fisheries Service, Northwest Region, Seattle, WA. http://www.nwr.noaa.gov/protected_species/salmon_steelhead/salmon_and_steelhead_listings/salmon_and_steelhead_listings.html *accessed October 13, 2013*.

NNR (Nooksack Natural Resources Department). 2001. Channel migration zone. GIS Shapefile. Deming, WA.

NNR (Nooksack Natural Resources Department). 2004. Salmonid Distribution Updates for WRIA 01 Watershed Management Project. 3/2/2004. Deming, WA.

NNR (Nooksack Natural Resources Department). 2008. South fork Nooksack large woody debris survey. Deming, WA.
NWIFC (Northwest Indian Fisheries Commission). 2008. WRIA 1 Salmonid Distribution. GIS Shapefiles. NWIFC North Sound Office, Mt. Vernon, WA.

Næsset, E., and K. O. Bjerknes. 2001. Estimating tree heights and number of stems in young forest stands using airborne laser scanner data. Remote Sensing of the Environment 78 (3): 328-340.

Næsset, E., T. Økland. 2002. Estimating tree height and tree crown properties using airborne scanning laser in a boreal nature reserve. Remote Sensing of the Environment 79 (1): 105-115.

Næsset, E. 2004. Practical large-scale forest stand inventory using a small-footprint airborne scanning laser. Scandinavian Journal of Forest Research 19 (2): 164-179.

Naiman, R. J., K. L. Fetherston, S. J. McKay, and J. Chen. 1998. Riparian forests. Pages 289-323. *In* B. E. Bilby and B. J. Naiman, editors. River ecology and management: lessons from the Pacific Coastal Ecoregion Springer Verlag Press, New York. River Ecology and Management: Lessons From the Pacific Coastal Ecoregion. New York. Springer-Verlag.

Naiman, R. J., R.E. Bilby, and P.A. Bisson. 2000. Riparian ecology and management in the Pacific coastal rain forest. BioScience 50 (11): 996-1011.

Naiman, R. J. and J. J. Latterell. 2005. Principles for linking fish habitat to fisheries management and conservation. Journal of Fish Biology 67(sB): 166-185.

Naiman, R. J., H. DéCamps, and M. E .McClain. 2005. Riparia: Ecology, Conservation, and Management of Streamside Communities. Elsevier Academic Press, San Francisco. Pp.156-158.

Nehlsen, W., J. E. Williams, and J. A. Lichatowich. 1991. Pacific Salmon at the Crossroads –Stocks at Risk from California, Oregon, Idaho, and Washington. Fisheries 16 (2): 4-21.

Nord-Larsen, T., and T. Riis-Nielsen. 2010. Developing an airborne laser scanning dominant height model from a countrywide scanning survey and national forest inventory data. Scandinavian Journal of Forest Research 25(3): 262-272.

Omar, H. 2010. Commercial timber tree species identification using multispectral WorldView-2 Data. DigitalGlobe 8-Band Research Challenge. http://dgl.us.neolane.net/res/dgl/survey/_8bandchallenge_winners.jsp?deliveryId=&id *accessed March 26, 2012.*

Ozdemir, I., and A. Karnieli. 2010. Predicting forest structural parameters using the image texture derived from WorldView-2 multispectral imagery in a dryland forest, Israel. DigitalGlobe 8-Band Research Challenge. http://dgl.us.neolane.net/res/dgl/survey/_8bandchallenge_winners.jsp?deliveryId=&id *accessed March 26, 2012.*

Packalen, P., and M. Maltamo. 2007. The k-MSN method for the prediction of species-specific stand attributes using airborne laser scanning and aerial photographs. Remote Sensing of the Environment 109 (3): 328-341.

Pascual, C., A. Garcia-Abril, L. García-Montero, S. Martin-Fernández, and W. B. Cohen. 2008. Object-based semi-automatic approach for forest structure characterization using LiDAR data in heterogeneous *Pinus sylvestris* stands. Forest Ecology and Management 255 (11): 3677-3685.

Popescu, S. C., R. H. Wynne, and J. A. Scrivani. 2004. Fusion of small-footprint LiDAR and multispectral data to estimate plot-level volume and biomass in deciduous and pine forests in Virginia, USA. Forest Science 50 (4): 551-565.

Popescu, S. C. 2007. Estimating biomass of individual pine trees using airborne LiDAR. Biomass and Bioenergy 31 (9): 656-655.

R Development Core Team. 2013. R: a language and environment for statistical computing. Available from www.R-project.org. *accessed May 30, 2008.*

Radoux, J., and P. Defourny. 2007. A qualitative assessment of boundaries in automated forest stand delineation using very high resolution imagery. Remote Sensing of the Environment 110 (4): 468-475.

Reutebuch, S. E., R. J. McGaughey, H. E. Andersen, and W. W. Carson. 2003. Accuracy of a high-resolution LiDAR terrain model under a conifer forest canopy. Canadian Journal of Remote Sensing 29(5): 527-535.

Rot, B.W., R. J. Naiman and R. E. Bilby. 2000. Stream Channel Configuration, Landform, and riparian forest structure in the Cascade Mountains, WA. Canadian Journal for Forest Research 5: 699-707.

Rutherford, J. C., S. Blackett, C. Blackett, L. Saito, and R. J. Davies-Colley. 1997. Predicting the effects of shade on water temperature in small streams. New Zealand Journal of Marine and Freshwater Research 31 (5): 707-721.

Sanborn. 2008. LiDAR Campaign Final Report for Puget Sound. Report to USGS. March 2008. Colorado Springs, CO.

Secrest, K. A. 2007. Combining LiDAR, multi-spectral imagery and GIS to assess riparian area conditions. Master's thesis, Western Washington University. Bellingham, Washington.

Sedell, J. R., and K. J. Luchessa. 1982. Using the Historical Record as an Aid to Salmonid Habitat Enhancement. Pages 201-223 in N. B. Armantrout, editor. Acquisition and utilization of aquatic habitat inventory information. Western Division, American Fisheries Society, Bethesda, Maryland, USA.

Shamsoddini, A., J. C. Trinder, and R. Turner. 2010. Quantization of Pinus forest biophysical parameters using WorldView-2. DigitalGlobe 8-Band Research Challenge. http://dgl.us.neolane.net/res/dgl/survey/_8bandchallenge_winners.jsp?deliveryId=&id *accessed March 26, 2012.*

Sheridan, W. L., and A. M. Bloom. 1975. Effects of canopy removal on temperature of some small streams in southeast Alaska. USDA Forest Service. Alaska Region, Juneau. 19p.

Sommer, T. R., M. L. Nobriga, W. C. Harrell, W. Batham, and W. J. Kimmerer. 2001. Floodplain rearing of juvenile chinook salmon: evidence of enhance growth and survival. Canadian Journal of Fisheries Science 58 (2): 325-333.

Spies, T. A. 1998. Forest structure: A key to the ecosystem. Northwest Science 72 (2): 34-39.

Spies, T. A., and J. F. Franklin. 1991. The structure of natural young, mature, and old-growth Douglas-fir forests in Oregon and Washington. In Wildlife and vegetation of unmanaged Douglas-fir forests. Edited by L. F. Ruggiero, K. B., Aubry, A. B., Carey, and M. H. Huff. U.S.For.Serv.Gen.Tech.Rep. PNW-GTR-285. Portland, OR: U.S. Department of Agriculture, Forest Service, Pacific Northwest Research Station.

Spence, B.C., G. A. Lomnicky, R. M. Hughes, and R. P. Novitzki. 1996. An ecosystem approach to salmonid conservation. Technical Report: RT-45501-96-6057. ManTech Environmental Research Services Corp., Corvallis, OR.

Sridharan, H. 2010. Multi-level urban forest classification using the WorldView-2 8-band hyperspatial imagery. DigitalGlobe 8-Band Research Challenge. http://dgl.us.neolane.net/res/dgl/survey/_8bandchallenge_winners.jsp?deliveryId=&id *accessed March 26, 2012.*

Steiger, J., A. M. Gurnell, and G. E. Petts. 2001. Sediment deposition along the channel margins of a reach in the Middel River Severn. UK. Regulated Rivers Research & Management 17 (4-5):443-460.

Sullivan, A. A., R. J. McGaughey, H. E. Andersen, and P. Schiess. 2009. Object-oriented classification of forest structure from light detection and ranging data for stand mapping. Western Journal of Applied Forestry 24(4): 198-204.

Suratno, A., C. Seielstad, and L. Queen. 2010. Tree species identification in mixed coniferous forest using airborne laser scanning. ISPRS Journal of Photogrammetry and Remote Sensing 64(6): 683-693.

USGS, 2002. WRIA 01 Watershed management project – introduction: surface water system. https://wa.water.usgs.gov/projects/wria01/sw_intro.htm *accessed 5 November 2007*.

USGS, 2006. LiDAR survey Western Whatcom Counties and Skagit Counties, Washington by Sanborn. Colorado Springs, CO.

Van Pelt, R., and J. F. Franklin. 2000. Influence of canopy structure on the understory environment in tall, old-growth, conifer forests. Canadian Journal of Forest Resources 30 (8): 1231-1245.

Volk, C. J., P. M. Kiffney, and R. L. Edmonds. 2003. Role of riparian red alder in the nutrient dynamics of coastal streams of the Olympic Peninsula, Washington, USA. American Fisheries Society Symposium 34: 213-225.

Voss, M., and R. Sugumaran. 2008. Seasonal effect on tree species classification in an urban environment using hyperspectral data, LiDAR, and an object-oriented approach. Sensors 8(5): 3020-3036.

WADNR (Washington State Department of Natural Resources). 1996. Field procedures for forest resource inventory system. Olympia: Washington State Department of Natural Resources.

WADNR (Washington Department of Natural Resources). 2010. Title 222-30 WAC – Forest practices rules: timber harvesting. Pages 30-1–30-36 in Washington forest practices rules (revised 12-06-2010). State of Washington Department of Natural Resources, Olympia, Washington. (Available from: http://www.dnr.wa.gov/Publications/fp_rules_title_222_wac.pdf *accessed September 10, 2013*

WDFW (Washington Department of Fish and Wildlife). 2013. Washington State Species of Concern Lists. Washington Department of Fish and Wildlife, Olympia, WA. http://wdfw.wa.gov/conservation/endangered/status/SC/ *accessed October 13, 2013.*

WFPB (Washington Forest Practices Board). 1997 Board Manual: Standard Methodology for Conducting Watershed Analysis under Chapter 222-22 WAC. Version 4.0., November 1997.

WRIA 01 SRB (WRIA 1 Salmon Recovery Board). 2005. WRIA 1 Salmon Recovery Plan. October 11, 2005. Bellingham, WA.

Wendler, H. O., and G. Deschamps. 1955. Logging dams on coastal Washington streams. Washington Department of Fisheries Research Papers 1 (3): 27-38.

Wolf, A. 2010. Using WorldView2 vis-NIR MSI imagery to support land mapping and feature extraction using normalized difference index ratios. DigitalGlobe 8-Band Research Challenge. http://dgl.us.neolane.net/res/dgl/survey/_8bandchallenge_winners.jsp?deliveryId=&id *accessed March 26, 2012.*

Wondzell, S. M., A. Przeszlowska, D. Pflugmacher, M. A. Hemstrom, and P. A. Bisson. 2011. Modeling the Dynamic Responses of Riparian Vegetation and Salmon Habitat in the Oregon Coast Range with State and Transition Models. *In* Kerns, B.K., A. J. Shlisky, and C. J. Daniel (Technical Editors). Proceedings of the First Landscape State-and-Transition Simulation Modeling Conference, June 14-16, 2011, Portland, OR. Gen.Tech. Rep. PNW-GTR-869, Portland, OR, U.S. Department of Agriculture, Forest Service, Pacific Northwest Research Station.

Yu, X., J. Hyyppä, M. Vastaranta, M. Holopainen, and R.Viitala. 2011. Predicting individual tree attributes from airborne laser point clouds based on the random forests technique. ISPRS Journal of Photogrammetry and Remote Sensing 66 (1): 28-37.

8.0 Appendices

Appendix A. Detailed LiDAR Data Flow Diagrams. LiDAR Plot Processing

Polyclip – extracts plot from raw LiDAR las file.	**Output** - Las file.	
Clipdata – normalizes las from polyclipp data to	**Output** - Las file normalized to bare earth model.	
Cloudmetrics – computes various statistical parameters for clipped LiDAR dataset.	**Output:** csv file. Subset metrics • **Maximum height**[1] • **Mean height**[1] • **SD height**[1] • **CV height**[1] • **P95 height**[1]	
Canopy Surface Model (CSM) – subtracts the ground elevations from the return to produce a canopy	**Output:** DTM grid file.	
SurfaceStats –computes surface area and volume under a surface or between the surface and ground for an entire	**Output:** csv file.	
Rumple –calculated in excel as the ratio of the canopy surface area to the ground area from	**Output: Rumple Index**[1]. For above CSM example, rumple index value of	

[1] **LiDAR Metrics used in correlation analysis**

LiDAR Grid Processing

```
┌─────────────────────────┐
│ First Returns LiDAR point│ ╲
│ data (las format)        │  ╲       ┌──────────────┐       Output: Raster grids
└─────────────────────────┘   ╲──────▶│              │          •  Maximum height
                               ╱       │  Gridmetrics │ ──────▶   •  Mean height
┌─────────────────────────┐   ╱        │              │          •  SD height
│ Bare Earth Surface Model │  ╱        └──────────────┘          •  CV height
│ (DTM format)             │ ╱ ╲                                 •  P95 height
└─────────────────────────┘    ╲                                 •  Cover
                                ╲      ┌──────────────┐
┌─────────────────────────┐     ╲────▶│GridSurfaceStats│─────▶  Output: Raster Grid
│ Canopy Surface Model     │    ╱      │              │             •  Rumple
│ (DTM format)             │ ──╱       └──────────────┘
└─────────────────────────┘
```

Appendix B. Summary Statistics from all field plots (n = 63). Grey shading indicates plots in WV-2 study area (n=22).

Plot #	DBH[1] SD[2] (cm)	DBH Mean (cm)	DBH Max (cm)	DBH Min (cm)	Dom[3]	BA[4] SD (m²)	BA Mean (m²)	BA Max (m²)	BA Min (m²)	Plot Area (ha)	BA Plot (m²/ha)	Density (trees/ha)	Density ≥ 50 cm DBH (trees/ha)	Density ≥ 30 cm < 50 cm DBH (trees/ha)	Density ≥ 10 cm < 30 cm DBH (trees/ha)	BFW[5] (m)	RM[6]	Min PFD[7] (cm)	Stream Name
1	14.75	21.84	65	10.2	M[8]	0.08	0.05	0.33	0.01	0.06	23.86	442.92	53.15	0	389.77	1.6	NA	4	UN[9] tributary
2	14.28	22.1	53.9	10.2	D[10]	0.07	0.05	0.23	0.01	0.06	16.75	313.2	34.8	34.8	243.6	1.4	NA	3.5	UN tributary
3	18.4	30.61	110.8	10.3	M	0.16	0.1	0.96	0.01	0.06	56.34	566.67	50	216.67	300	0.83	NA	2.08	UN tributary
5	19.56	37.76	104.8	11.9	M	0.16	0.14	0.86	0.01	0.06	63.42	450	66.67	216.67	166.67	6.3	NA	15.75	UN tributary
10	33.35	47.94	88	10	C[11]	0.28	0.25	0.61	0.02	0.06	20.87	83.33	33.33	16.67	33.33	4	1.95	10	Black Slough
11	9.06	17.5	58.9	10	D	0.04	0.03	0.27	0.01	0.06	22.25	733.33	16.67	33.33	683.33	2.7	1.95	6.75	Black Slough
12	14.84	30.2	82.5	10.7	M	0.1	0.09	0.53	0.01	0.06	59	666.67	66.67	200	400	3.8	NA	9.5	UN tributary
13	10.27	24.44	52	10.5	D	0.05	0.05	0.21	0.01	0.06	33.91	616.67	16.67	133.33	466.67	3.1	NA	7.75	UN tributary
15	16.06	33.83	75.3	10	C	0.11	0.11	0.45	0.01	0.06	52.79	482.27	62.23	155.57	264.47	NA	16.5	NA	Cavanaugh Creek
17	18.03	27.08	75.6	10.8	C	0.12	0.08	0.45	0.01	0.07	31.49	383.57	46.03	76.71	260.83	NA	16.5	NA	Cavanaugh Creek
19	17.92	34.4	84.6	15.9	C	0.13	0.12	0.56	0.02	0.06	67.47	574.6	118.3	135.2	321.1	NA	16.5	NA	Cavanaugh Creek
20	13.59	33.37	63.1	12.3	C	0.08	0.1	0.31	0.01	0.07	38.63	381.07	45.73	182.91	152.43	NA	20.1	NA	Deer Creek
21	12.43	30.88	55.8	11.3	M	0.06	0.09	0.24	0.01	0.06	28.34	327.9	15.61	156.14	156.14	NA	20.1	NA	Deer Creek
22	11.65	28.02	53	12.3	M	0.06	0.07	0.22	0.01	0.06	25.61	356.5	15.5	93	248	8	20.1	20	Deer Creek
23	11.44	29.11	62.7	11	D	0.06	0.06	0.31	0.01	0.06	46.76	610.8	33.93	254.5	322.37	NA	4.6	NA	UN tributary
25	15.98	19.7	68.5	10	C	0.09	0.05	0.37	0.01	0.06	24.16	484.87	51.95	34.63	398.28	3.2	4.6	8	UN tributary
26	13	28.91	63.8	10.1	C	0.07	0.08	0.32	0.01	0.06	77.03	978.61	48.13	417.11	513.37	36	15.85	90	SF[12] Nooksack River
27	17.72	40.23	72.7	10.2	C	0.12	0.15	0.42	0.01	0.07	69.14	457.91	162.49	147.71	147.71	34	15.75	85	SF Nooksack River
28	17.73	34.34	80.8	10.6	C	0.12	0.12	0.51	0.01	0.07	70.7	605.63	126.76	197.18	281.69	5.8	15.25	14.5	Edfro Creek
29	15.36	34.94	86.5	12.5	C	0.11	0.11	0.59	0.01	0.06	83.6	733.33	66.67	416.67	250	8.4	15.25	21	Edfro Creek
30	12.49	37.03	63.3	13.7	C	0.08	0.12	0.31	0.01	0.06	51.78	433.33	66.67	266.67	100	NA	15.25	NA	Edfro Creek
35	27.37	46.9	110.2	13	M	0.26	0.23	0.95	0.01	0.06	56.91	250	83.33	133.33	33.33	13.8	10.25	34.5	Hutchinson Creek
36	32.92	43.64	116.4	13.4	C	0.33	0.23	1.06	0.01	0.06	72.91	316.67	100	66.67	150	11.7	10.25	29.25	Hutchinson Creek
37	23.03	39.35	69.1	10.1	D	0.14	0.16	0.38	0.01	0.06	29.23	183.33	66.67	50	66.67	10.6	10.25	26.5	Hutchinson Creek
38	2.94	12.21	21	10	D	0.01	0.01	0.03	0.01	0.05	3.46	280	0	0	280	6.9	27.2	17.25	Anderson Creek
39	26.72	53.24	90.5	27.5	M	0.25	0.27	0.64	0.06	0.03	63.17	233.33	100	66.67	66.67	7.2	27.2	18	Anderson Creek
40	4.92	17.55	23.7	10	D	0.01	0.03	0.04	0.01	0.01	23.94	923.08	0	0	923.08	7.7	27.2	19.25	Anderson Creek
41	14.16	22.37	74	10	M	0.09	0.05	0.43	0.01	0.06	35.2	644	48.3	32.2	563.5	25.2	14.3	63	Skookum Creek
42	15.73	30.18	74.5	11.2	M	0.1	0.09	0.44	0.01	0.07	33.29	369.23	46.15	92.31	230.77	38.6	14.3	96.5	Skookum Creek
43	10.43	29.66	60.2	13.2	C	0.06	0.08	0.28	0.01	0.06	56.27	726.63	16.51	297.26	412.86	21.2	14.3	53	Skookum Creek
44	10.79	27.69	51.7	10.7	M	0.05	0.07	0.21	0.01	0.07	54.99	795	30	315	450	13.5	14.3	33.75	Arlecho Creek
45	12.91	23.93	72.5	10.9	C	0.08	0.06	0.41	0.01	0.03	72.14	1250	71.43	107.14	1071.43	12.3	14.3	30.75	Arlecho Creek
46	11.17	39.99	59.9	20.7	C	0.07	0.13	0.28	0.03	0.07	45.33	335.8	58.4	189.8	87.6	6.5	14.3	16.25	UN tributary
47	5.26	20.38	31.3	10.7	D	0.02	0.04	0.08	0.01	0.06	17.36	500	0	15.63	484.38	2.4	14.3	6	UN tributary
48	15.2	27.39	58.7	13	D	0.08	0.08	0.27	0.01	0.07	10.75	142.86	14.29	42.86	85.71	78	0.7	195	SF Nooksack River
49	14.54	27.93	67.5	10.9	D	0.08	0.08	0.36	0.01	0.07	21.17	275.14	15.29	107	152.86	56	0.75	140	SF Nooksack River
50	19.05	36.92	65.1	10	D	0.11	0.13	0.33	0.01	0.06	53.75	400	133.33	100	166.67	58	0.8	145	SF Nooksack River
51	31.53	50.54	104.9	11.3	D	0.28	0.27	0.86	0.01	0.06	73.02	266.67	150	33.33	83.33	166	26.8	415	MS[13] Nooksack
53	14.65	29.64	61.1	10	M	0.08	0.09	0.29	0.01	0.06	35.5	416.67	66.67	100	250	NA	NA	NA	UN tributary
54	10.63	26.2	47.8	10	M	0.05	0.06	0.18	0.01	0.06	41.71	666.67	0	216.67	450	NA	NA	NA	UN tributary
55	35.66	38.03	99.7	10	D	0.3	0.2	0.78	0.01	0.04	52.04	257.14	85.71	0	171.43	5.2	1	13	Silver Creek
56	10.08	35.14	46.7	22.2	D	0.05	0.1	0.18	0.04	0.02	24.61	238.1	0	142.86	95.24	4.9	1	12.25	Silver Creek
57	21.03	30.99	70	11.1	C	0.13	0.11	0.38	0.01	0.01	169.3	1600	400	400	800	10	29.8	25	Smith Creek
58	35.51	47.07	116.9	24.5	M	0.4	0.26	1.07	0.05	0.01	128.27	500	83.33	166.67	250	6.3	29.8	15.75	Smith Creek
59	13.34	50.37	61.3	35.5	M	0.1	0.21	0.3	0.1	0.02	41.71	200	133.33	66.67	0	7.6	29.8	19	Smith Creek
60	11.65	25.06	61	10.2	M	0.06	0.06	0.29	0.01	0.06	47.14	788.9	32.2	161	595.7	51	13	127.5	SF Nooksack River
61	16.03	28.38	83.2	11.7	M	0.12	0.08	0.54	0.01	0.06	47.37	571.69	33.63	134.51	403.54	54	13	135	SF Nooksack River
62	19.2	27.39	101.2	10	C	0.14	0.09	0.8	0.01	0.07	62.79	719.32	88.08	132.12	499.12	38	13.1	95	SF Nooksack River
63	25.32	34.78	142.4	12.4	M	0.3	0.14	1.59	0.01	0.05	77.49	540	60	240	240	13.3	NA	33.25	SF Anderson Creek
64	16.83	38.08	75	12.5	M	0.11	0.14	0.44	0.01	0.06	94.93	700	183.33	283.33	233.33	8.4	21	SF Anderson Creek
65	20.21	36.84	80.5	10	M	0.13	0.14	0.51	0.01	0.06	84.97	616.67	133.33	250	233.33	11.6	NA	29	SF Anderson Creek
66	9.36	26.04	41.8	11.7	D	0.04	0.06	0.14	0.01	0.07	23.96	400	0	142.86	257.14	38	30.05	95	SF Nooksack River
67	14.21	28.78	65.1	10.4	M	0.08	0.08	0.33	0.01	0.07	40.84	507.69	46.15	153.85	307.69	42	30.07	105	SF Nooksack River
68	33.13	38.22	141	12	D	0.38	0.22	1.56	0.01	0.06	55.5	283.33	33.33	100	150	29	22.3	72.5	SF Nooksack River
69	43.7	42.33	213.5	10.3	M	0.7	0.29	3.58	0.01	0.06	125.68	440.4	125.83	47.19	267.39	41	22.35	102.5	SF Nooksack River
70	11.39	22.67	65.3	11.1	D	0.06	0.05	0.33	0.01	0.06	21.74	433.33	16.67	50	366.67	41	22.35	102.5	SF Nooksack River
71	5.01	19.95	37.4	11	M	0.02	0.03	0.11	0.01	0.06	33.21	1000	0	16.67	983.33	10	24.2	25	SF Nooksack River
72	8.21	19.67	51.3	10	D	0.04	0.04	0.21	0.01	0.06	22.5	633.33	16.67	33.33	583.33	48	24.25	120	UN tributary
73	13.42	23.16	52.8	10.3	D	0.06	0.06	0.22	0.01	0.06	23.22	416.67	33.33	83.33	300	1.45	12	3.63	Nessett Creek
74	22.11	32.85	72.2	11.9	M	0.14	0.12	0.41	0.01	0.06	26.04	216.67	50	33.33	133.33	3	4.6	7.5	UN tributary
75	44.09	69.49	153.2	12.5	M	0.59	0.52	1.84	0.01	0.09	89.44	171.2	96.3	42.8	32.1	62	13.48	155	SF Nooksack River
76	29.3	31.3	151.3	10.2	M	0.33	0.14	1.8	0.01	0.09	65.29	457.38	65.34	87.12	304.92	50	13.6	125	SF Nooksack River
78	3.65	14.46	21.3	10.1	D	0.01	0.02	0.04	0.01	0.06	8.13	466.67	0	0	466.67	139	9.6	347.5	SF Nooksack River

[1] DBH - Diameter at breast height
[2] SD - Standard deviation
[3] Dom - Dominance - Defined as C ≥ 75% Conifer Species, D ≥ 75% Deciduous Species, M - Mixed neither Conifer or Deciduous dominant.
[4] BA - Basal area
[5] BFW- Bankfull width
[6] RM - River Mile
[7] Min PFD - Minimum pool forming diameter - (Bankfull width x 0.025) x 100 (Hyatt et al. 2004; Beechie et al. 2000)
[8] C - Conifer dominated forest
[9] UN - Unnamed
[10] M - Mixed forest
[11] D - Deciduous dominated forest
[12] SF - South Fork
[13] MS - Mainstem

Appendix B continued. Summary Statistics from all field plots (n = 63). Grey shading indicates plots in WV-2 study area (n=22).

Plot #	Point Density (first returns/m²)	First Return Count	Minimum Height(ft)	Maximum Height (ft)	Mean Height (ft)	SD Height (ft)	CV Height	95th % Height (ft)	Percent first returns above 10 ft	Percent all returns above 10 ft	Percent first returns above mean	Rumple Index	Corner 1 Northing	Corner 1 Easting	Corner 2 Northing	Corner 2 Easting	Corner 3 Northing	Corner 3 Easting	Corner 4 Northing	Corner 4 Easting
1	2.04	1151	0.04	82.27	25.5	18.58	0.73	60.24	74.11	67.87	44.74	2.33	5400684.89	545164.25	5400676.23	5400676.23	5400714.89	545213.14	5400706.23	545218.14
2	2.23	1280	0.05	105.05	37.6	28.29	0.75	96.97	86.09	70.85	32.81	2.6	5400858.12	545172.64	5400866.78	545167.64	5400828.12	545122.87	5400836.78	545117.87
3	5.18	3110	0.57	127.66	86.4	16.28	0.19	115.19	99.68	90.84	46.98	2.5	5401569.19	545123.02	5401561.52	545116.59	5401607.75	545077.14	5401600.09	545070.72
5	2.26	1357	2.76	114.31	81.21	19.24	0.24	102.69	99.41	94.01	63.6	2.09	5401429.64	545182.80	5401421.55	545188.68	5401464.91	545231.10	5401456.82	545236.98
10	0.97	584	0	60.58	4.23	8.72	2.06	24.02	9.42	8.77	19.18	1.69	5398976.06	559864.25	5398972.97	559873.76	5399033.13	559882.80	5399030.04	559892.31
11	0.91	546	0.02	84.28	48.26	19.07	0.4	77.34	91.94	86.26	55.86	2.7	5398766.37	559978.16	5398765.68	559988.13	5398706.52	559973.97	5398705.82	559983.95
12	2.76	1655	0.07	105.58	62.29	17.48	0.28	85.33	96.92	84.11	58.43	2.13	5423560.69	520769.15	5423651.30	520765.73	5423581.21	520712.82	5423571.82	520709.40
13	2.63	1576	0	95.12	60.74	18.09	0.3	85.02	95.3	71.1	67.45	1.88	5423646.40	520726.90	5423651.40	520718.24	5423698.36	520756.87	5423703.36	520748.21
15	0.98	627	0.02	190.31	107.46	50.54	0.47	169.92	87.24	83.04	64.75	6.47	5387774.33	568180.71	5387780.76	568173.05	5387809.33	568236.38	5387815.76	568228.71
17	0.95	621	0.01	169.86	114.9	30.95	0.27	150.99	98.23	94.42	62.48	4.19	5387905.54	568278.39	5387907.28	568268.54	5387844.92	568245.80	5387846.66	568235.96
19	3.43	2027	0	172.21	86.12	45.64	0.53	145.53	87.27	82.5	60.09	4.74	5387795.49	568333.34	5387797.23	568343.18	5387864.43	568323.06	5387866.17	568332.91
20	1.34	882	0	114.24	57.35	26.86	0.47	91.21	90.02	85.67	62.24	4.37	5383755.03	566948.55	5383753.29	566958.39	5383823.96	566959.94	5383822.23	566969.79
21	1.11	708	0.02	117.86	53.85	40.39	0.75	103.6	75.14	69.27	53.25	3.25	5383704.19	566992.45	5383699.19	567001.11	5383643.57	566960.43	5383638.57	566969.09
22	1.22	785	0.02	124.67	66.28	30.24	0.46	103.99	88.92	86.46	59.49	3.89	5383670.14	567084.53	5383675.14	567075.87	5383730.76	567116.79	5383735.76	567108.13
23	1.3	764	0.02	101.32	69.04	25.38	0.37	95.31	96.73	92.91	62.96	2.22	5390651.92	564051.20	5390650.18	564041.36	5390711.01	564040.97	5390709.27	564031.12
25	1.25	720	0	91.47	14.45	19.28	1.33	61.04	39.72	39.44	24.31	2.15	5390691.63	564147.69	5390701.03	564151.11	5390671.11	564201.96	5390680.51	564205.38
26	1.41	881	0.15	140.15	94.11	25.62	0.27	123.72	98.3	95.96	63.11	3.29	5389162.56	564498.80	5389171.39	564503.49	5389195.42	564443.76	5389204.25	564448.46
27	0.8	540	0.01	166.44	104.7	25.41	0.24	137.58	97.22	95	56.3	4	5389304.72	564572.83	5389295.32	564569.41	5389328.66	564509.22	5389319.26	564505.80
28	1.25	886	0.15	153.18	109.45	28.56	0.26	141.37	97.86	90.97	62.19	4.45	5390821.13	565787.84	5390813.47	565781.41	5390775.50	565842.01	5390767.84	565835.58
29	0.99	592	17.88	155.32	109.91	19.18	0.17	139.58	100	98.38	42.4	2.52	5390919.45	565807.42	5390927.87	565816.82	5390863.07	565827.94	5390866.49	565837.34
30	1.02	610	0.04	163.5	98.83	33.39	0.34	146.91	94.1	90.51	60.98	4.6	5390816.37	565933.51	5390809.94	565925.85	5390862.33	565895.06	5390855.90	565887.40
35	0.87	523	0	157.36	58.12	44.8	0.77	136.1	78.97	73.13	44.93	6.08	5396856.68	562106.66	5396863.62	562099.46	5396813.52	562065.14	5396820.46	562057.95
36	0.83	500	0.01	139.39	62.1	35.42	0.57	108.74	85.6	83.5	54.6	4.25	5396781.71	562016.14	5396787.01	562024.62	5396832.59	561984.41	5396837.89	561992.89
37	1	601	0.05	150.46	88.78	40.02	0.45	131.6	92.18	87.45	67.22	3.79	5396745.78	562009.14	5396755.39	562011.90	5396729.24	562066.70	5396738.85	562069.46
38	0.54	270	0	63.1	9.75	16.62	1.71	45.15	26.3	27.59	26.3	1.98	5409061.74	548501.83	5409060.00	548511.67	5409110.98	548510.50	5409109.24	548520.35
39	0.59	176	0	118.66	66.16	30.76	0.46	103.4	88.07	77.84	52.84	4.24	5409180.03	548487.26	5409171.37	548492.26	5409165.03	548461.31	5409156.37	548466.31
40	0.68	89	0.15	95.22	49.77	29.85	0.6	91.23	85.39	74.29	55.06	4.36	5409215.02	548438.57	5409205.62	548441.99	5409219.60	548450.75	5409210.21	548454.17
41	0.99	615	0.05	126.93	54.78	26.28	0.48	101.95	95.45	91.22	45.04	3.87	5393096.55	565628.18	5393166.38	565632.52	5393097.25	565622.54	5393167.08	565622.54
42	1.4	911	0.01	129.49	58.08	28.4	0.49	99.79	89.35	82.96	59.28	3.44	5393072.07	565558.12	5393063.40	565553.12	5393104.57	565502.38	5393095.90	565497.38
43	1.62	979	0.27	126.03	92.53	16.31	0.18	112.28	99.28	95.27	54.24	2.11	5392876.34	565539.71	5392881.34	565548.37	5392936.96	565509.43	5392941.96	565518.09
44	1.06	707	0.03	109.24	75.86	20.43	0.27	95.19	95.47	86.26	67.75	2.12	5393144.91	569175.56	5393151.33	569167.90	5393198.53	569218.42	5393204.96	569210.76
45	1.15	321	0.05	113.26	77.24	15.62	0.2	94.58	98.44	94.96	55.76	2.15	5393233.02	569068.84	5393233.02	569058.84	5393261.02	569068.84	5393261.02	569058.84
46	1.56	1069	0	123.21	82.58	23.14	0.28	111	96.3	93.54	57.34	3.55	5394529.29	565591.18	5394484.29	565643.65	5394529.29	565643.65	5394476.63	565637.22
47	1.28	818	0.08	106.53	46.77	19	0.41	83.52	96.94	90.55	45.6	2.04	5394474.46	565534.11	5394464.61	565535.83	5394463.35	565471.52	5394453.50	565473.26
48	1.15	804	0.07	106.58	57.24	26.69	0.47	92.1	93.53	91.3	61.07	3.52	5405621.99	558481.96	5405631.39	558485.38	5405655.33	558420.26	5405645.93	558416.84
49	1.53	1000	0.13	108.06	70.03	26.78	0.38	96.28	91.3	88.48	69.7	3.39	5405525.14	558440.81	5405534.54	558444.23	5405558.48	558382.75	5405549.08	558379.33
50	1.2	717	0	140.46	80.62	46.56	0.58	131.99	85.08	82.12	59.69	5.91	5405422.44	558500.10	5405432.28	558501.84	5405412.02	558558.95	5405421.87	558560.69
51	0.77	464	0.64	155.28	110.61	38.89	0.35	149.4	94.4	87.49	63.36	5.69	5414436.12	548487.25	5414427.24	548493.30	5414409.12	548433.85	5414399.88	548439.77
53	1.93	1158	0.01	119.18	56.22	27.98	0.5	99.34	88.6	68.18	58.13	2.73	5421136.79	519295.12	5421136.79	519305.12	5421076.79	519305.12	5421076.79	519305.12
54	0.26	157	1.62	110.71	92.12	17.46	0.19	109.27	99.36	87.82	66.88	3.84	5421115.53	519366.63	5421115.53	519376.63	5421055.53	519366.63	5421055.53	519376.63
55	0.63	222	0	102.54	44.25	29	0.66	94.32	83.3	69.97	48.2	3.99	5406739.70	534883.41	5406741.43	534893.26	5406774.17	534877.37	5406772.44	534887.22
56	0.62	131	0.86	73.93	29.73	21.1	0.71	65.25	74.81	66.51	45.8	3.8	5406705.30	534963.39	5406697.64	534969.82	5406718.80	534979.29	5406711.14	534985.72
57	1.24	62	1.76	62.95	40.6	18.01	0.44	62.49	95.16	93.6	54.84	3.44	5410659.87	552781.21	5410654.87	552789.87	5410655.53	552778.77	5410650.53	552787.43
58	1.44	173	0.28	117.36	94.92	25.72	0.27	114.7	98.7	97.99	66.47	2.41	5410729.31	552729.04	5410731.05	552719.19	5410741.13	552731.63	5410742.86	552721.78
59	1.18	177	0.71	112.74	51.55	31.07	0.6	108.21	89.27	88.39	40.11	4.51	5410730.78	552644.79	5410727.36	552654.19	5410716.69	552640.71	5410713.27	552650.11
60	1.12	697	0.2	120.93	57.66	28.21	0.49	96.27	94.4	91.11	47.49	2.54	5391872.04	561507.24	5391867.04	561515.90	5391811.41	561476.18	5391806.41	561484.84
61	1.13	671	0.03	113.78	53.43	27.34	0.51	96.51	96.76	92.17	41.88	2.65	5391867.04	561515.90	5391862.04	561524.56	5391806.41	561486.16	5391801.41	561494.82
62	1.35	920	0	128.08	58.1	35.59	0.61	112.08	83.8	79.71	55.22	4.17	5391796.66	561630.10	5391801.81	561621.53	5391732.37	561595.02	5391737.52	561586.45
63	3.41	1704	1.41	149.69	100.91	32.66	0.32	138.82	99.59	91.81	54.4	3.32	5404024.41	549357.49	5404032.07	549351.07	5404065.94	549395.45	5404064.21	549389.03
64	1.94	1163	13.25	142.99	93.52	18.26	0.2	129.66	100	97.96	43.16	2.6	5403983.54	549345.85	5403993.39	549344.11	5403993.96	549404.35	5404003.80	549402.62
65	1.05	631	0.05	127.55	77.67	21.31	0.27	103.98	97.62	94.82	72.42	2.27	5403893.91	549381.77	5403903.75	549383.51	5403883.49	549440.27	5403893.34	549442.01
66	0.97	678	0.02	102.57	70.39	30.49	0.43	97.51	90.71	76.37	66.96	1.88	5384191.20	579655.32	5384188.61	579645.65	5384123.58	579712.85	5384121.00	579663.65
67	0.97	632	0	132.95	72.52	32.05	0.44	114.64	91.77	84.97	57.75	4.3	5384188.99	579733.85	5384188.29	579743.82	5384124.15	579729.34	5384123.45	579739.31
68	0.97	581	0.15	150.15	75.22	35.68	0.47	131.93	88.81	82.43	60.07	3.86	5383540.19	569360.46	5383541.92	569370.31	5383599.27	569350.12	5383601.01	569359.97
69	0.8	507	0.08	190.25	75.79	35.89	0.47	159.31	97.63	95.59	36.88	4.16	5383537.95	569473.56	5383537.95	569463.56	5383601.53	569473.56	5383601.53	569463.56
70	1.26	755	0.07	108.68	40.62	19.32	0.48	69.89	95.89	91.92	53.77	2.63	5383505.28	569451.12	5383504.93	569461.11	5383445.32	569449.03	5383444.97	569459.03
71	0.97	581	0.28	76.07	61.11	8.91	0.15	72.29	99.48	96.24	50.6	1.71	5383170.47	571847.73	5383180.32	571845.99	5383180.89	571906.58	5383190.74	571904.85
72	1.4	838	0.25	68.81	42.04	16.47	0.39	63.26	93.79	86.86	57.64	2.3	5383386.15	571824.04	5383384.41	571814.19	5383327.06	571834.42	5383325.33	571824.57
73	1.47	883	0.18	108.29	43.93	22.24	0.51	86.39	99.43	98.85	44.85	3.69	5393285.93	562425.92	5393292.36	562418.26	5393331.89	562464.30	5393338.32	562456.63
74	1.18	710	0.07	120.07	47.37	31.94	0.67	92.92	81.55	78.22	50.14	3.36	5390640.61	564106.26	5390637.19	564115.66	5390584.23	564085.84	5390580.81	564095.24
75	1.6	1498	0.01	160.98	62.1	42.24	0.68	123.83	81.04	76.43	55.41	4.39	5391506.66	562091.90	5391501.66	562100.56	5391593.27	562138.63	5391588.27	562147.29
76	1.28	1174	0	160.99	77.92	40.67	0.52	141.29	94.29	92.22	55.11	3.77	5391418.16	562257.60	5391410.75	562263.41	5391354.01	562194.44	5391348.07	562202.40
78	1.18	707	0.01	44.94	20.06	9.15	0.46	34.01	86.85	83.97	53.04	2.12	5395464.44	559941.48	5395467.86	559932.08	5395408.06	559920.95	5395411.48	559911.56